Development of a volumetric solar thermal absorber

Franz-Dominik Treikauskas

PhD

2009

Development of a volumetric solar thermal absorber

Franz-Dominik Treikauskas

A thesis submitted in partial fulfilment
of the requirements of De Montfort University
for the degree of Doctor of Philosophy (PhD)

January 2009

Institute of Energy and Sustainable Development
De Montfort University Leicester

Centre of Excellence for Solar Engineering
Ingolstadt University of Applied Sciences

Abstract

Thermal collectors are the central part of a solar energy system. Within the collector, the absorber is the most essential component and contributes about 46% to the total costs of a collector. These absorbers are typically based on the sheet-pipe design. Hence, further improvements of the absorber performance are hard to carry out without increasing costs and weight for the collector significantly. Against this background, current absorber designs are investigated and new possibilities are selected, calculated, optimised and experimentally tested.

An analysis of former and current absorber designs is carried out. It can be seen, that during the energy crisis more innovative systems were developed, while in recent years the state-of-the-art is based on the sheet-pipe design. A lot of different connections are applied to join the header and riser pipes to the selectively coated absorber sheet. However, weaknesses in manufacturing and operation as well as those regarding efficiency and costs make it hard to improve this design.

In an engineering design process the absorber is analysed and together with a requirements list, new approaches have been developed. New absorber materials are suggested as well as absorber design possibilities for fluid and heat conduction. Based on the solutions several concepts are derived, which are evaluated to select the best for further optimisation and experimental testing.

In the course of fluid simulation, the chosen concepts are modelled and optimised regarding flow distribution. This approach is novel as former absorber designs lack homogenous flow, or the distribution was optimised experimentally. The simulation results show a more equal flow distribution for the concepts than is the case for the state-of-the-art absorbers. Calculations of the collector efficiency factor show superior values for volumetric absorbers, while typical values are gained for sheet-pipe-absorbers.

Infrared, pressure drop and collector efficiency tests confirm the results of simulation and calculation for both the new designs and the state-of-the-art. The developed absorber with corrugated pattern shows a more homogeneous flow distribution and a higher measured collector efficiency factor than typical state-of-the-art absorber.

Acknowledgements

This research project was carried out at the Institute of Energy and Sustainable Development at De Montfort University Leicester in cooperation with the Centre of Excellence for Solar Engineering at Ingolstadt University of Applied Sciences.

I would like to thank Prof. Vic Hanby, Dr. Simon Rees and Prof. Wilfried Zörner for the initiation of this research work, for their excellent support and guidance as well as for their revision of this thesis.

Furthermore, I would like to give special thanks to the industrial project partner CitrinSolar, in particular to Hanns Koller with whom it was a pleasure to work and who was always willing to give support.

Moreover, I am very grateful to the students and colleagues who accompanied me during the years at the Centre for Excellence for Solar Engineering, especially to Sebastian Brandmayr, Achim Haller, Holger Müller, Matthias Sonnleitner, Dr. Christoph Trinkl and Roland Wittmann. They made the university much more than just a place to work.

I have to express my special thanks to Michael Rebele who always helped when problems occurred with the Linux operating system environment or the running of the solver.

Finally, I would like to thank my parents for their enduring support and their encouragement throughout the work. I also would like to thank my girl-friend Christiane for her patience and her encouragement in difficult times.

I declare that the content of this submission is my own work. The contents of the work have not been submitted for any other academic or professional award. I acknowledge that this thesis is submitted according to the conditions laid down in the regulations. Furthermore, I declare that the work was carried out as part of the course for which I was registered. I draw attention to any relevant considerations of rights of third parties.

Table of Contents

List of Figures

List of Tables

Abbreviations

BC	Boundary Condition
CAD	Computer Aided Design
CFD	Computational Fluid Dynamics
CVD	Chemical Vapour Deposition
HVAC	Heating Ventilation and Air Conditioning
IEA-SHC	International Energy Agency – Solar Heating and Cooling Programme
IGES	Initial Graphics Exchange Specification
PMMA	Polymethyl Methacrylate
PVD	Physical Vapour Deposition
SDHW	Solar Domestic Hot Water
UTF	Unicode Transformation Format
VBA	Visual Basic for Applications

Symbols

a_1	Linear heat loss coefficient	W $m^{-1}K^{-1}$
a_2	Quadratic heat loss coefficient	W $m^{-1}K^{-2}$
A_A	Absorber area	m²
A_{CH}	Cross sectional area of converging header	m²
A_{DH}	Cross sectional area of diverging header	m²
A_{Fin}	Fin area	m²
A_H	Cross sectional area of header (either diverging or converging)	m²
$A_{i+1,j}$	Cross sectional area of duct j in model i+1	m²
A_j	Cross sectional area of pipe or duct j	m²
A_{Rj}	Cross sectional area of riser j	m²
b	Width of duct	m
$b_{i,j}$	Width of duct j in the current model i	m
$b_{i+1,j}$	Width of duct j in model i+1	m
b_I	Width of island	m
b_j	Width of duct j	m
b_{left}	Width of channel on the left side of an island	m
b_{right}	Width of channel on the right side of an island	m
b_{RW}	Width of riser	m
C_b	Bond conductance between riser and sheet	W $m^{-1}K^{-1}$
D	External diameter of riser pipe	m
d_{CH}	Diameter of converging header	m
d_{DH}	Diameter of diverging header	m
d_{h_j}	Hydraulic diameter of duct j	m

d_H	Header diameter (either diverging or converging)	m
d_j	Diameter of pipe j	m
d_R	Diameter of riser	m
d_{Rj}	Diameter of riser j	m
f_{HT}	Factor for header types	-
F	Fin efficiency factor	-
F_{as}	Fin efficiency factor for asymmetric fin	-
F'	Collector efficiency factor	-
F'_{as}	Collector efficiency factor for asymmetric fin	-
F'_{FN_j}	Normalised collector efficiency factor of fin j	-
F'_m	Averaged collector efficiency factor	-
g	Bond conductance width	m
G	Irradiance	W m^{-2}
h	Height of duct	m
h_{fi}	Heat transfer coefficient	W $m^{-2}K^{-1}$
k_{gF}	Heat transmission coefficient	W $m^{-2}K^{-1}$
l	Pipe length	m
L_H	Length of header	m
L_R	Length of riser	m
m	Maximum number of layers	-
n	Number of risers / ducts (in layer)	-
n_k	Maximum number of channels in layer k	-
n_R	Number of risers	-
$Nu_{m,q}$	Averaged Nusselt number	-
$Nu_{m,q,1}$	First asymptote for the averaged Nusselt number	-

$Nu_{m,q,2}$	Second asymptote for the averaged Nusselt number	-
$p_{s,in}$	Static pressure at inlet cross section	Pa
$p_{s,out}$	Static pressure at outlet cross section	Pa
Pr	Prandtl number	-
$\dot{q}_{use}$	Usable heat flux	W m^{-2}
Q_{abs}	Usable heat flow	W
R_{RT}	Top radius of riser	m
Re	Reynolds number	-
T_a	Ambient temperature	K
T_{abs}	Mean absorber sheet temperature	K
T_f	Local fluid temperature	K
T_{in}	Temperature at collector inlet	K
T_m	Mean fluid temperature	K
T_{out}	Temperature at collector outlet	K
T_{Pt}	Local plate temperature	K
U_j	Perimeter of duct j	m
U_L	Collector overall heat loss coefficient (based on T_{abs})	W m^{-2}K^{-1}
V_F	Fluid volume of absorber	l
$v_{i,j}$	Flow velocity in duct j of model i	m s^{-1}
v_j	Flow velocity in pipe or duct j	m s^{-1}
$\dot{V}_H$	Ideal flow rate of layer (homogenous flow distribution in all channels)	m³ s^{-1}
$\dot{V}_{Hn}$	Normalised ideal flow rate	-
$\dot{V}_{i+1,j}$	Flow rate in duct j in model i+1	m³ s^{-1}
$\dot{V}_j$	Flow rate in pipe or duct j	m³ s^{-1}

$\dot{V}_{nH_j}$	Normalised flow rate of channel j	-
$\dot{V}_{nH_{i+1,j}}$	Normalised flow rate of duct j in model i+1	-
$\dot{V}_O$	Flow rate at absorber inlet	$m^3\ s^{-1}$
W	Distance between risers	m
W_A	Absorber width	m
W_L	Left fin width	m
W_R	Right fin width	m
x	Channel position in direction of the absorber width	m
$(\tau\alpha)_{eff}$	Effective transmittance absorptance product	-
α	Absorptance of absorber coating	-
δ	Sheet thickness	m
η	Collector efficiency	-
η_0	Zero loss efficiency	-
λ_f	Thermal conductivity of heat transfer fluid	$W\ m^{-1}K^{-1}$
λ_S	Thermal conductivity of absorber sheet	$W\ m^{-1}K^{-1}$
ρ_c	Reflectance of transparent cover	-
τ	Transmittance of transparent cover	-
ΔL_R	Distance between riser pipes	m
Δp	Pressure loss of absorber	Pa
$\Delta\dot{V}_{n_{i+1,j}}$	Normalised flow rate deviation of channel j in model i+1	-
$\Delta\dot{V}_{O_i}$	Overall normalised flow rate deviation of model i	-

1 Introduction

Solar thermal collectors for domestic hot water and space heating applications have been increasingly used in recent years. Higher costs for fossil fuel on the one hand and an increasing environmental awareness on the other hand maybe the cause for this development. Collector manufacturers, however, have to face new challenges due to the need for higher quantities. State-of-the-art absorbers based on the sheet-pipe design are not optimised for mass production. Especially, soldered absorbers face this problem (Epp 2002) driven by improved collector efficiency and the resulting higher stagnation temperatures. Although, alternative absorber designs existed as shown in Appendix A manufacturers and research institutes stuck with the sheet-pipe absorber design and concentrated on alternatives for connecting the absorbing sheet to the fluid conducting pipes (section 2.4.2). Sheet-pipe absorbers are mainly based on the header riser designs as shown in chapter 4.2.1 / Figure 4.1 and to a lesser extent on the meander design. The latter one is not considered in this work as there is just one flow path without any mass flow distribution. In some cases, however, the meander absorber is used for a comparison with other designs. An alternative to the state-of-the-art are volumetric or flooded sheet absorbers like the steel panel and the steel cushion absorber illustrated in Appendix A.

Furthermore, absorber costs are difficult to reduce with sheet-pipe designs as many different steps are needed for manufacturing. Mangold (1996) showed that nearly half of the collector costs are incurred by the absorber as illustrated in Figure 1.1. Cost reductions accompanied by new sheet-pipe manufacturing methods could not be identified (Mangold 2004). It is shown in section 2.4.3 that the sheet-pipe absorber design requires high heat conduction, hence, copper is the material of choice for the absorbing sheet and the piping. Copper prices, however, increased significantly during recent years as shown in

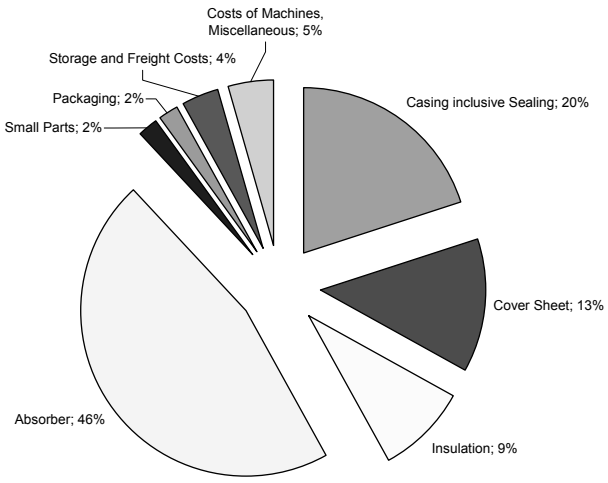

Figure 1.1: Distribution of Collector Costs, data from Mangold (1996)

Figure 1.2. As can be seen the price for aluminium also increased, however, it is still more than 2 times lower than that of copper. This is the major reason for absorber manufacturers to switch from a copper sheet to an aluminium sheet.

Nevertheless, the improvement of manufacturing processes as well as cost reductions based on the sheet-pipe absorber design cannot increase the collector efficiency factor. A significant improvement in efficiency is strongly dependent on the number of risers used in the header riser design of a sheet-pipe absorber as shown in sections 2.4.3 and 4.4.1. Hence, the material content of the copper piping within the absorber is increased, accompanied by higher material cost.

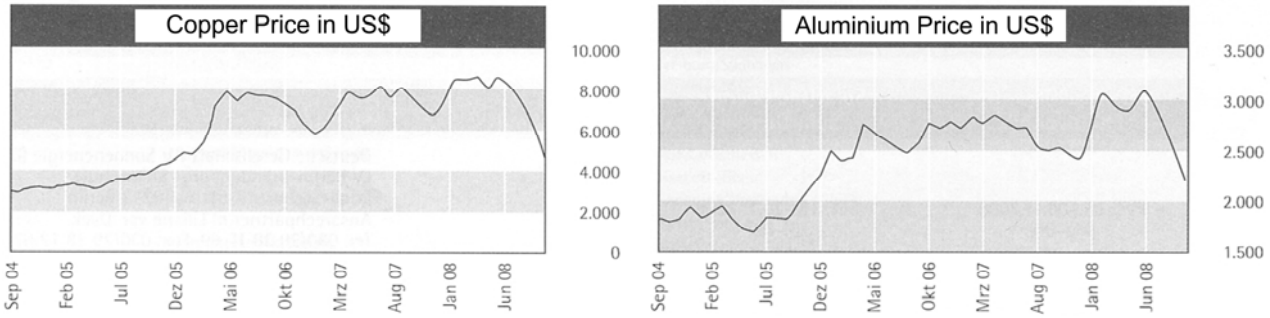

Figure 1.2: Price Trend of Copper and Aluminium (Anon 2008)

In order to avoid the above mentioned weaknesses of the sheet-pipe absorber design this research had to main objectives:

- the application of new manufacturing processes accompanied by new absorber materials (aspects: cost reduction and mass production)
- the efficiency improvement of the solar-thermal absorber

Hence, this research was aimed at the development of a new absorber design providing significant area for heat transfer between the absorbing surface and the heat carrier fluid. In subsequent chapters absorbers based on this concept are called ‘volumetric absorbers’. As a first step towards concept development absorbers are analysed in chapter 0 regarding designs, quality and manufacturing. This information is used in chapter 3 to define a specification and a function structure as a basis for the subsequent concept development process. In the concept phase and the subsequent steps attention is drawn to realisable manufacturing processes ready for mass production in combination with lower priced absorber materials. Due to the design approach based on a volumetric absorber, a higher collector efficiency factor is anticipated and can be realised as shown in sections

4.4 and 5.5. In chapter 3 the concept development is followed by numerical simulations and an optimisation process aiming at a homogenous flow distribution. The state-of-the-art header-riser absorber design is analysed in detail showing improvements for a more homogenous flow distribution and a lower pressure loss. Furthermore, two different designs from chapter 2 are investigated and optimised. Efficiency calculations are in turn calculated analytically and use empirical formulae for heat transfer as well as models for different absorber designs. Finally, chapter 0 illustrates the experimental investigations carried out at the University of Ingolstadt. Prototypes of the state-of-the-art absorber design as well as the new volumetric absorber were tested and the results were compared with calculated values proofing in both cases the quality of the simulations and the advantage of the new design. Chapter 5 provides a conclusion to the work with notes on the further work.

Within the project collaboration between the University of Applied Sciences Ingolstadt and the company CitrinSolar existed. CitrinSolar is a local collector manufacturer, who is interested in a new, optimised absorber as mentioned in the previous paragraphs. Throughout the research project information on the work packages were exchanged, while CitrinSolar was particularly involved in the specification for the new absorber design and provided support for test rigs and prototypes.

2 Solar Thermal Collectors

2.1 Application Areas

In the beginnings of solar technology for low temperature applications at the end of the seventies, collectors were almost exclusively used for domestic hot water preparation. Nowadays, however, they are increasingly used to support space heating in houses. Moreover, various applications for HVAC-systems can be considered as state-of-the-art. Figure 2.1 shows today's applications of solar thermal collectors in the field of low temperature applications. As a consequence of increased adoption of glass and steel in the building industry, thermal air conditioning processes have been developed, especially for small refrigerating capacities. This provides another possibility to use thermal collectors as an energy source. Furthermore, process heat applications in the industry will become more important in future, due to rising energy costs.

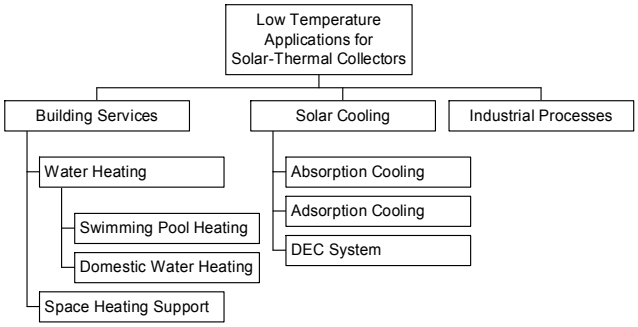

Figure 2.1: Employment of Thermal Low Temperature Collectors

The temperature level of a collector has to be considered before choosing a collector type for a certain application. Figure 2.2 shows various collector types for low temperature applications. In principle, all collectors listed use the same absorber design, apart from water storage and air heating collectors.

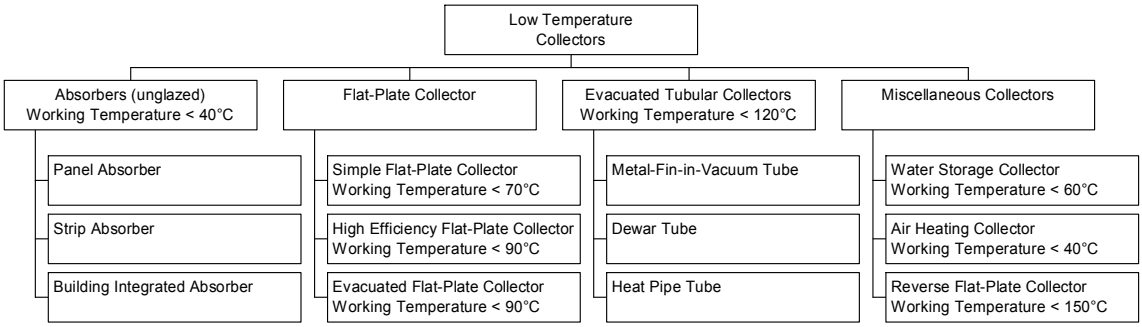

Figure 2.2: Types of Low Temperature Collectors

2.2 Absorber Components

Absorber Materials

The main technical demand for materials of absorbers is high temperature stability because of stagnation periods during collector operation. Moreover, good corrosion resistance is very important for a reliable and durable operation that can last more than 20 years. Particularly in the beginning of solar technology many different materials for absorbers were employed. This variety is mainly reduced to copper for the piping and the sheet caused by various reasons, e.g. corrosion aspects. Due to economic factors and accompanied by the laser welding technology the copper sheet can be replaced by an aluminium sheet nowadays. Table 2.1 gives an overview of employed materials for the last 30 years and shows their assets and drawbacks.

Table 2.1: Overview of Absorber Materials

Materials	Advantages	Disadvantages
Aluminium	● high thermal conductivity ● low density ➔ low weight ● easy to process ● inexpensive	● low corrosion resistance ● high energy input for Al production (relating to primary Al / In case of recycled Al the energy demand is no longer a disadvantage as it is much lower.)
Steel	● easy to process ● inexpensive ● low energy input for steel production	● low thermal conductivity ● high density ➔ high weight ● low corrosion resistance
Stainless Steel	● corrosion resistant ● high durability ● low energy input for steel production	● low thermal conductivity ● high density ➔ high weight ● expensive
Copper	● high thermal conductivity ● corrosion resistant ● high durability ● easy to process	● high density ➔ high weight ● expensive
Plastics	● low density ➔ high weight ● corrosion resistant ● low energy input for polymer production	● very low thermal conductivity ● low temperature durability
Engineering Fibres	● low density ➔ low weight ● corrosion resistant	● very low thermal conductivity ● low temperature durability
Glass	● corrosion resistant ● high durability ● easy to process	● very low thermal conductivity ● low ductility ● expensive

Absorber Coatings

Absorber coatings are used to significantly improve the energy efficiency of collectors in two ways. Selective coatings increase the absorptance α of the absorber surface for short-wave radiation and reduce the temperature dependent emittance ε for long-wave radiation (thermal radiation), as shown in Figure 2.3.

Selective coatings exploit two physical effects, which are based on the different wavelengths of the solar spectrum and the infrared radiation. Figure 2.4 implicates the short-wave radiation for solar irradiance on the ground with an air mass spectrum 2 (AM 2) at wavelengths $\lambda < 3\ \mu m$ and the long-wave radiation of a black body at $\lambda > 3\ \mu m$. Kirchhoff's Law constitutes that a surface has a high emittance at a given wavelength if it has a high absorptance at the same wavelength. At a certain wavelength, however, the emittance is low when the surface exhibits high reflectance – being a mirror at this wavelength. Therefore, the ideal surface does not reflect radiation below $\lambda < 3\ \mu m$ and reflects in the range above $\lambda > 3\ \mu m$ as illustrated in Figure 2.5.

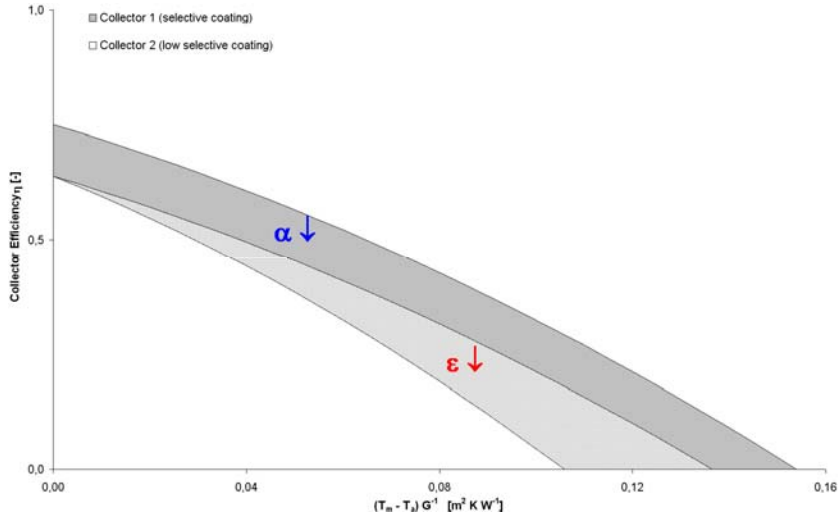

Figure 2.3: Influence of the Selective Coating on the Collector Efficiency

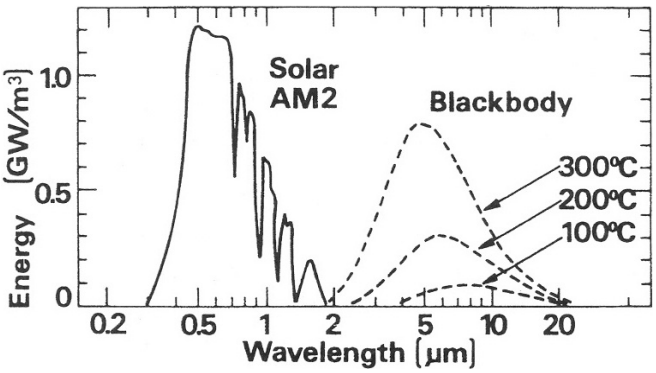

Figure 2.4: Spectra for Characteristic Solar and Black Body Radiation (Niklasson & Granqvist 1991)

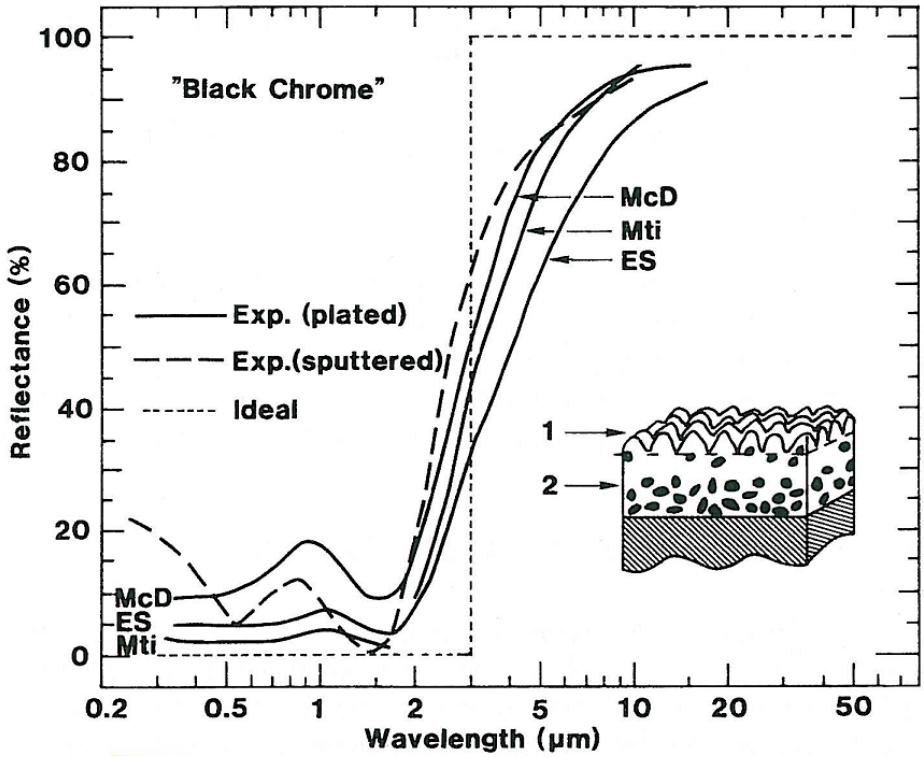

Figure 2.5: Reflectance of Ideal and Black-Chrome Selective Coatings (Niklasson & Granqvist 1991)

Until the seventies, non-selective coatings, like black paint, were applied to the absorber surface. Nevertheless, research regarding selective coatings already started in the fifties and had a big increase in the seventies due to the oil crisis. A detailed bibliography of this vast field of research is given in Bogaerts and Lampert (1983), Niklasson and Granqvist (1983) as well as Lampert (1997). The coatings developed then such as black chrome are still employed nowadays. Compared to new coatings, however, they suffer from a higher emission rate, susceptibility to moisture, fouling and especially grease. Even then these coatings can reach a lifetime of around 20 years and more when they are protected in a collector casing, as described by Peuser et al (1997).

State-of-the-art is a selective coating like PVD- (Physical Vapour Deposition), CVD- (Chemical Vapour Deposition) or a PECVD-coating (Plasma Enhanced Chemical Vapour Deposition). The layers are based upon physical or chemical processes known from coatings applied to milling cutters in order to gain higher abrasion resistance. Furthermore, some other possibilities have been developed to achieve selective attributes, for example solar selective paints (Orel 2007a, 2007b) or by mechanical and chemical treatment of the surface (Konttinen et al 2003). The advantages of these new kind of coating processes are lower energy consumption, less environmental pollution and lower

emission rates. A drawback is the high investment for industrial production facilities. Table 2.2 describes current absorber coatings.

Table 2.2: State-of-the-Art Absorber Coatings (according to Berner 2004)

Manufacturer	Product	α [%]	ε [%]	Coating	Process	Substrate
Alanod	Miro-Therm	94 ±2	5 ±2	Cermet	PVD	Al
European Solar Engineering S.A.	Epsilon	95 ±1	4 ±1	n. s.	PVD	Cu
Tinox	Tinox classic	9 ±2	5 ±2	Titan-Nitrite-Oxide	PVD	Cu
	Tinox art-line	91 ±2	5 ±2			
Ikarus Coatings	Brillanta	92 ±1	4 ±1	Amorphous, chrome containing hydro-carbon layer	Magnetron-sputter-CVD-process	Cu
Interpane	Sunselect	95 ±1	5 ±1	Cermet	Magnetron-sputter-prozess	Cu
Sunstrip AB	Sunstrip	96 ±2	7 ±2	Cermet	Magnetron-sputter-prozess	Al
Alternate Energy Technologies LLC	Crystal Clear	94-96	4-9	Ni layer in crystal structure	Galvanic process	Cu
ChromeCoat A/S	ChromeCoat	95 ±1	10 ±2	Black chrome with Ni intermediate layer	Galvanic process	Cu
Energie Solaire SA	AS	95	15	Black chrome with Cu intermediate layer	Galvanic process	Stainless steel
	AS+	95	5			
Fentek Fenis Teknik Ürünler	Solartek	95 ±2	15 ±2	Ni pigmented anodic Al_2O_3	Galvanic process	Al
Materials Technology Inc.	Krosol	96 ±2	8 ±3	Black chrome with Ni intermediate layer	Galvanic process	Cu
Solchrome Systems India Ltd.	Solchrome	96 ±2	12 ±2	Black chrome with Ni intermediate layer	Galvanic process	Cu
Target	Nirabo	96 ±1	7 ±1	Black nickel	Galvanic process	Al, Cu, steel
Thermo|Solar	AlOx	95 ±1	16 ±1	Ni pigmented anodic Al_2O_3	Galvanic process	Al
Jacques Giordano Industries	Cumox	95 ±1	9 ±1	n. s.	n. s.	Cu

2.3 Previous Absorber Designs

In 1978 the German government published a new funding programme to promote the applicability of solar thermal systems. Within this research programme 141 solar thermal systems were installed on public buildings between 1978 and 1983 (Peuser & Riemer 1985). By comprehensive measurements Peuser and Riemer (1985) analysed and optimised these systems in the following years. About 20 years later these systems were investigated concerning durability and characteristics in long-term operation within the funding programme “Solarthermie2000”. Peuser et al (1997) analysed the whole solar system, starting with collectors on the roof, fittings, controllers and ending with storages in the cellar. Transparent covers, insulations and absorber coatings were inspected in

detail, however, documented the situation 20 years ago. Furthermore, Peuser et al (1997) presented results for different absorbers in operation without giving detailed information on designs. Therefore, this chapter describes the main designs together with their processes and materials.

2.3.1 Overview of Former Designs

During the oil crises in the seventies and early eighties the solar technology boomed and a much larger variety of absorber designs used to be applied than today. Bigger efforts in production, problems in process management or lower durability of the materials used, however, reduced the design types to sheet-pipe absorbers. Appendix A / Table A.1 gives an overview of formerly employed absorber designs. Some of these options were already based on a volumetric absorber design.

2.3.2 Analysis of Used Collectors

This chapter describes the analysis of collectors / absorbers regarding deterioration and design carried out at Ingolstadt University. Unfortunately, some of the absorber designs described in Appendix A / Table A.1 ceased to exist on the market. Therefore, the sourcing of former absorbers aged twenty years or more proved difficult and time-consuming. New sheet-pipe absorbers are also included into the tests as they are useful for comparison with older types. Table 2.3 gives an overview of collectors that were disassembled and analysed in the laboratories.

Table 2.3: Data of Analysed Absorbers

Manufacturer	Product	Design	Sheet	Pipe	Connection	Coating	Built
Thermo|Solar	HVL 20	Sheet-pipe	Aluminium	Copper	Cramped	Selective film	~1988
Thermo|Solar	HVL 20	Sheet-pipe	Aluminium	Copper	Pressed	Selective coating	~1989
self made	–	Sheet-pipe	Copper	Copper	Soldered	Non-selective paint	~1980
SOLTEC	F50	Sheet-pipe	Aluminium	Copper	Rolled	Selective coating	1980
Bittner	Bita	Sheet duct	Steel	–	Seam welded	Non-selective paint	1973
Stiebel Eltron	SOL 20	Steel cushion	Steel	–	Spot welded	Non-selective paint	1978
BBC	Solektor	Rollbond	Aluminium	–	Rollbonding	Non-selective paint	~1980
Walo	WK12	Rollbond	Aluminium	–	Rollbonding	Non-selective paint	1978
Wolf	TopSon F3	Sheet-pipe	Copper	Copper	Ultrasonic welded	Selective coating	2004
Thermo|Solar	300N	Sheet-pipe	Aluminium	Copper	Pressed	Selective coating	2004
Böhm	–	Sheet-pipe	Copper	Copper	Soldered	Selective coating	2004

Compared to current collector configurations, former products were more complex due to the frame structure or the implementation of the insulation or the absorber. Nevertheless, their efficiency was low because of non-selective coatings as illustrated in Figure 2.6 with a high solar absorptance but an also high thermal emittance (strongly decreasing collector efficiency graph). Furthermore, Figure 2.6 shows two different graphs, one for a collector which was in operation for 13 years and one unused collector. However, no important differences in efficiency are visible between both graphs showing that no significant deterioration occurred. Only in the zero loss coefficients (intersection with the ordinate) a greater difference is visible and the unused collector is even below the used one. This anomaly can be attributed to the ordinary window panes that were used in these collectors (Peuser et al 1997). Compared to low-iron solar glasses the formerly used window panes did not have to meet the requirements applied nowadays and greater quality differences could occur.

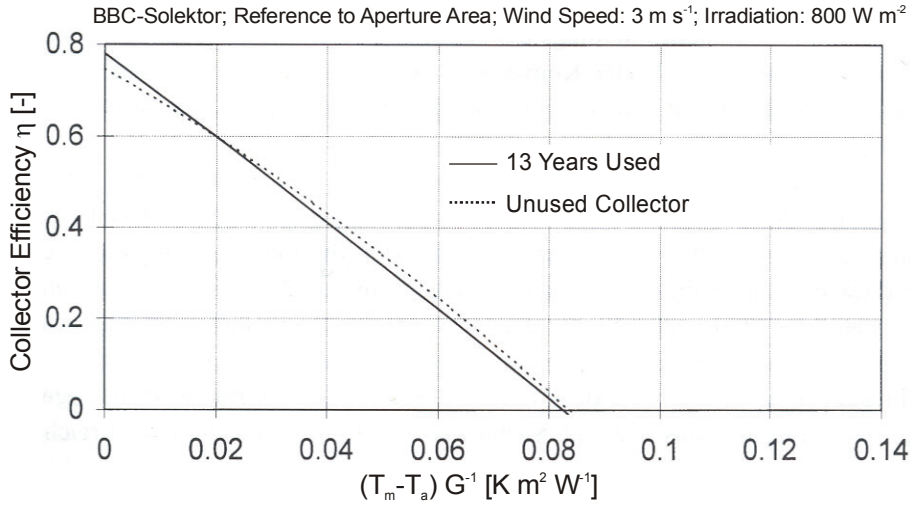

Figure 2.6: Collector Efficiency Curves for a BBC Solektor (Peuser et al 1997)

Another weakness of these collectors is the use of materials of insufficient quality. The collector in Figure 2.7 for example uses a fibre-reinforced plastic plate as transparent cover. Hence, transmission of the cover even in new condition was much lower than of a simple shatterproof glass. On the contrary, Figure 2.8 shows a convex PMMA cover with still high transparency and elasticity. However, the second cover used to suppress convection is destroyed and extremely brittle due to ultraviolet radiation and thermal exposure. Cracks and delamination of the selective film are also visible in the Thermo|Solar absorber HVL 20 as Figure 2.9 illustrates.

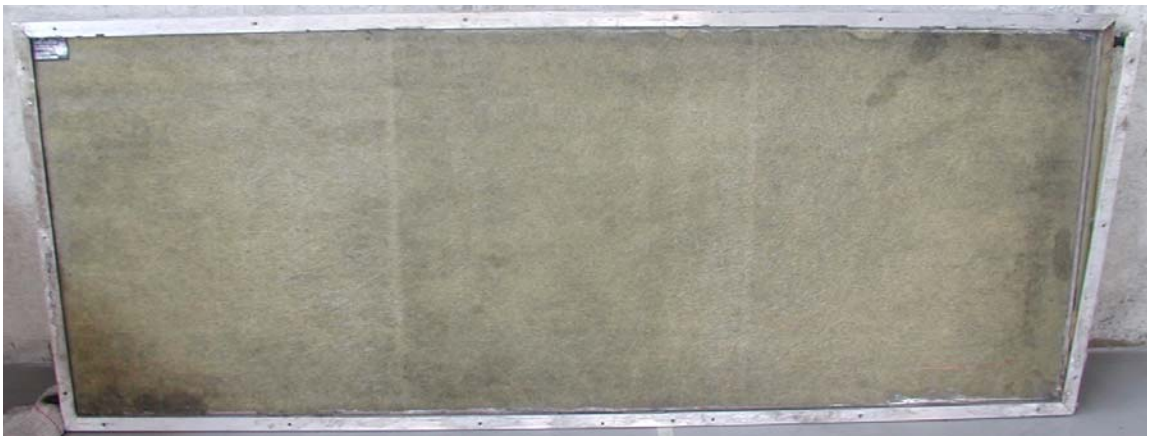

Figure 2.7: Fibre-Reinforced Transparent Cover after 23 Years of Operation (Bittner-collector)

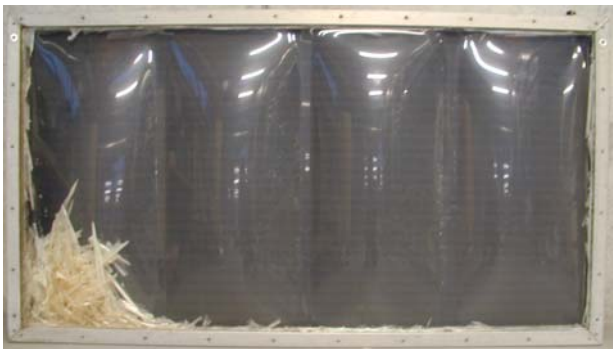

Figure 2.8: Polyester Foil to Avoid Convection after 25 Years of Operation (Stiebel Eltron-collector)

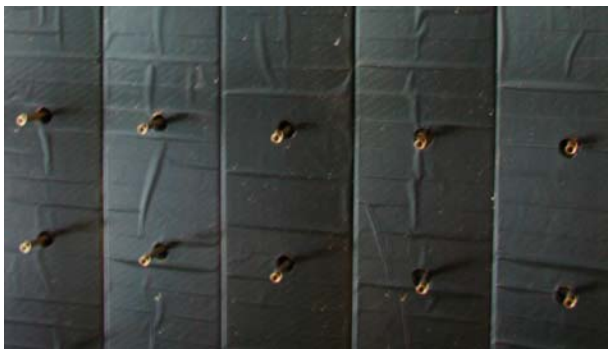

Figure 2.9: Cracks and Delaminating of the Selective Foil after 15 Years of Operation (Thermo|Solar Absorber)

Thermal Behaviour of Sheet-Pipe Absorbers

In this section the absorbers of Table 2.3 are investigated in the university laboratories concerning their thermal behaviour by infrared images. The absorbers are heated by the flow with a temperature of 60°C, while the transient heating phase is recorded with an infrared camera. The tests and the set-up are carried out according to the detailed information given in chapter 5.2.1. The images show the flow distribution of each absorber design. Hence, qualitative conclusions can be drawn from these results about the efficiency.

The sheet-pipe design of older absorbers still equals to those of the state-of-the-art absorbers. In former times, however, the most popular connection techniques between sheet and pipe were clamping/pressing or soldering. All of these former connection processes are still applied whereas clamping and even soldering are becoming increasingly less used. Figure 2.10 shows a home-made absorber whose pipes detached due to high stagnation temperatures accompanied by a reduced strength of the solder and increasing

thermal expansion of the absorber components. In areas of detached fins and tubes, a higher thermal resistance occurs, resulting in degraded absorber efficiency.

The absorber presented in Figure 2.11 is made up of aluminium extruded sections that are connected by hooking them into each other. Every extruded section is connected with one loop of the serpentine. The disadvantage of this process is shown by the temperature distribution in the lower and upper centre caused by some badly pressed sheet-pipe sections. The low heat transfer of the left and right areas of the absorber is caused by the pipe bends that have no contact with the absorber sheet.

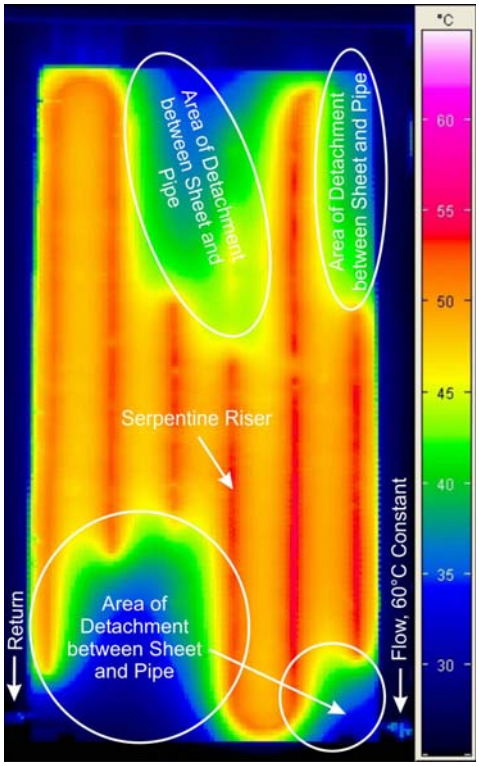

Figure 2.10: Thermal Behaviour of a Soldered Sheet-Pipe Absorber (self-made, 120 l h^{-1}) (Time from starting the test = 548 s)

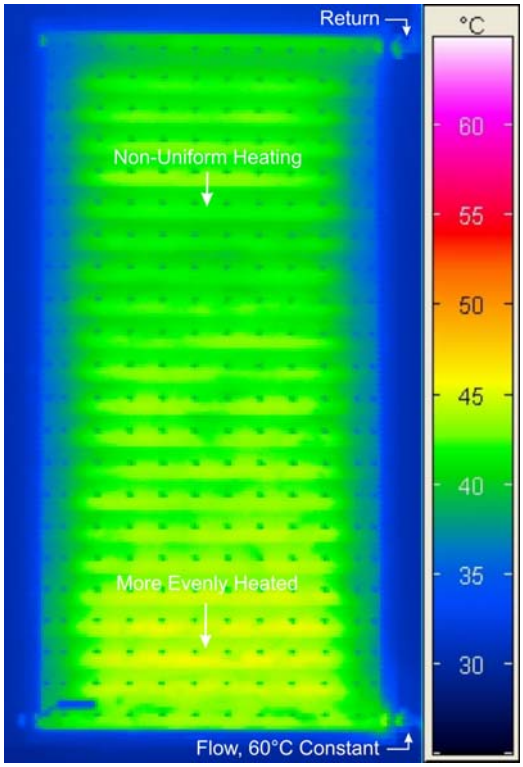

Figure 2.11: Thermal Behaviour of a Pressed Sheet-Pipe Absorber (Thermo|Solar, 120 l h^{-1}) (Time from starting the test = 215 s)

Figure 2.12 and Figure 2.13 characterise absorbers that are up-to-date concerning their production process. Figure 2.12 illustrates a header-riser absorber with parallel risers soldered to the sheet. The following Figure 2.13 presents an absorber with a serpentine riser, which is ultrasonic welded to the sheet between the pipe bends on the left and the right side. Compared to Figure 2.10 the risers of the new absorbers are arranged more closely. The Thermo|Solar absorber in Figure 2.11 is an exception with a distance of 88 mm. However, this implies other problems, e.g. high pressure losses. Furthermore,

the last figures indicate a more uniform temperature distribution than the preceding two images. This is due to a better connection process.

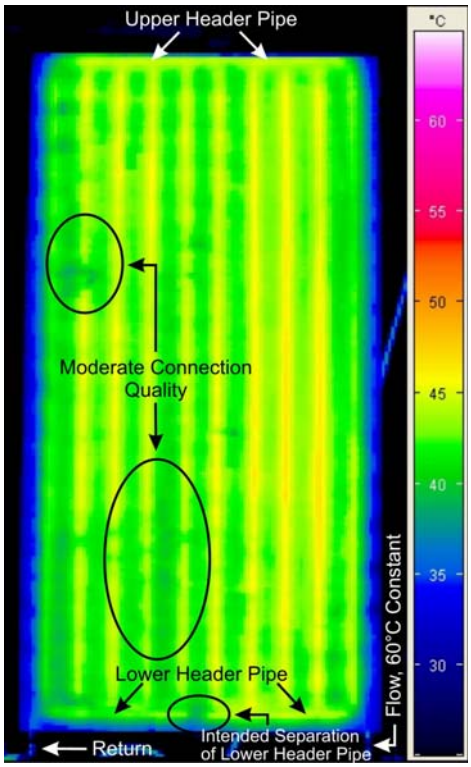

Figure 2.12: Thermal Behaviour of a Soldered Sheet-Pipe Absorber (Böhm, 120 l h^{-1}) (Time from starting the test = 198 s)

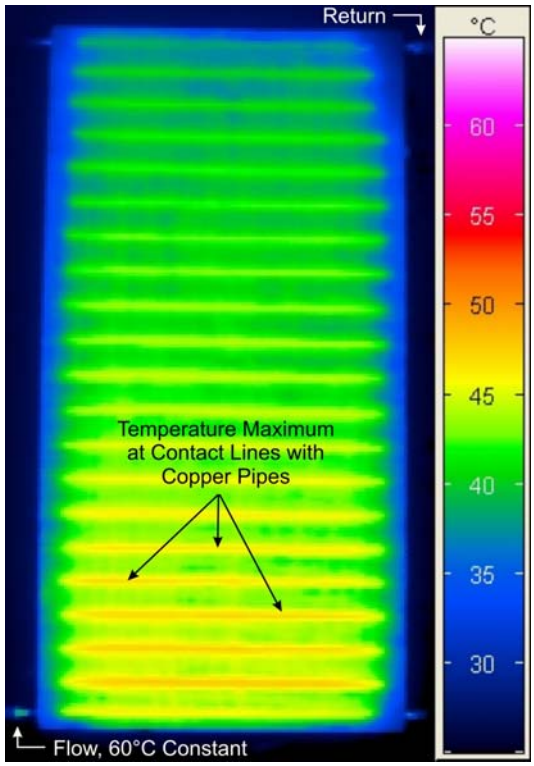

Figure 2.13: Thermal Behaviour of a Ultrasonic Welded Sheet-Pipe Absorber (Wolf, 120 l h^{-1}) (Time from starting the test = 166 s)

Thermal Behaviour of Volumetric Absorbers

Absorber designs which incorporate fluid channels made by different processes have the advantage of a closer arrangement of fluid channels and a bigger surface that is in contact with the heat carrier fluid. This results in a more uniform temperature distribution.

Figure 2.14 shows the analysis of a meander-shaped steel panel absorber with extensive fluid channels. The thermal capacity of this absorber is rather high due to the unfavourable material, a large sheet thickness of 1 mm and a high amount of heat carrier fluid. This results in a higher response time in collector operation. The absorber takes some time to reach the temperature level at the right side (green area: ~ 45°C). The temperature distribution, however, is uniform compared to the previous samples.

The response time can be improved by applying aluminium and the rollbond process (Figure 2.15). Nearly 30 years ago absorbers of this type were already in use. They are characterised by little weight, low thermal capacity and high thermal conductivity.

Figure 2.15 shows the heating phase of the absorber to a temperature level of 45°C in the riser duct area. The flow distribution is not completely homogenous as the flow velocity is higher in the outer channels than in the inner channels. Chapter 4.2 shows details on how to design the header and riser channels more carefully. However, Figure 2.15 also shows a very homogenous temperature distribution without any temperature peaks between the riser channels as they normally occur in header-riser or meander absorbers (see Figure 2.12 and Figure 2.13). Hence, the area with heat conduction is decreased.

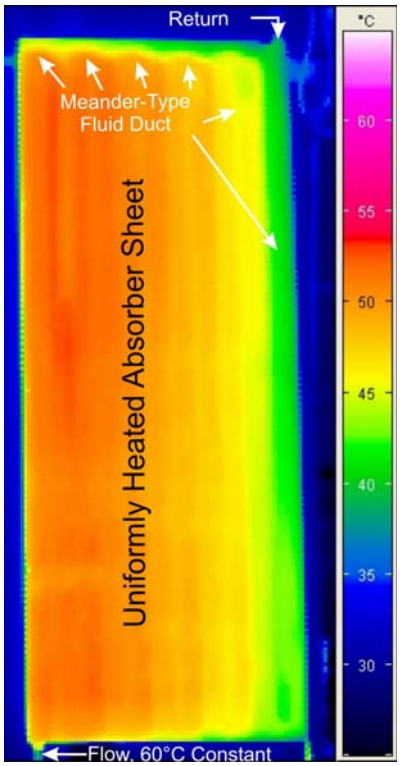

Figure 2.14: Thermal Behaviour of a Seam Welded Steel Panel Absorber
(Bittner, 120 l h^{-1})
(Time from starting the test = 334 s)

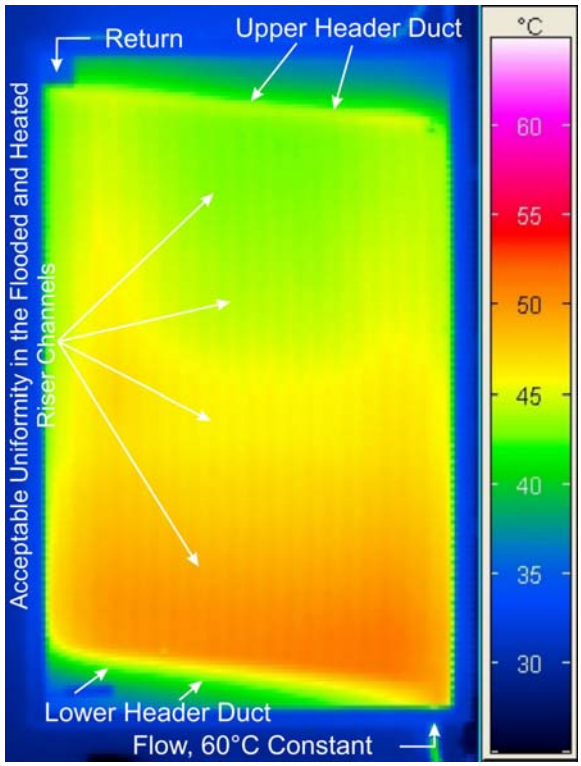

Figure 2.15: Thermal Behaviour of a Rollbond Absorber
(Walo, 120 l h^{-1})
(Time from starting the test = 152 s)

Unlike the Walo WK12, the rollbond BBC Solektor has a more complex fluid channel structure. Despite the elaborate structure around the top and bottom header area, a non-uniform temperature distribution was found (Figure 2.16). Apparently, the central part has poor circulation. This phenomenon may have different reasons: on the one hand, it is possible that air remains in the absorber despite extensive arrangements to bleed the absorber; on the other hand, higher flow resistances occur in the centre causing the fluid to flow to the left and right sections of the absorber. Therefore, further tests were carried out with a volume flow increased from 120 l h^{-1} to 240 l h^{-1}. Figure 2.17 shows the result with improved flow conditions in the centre. It can be concluded that flow rate requires

exact adjustment to achieve a more uniform flow and temperature distribution, respectively.

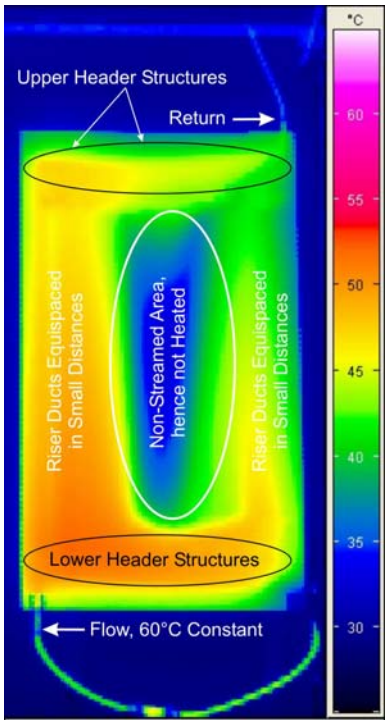

Figure 2.16: Thermal Behaviour of a Rollbond Absorber at Low Flow Conditions (BBC Solektor, 120 l h^{-1}) (Time from starting the test = 175 s)

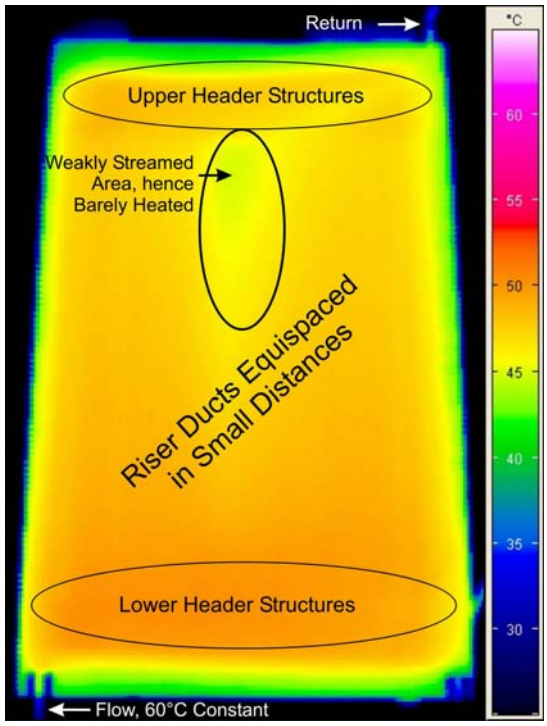

Figure 2.17: Thermal Behaviour of a Rollbond Absorber at High Flow Conditions (BBC Solektor, 240 l h^{-1}) (Time from starting the test = 399 s)

The only available spot welded steel panel absorber based on the volumetric flow system, the Stiebel Eltron SOL 20 collector, was leaking at the welding points (7 collectors of this type were disassembled). Therefore, investigations of that type of absorber were not possible. It is generally agreed that even the short time between dismounting of collectors and disassembling may lead to corrosion.

Conclusion of Thermal Analysis

The investigations of various absorbers illustrate that volumetric absorbers have the potential of a more uniform temperature and flow distribution than sheet-pipe absorbers. Moreover, an acceptable response time can be achieved. Nevertheless, a detailed adjustment of components and flow conditions is necessary to avoid aspects as shown in Figure 2.16 or Figure 2.17. An optimised flow distribution and increased temperature stability is necessary for new volumetric absorbers as the performance of the absorber will be improved and thereby the stagnation temperature will be increased.

2.4 State-of-the-Art

2.4.1 Research and Development

The status quo in the design layout of an absorber has not changed since the eighties. The current sheet-pipe system is only varied by different connection processes, which are described in section 2.4.2.

Only few research projects or application developments work fundamentally on a new design layout. Hermann (2005) has worked on an absorber with fluid channel structures based upon natural structures like blood vessels as shown in Figure 2.18. These structures are described mathematically by fractals. With the generated pipe network, various simulations and optimisations were carried out to fully utilise the absorber area and to gain an optimum flow distribution within the channels.

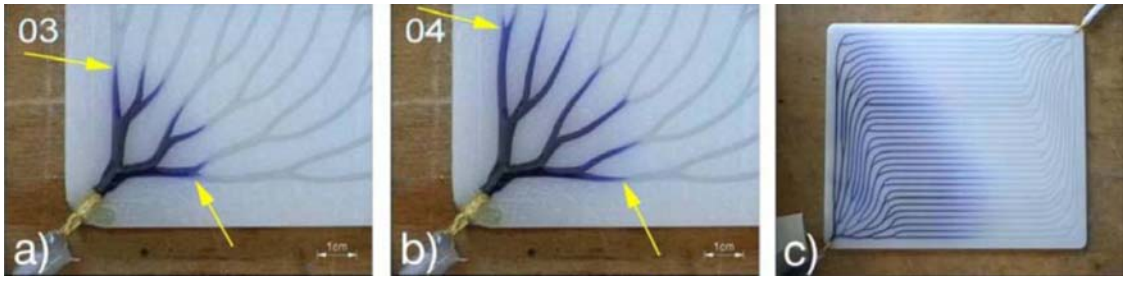

Figure 2.18: Flow Experiments with an Absorber Based upon Natural Structures (Hermann 2005)

Sandler (2004) is aiming at a volumetric absorber designed by steel panels with integrated headers. The upper and lower steel panels are connected by seam welding along the margins, while the inner areas are spot welded in a defined pattern. Finally, the fluid channels are produced by hydroforming between the welding points. Figure 2.19 shows infrared images of this absorber in a transient heating condition. The absorber is heated by hot water entering at the inlet on the lower left side as shown in the left image. In contrast to the investigations carried out in chapter 5.2 the flow distribution of the hydroformed absorber presented by Sandler (2004) does not start along the absorber width. The flow preferentially enters the riser channels in the lower left side as shown in the images of Figure 2.19 and mainly propagates from this area.

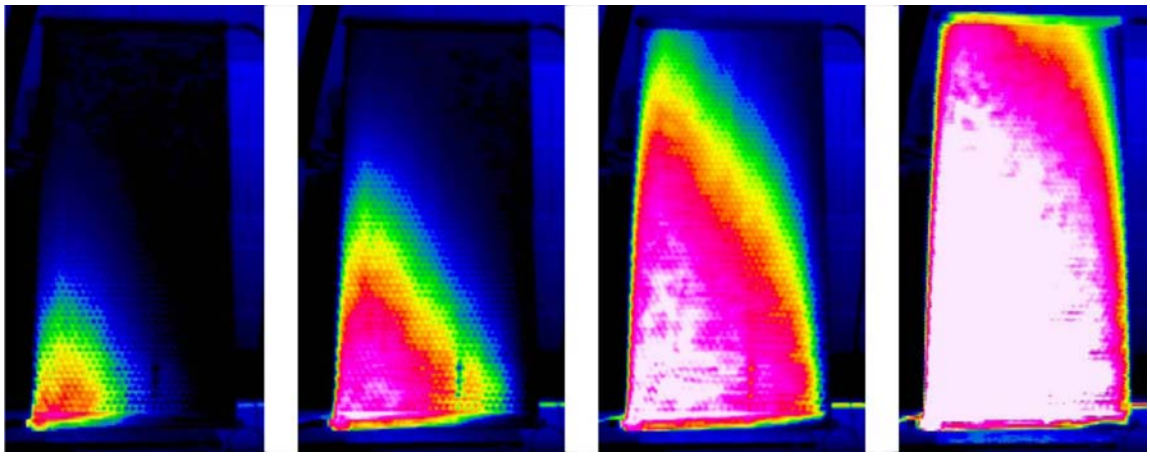

Figure 2.19: Thermography of the Steel Panel Absorber with Hexagonal Fluid Structures (Sandler 2004)

Very little research and development has been carried out concerning alternative materials, such as plastics. In contrast to glazed absorbers like flat-plate collectors unglazed absorbers are often made of polymers; however, they do not have to withstand temperatures above 90°C. Henden (2000) as well as Meir and Rekstad (2003) worked on an absorber implemented in a collector made entirely of plastic. Due to high demands on the material at collector stagnation, special protective measures were implemented. Cristofari et al (2002) also suggest a plastic absorber for solar water heating systems. The intention is to reduce investment costs for a SDHW system by providing a low-cost collector. The collector, which is theoretically investigated, is based on a copolymer that is formed to an absorber by rectangular fluid channels with integrated upper and lower headers. An overview of testing, application and use of polymers in solar thermal collector systems is given by Davidson et al (2003).

An international project on polymeric materials for solar thermal applications started in October 2006 in the Task 39 within the Solar Heating and Cooling Programme of the International Energy Agency (IEA-SHC). This task is aiming at the development of a polymeric solar thermal system incorporating storage, collector and system design (e.g. overheating protection) as well as material selection.

2.4.2 Overview of Sheet-Pipe Connections

In recent years absorber manufacturers were focusing on the improvement of sheet and pipe connections. Table 2.4 gives an overview of possibilities for sheet and pipe connection.

Furnace soldering or flow soldering adapted from the electronic industry are increasingly less used. They are substituted by processes that are more stable in manufacturing and during collector operation. Even the ultrasonic welding process is likely to be replaced by laser welding due to increasing copper prices as shown in Figure 1.2.

Table 2.4: Overview of Sheet-Pipe Connections

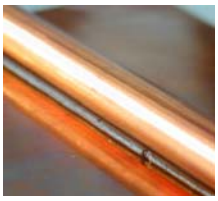

Bonding Processes
- Piping connected to absorber sheet by high temperature stable adhesive
- No substance-to-substance bond
- Material combination: Al / Cu and Cu / Cu
- Barely used

Clamping and Pressing Processes
- Piping connected to absorber sheet by clamping or pressing
- No substance-to-substance bond
- Material combination: Al / Cu and Cu / Cu
- Barely used nowadays

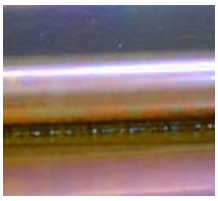

Furnace Soldering
- Piping and sheet are heated in a furnace
- Coating of both parts with a compound of flux and solder in preheated condition
- Final heating process in the furnace
- Substance-to-substance bond
- Material combination: Cu / Cu

Flow Soldering
- Waves of a solder bath coat the piping and the sheet moving above the bath
- Wave peaks only get in contact in areas where pipes are
- Substance-to-substance bond
- Material combination: Cu / Cu
- Manufacturing stopped in 2005

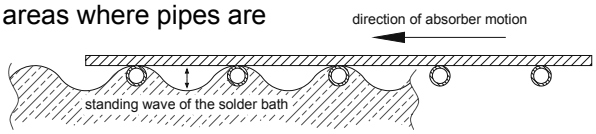

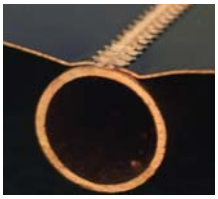

Ultrasonic Welding
- Sonotrode and ambos fix the piping and the sheet
- The sonotrode is oscillating with high frequency, oxide layers are destroyed accompanied by extended contact surfaces which facilitate the diffusion process
- Substance-to-substance bond
- Material combination: Cu / Cu

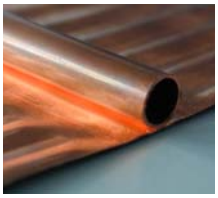

Plasma Welding
- Enhancement of the TIG-welding process
- Substance-to-substance bond
- Material combination: Cu / Cu
- Barely used

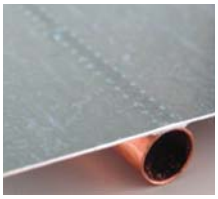

Laser Welding
- Piping and sheet are melted by a pulsed laser beam
- Substance-to-substance bond
- Material combination: Al / Cu and Cu / Cu
- Currently the preferred process

2.4.3 Weaknesses of the Sheet-Pipe Connection

Current absorber designs suffer from disadvantages in manufacturing processes, cost and efficiency. These disadvantages interact as for example the efficiency can not be significantly improved without more riser pipes, hence, time, effort for manufacturing and overall costs are increased. The following aspects characterise the situation of state-of-the art absorbers.

High Thermal Resistance

As illustrated in Figure 3.1 the most important functions of the absorber are the

- conversion of radiation into thermal energy and
- heat transport to the heat carrier fluid.

These functions are realised by various components in state-of-the art absorbers:

- absorber sheet,
- connection between sheet and piping,
- piping.

Figure 2.20 illustrates the thermal resistances caused by the absorber design and its components. The thermal resistances can be accumulated as they are connected in series. Moreover, a temperature peak occurs on the absorber sheet between the energy gathering pipes as shown in Figure 2.21, which is necessary for the heat flow from the sheet to the pipe.

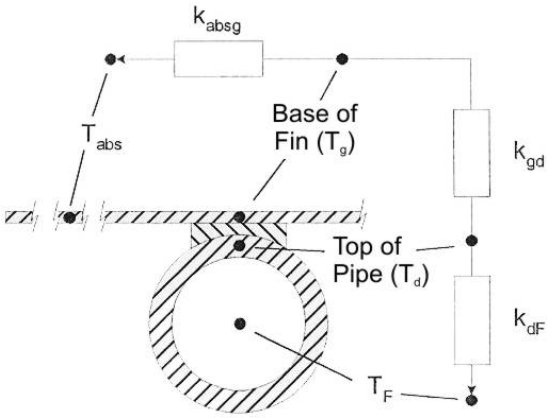

Figure 2.20: Thermal Equivalent Network of Absorber (Eisenmann 2003)

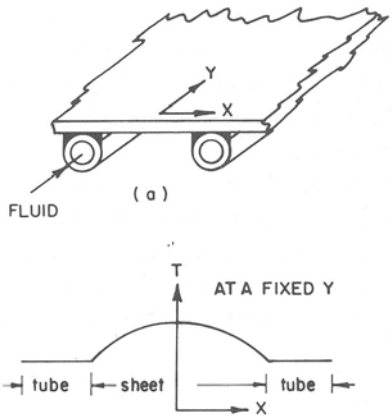

Figure 2.21: Temperature Distribution Across an Absorber Fin (Duffie & Beckman 2006)

An indicator for the performance of solar absorbers is the collector efficiency factor *F'*. It is the ratio of the actual useful energy gain to the useful gain that would occur if the absorbing surface had been at the local fluid temperature. Due to the specific design the collector efficiency factor of sheet-pipe absorbers is influenced by several parameters. Figure 2.22 shows these parameters and their influence on the efficiency and indicates the standard values that are described in Appendix D / Table D.1. The formulae applied for calculating the collector efficiency factor *F'* are discussed in detail in section 4.4.1.

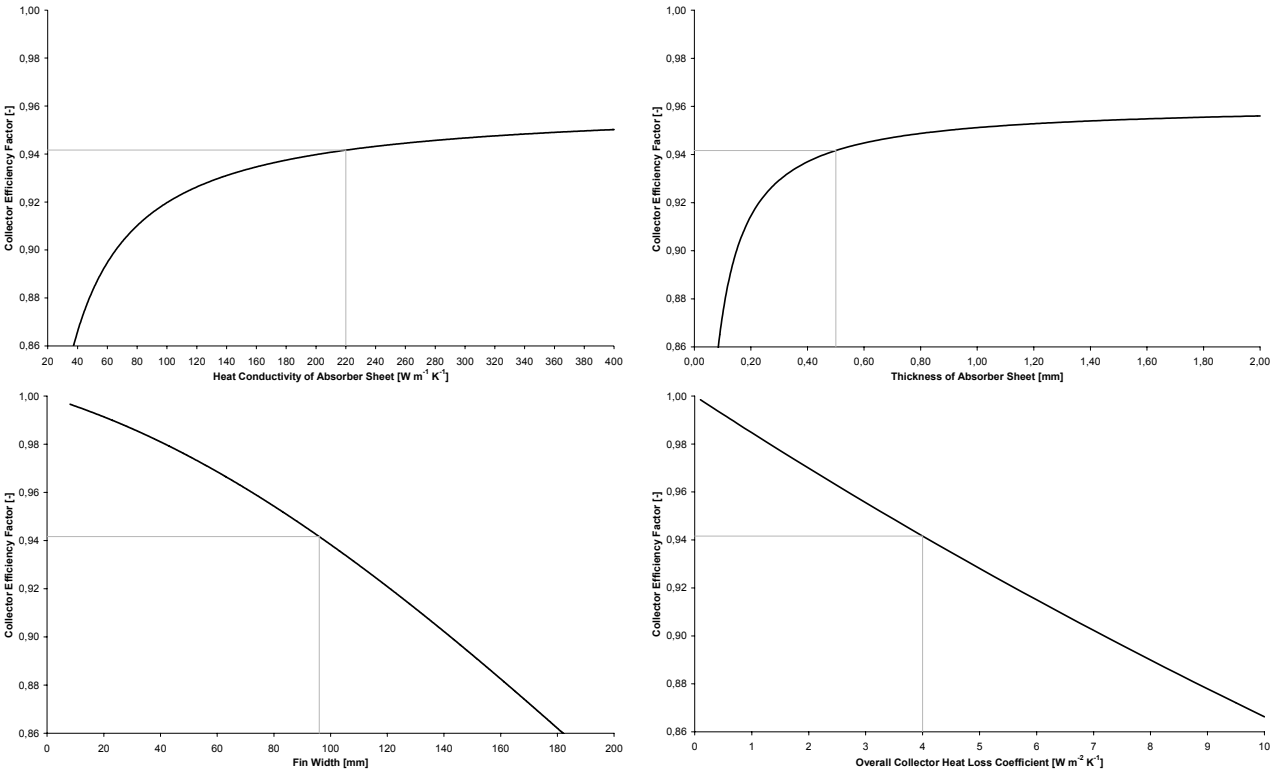

Figure 2.22: Influence of Various Collector Parameters on the Collector Efficiency Factor *F'*

Three parameters show a strong impact on the thermal resistances of the sheet-pipe absorber network, thereby on the collector efficiency factor. The parameters are the heat conductivity of the absorber sheet, its thickness and the distance of the risers, the fin width. The heat conductivity of the absorber sheet illustrated in the upper left diagram of Figure 2.22 shows a lower impact on the efficiency, when aluminium (220 W m^{-2} K^{-1}, marked) or copper (385 W m^{-2} K^{-1}) are used. However, the use of materials with lower heat conductivity like steel or stainless steel has a strong influence on the performance as their values are below 50 W m^{-2} K^{-1} with a corresponding *F'* of less than 0.88. Polymers have an even lower heat conductivity of less than 2 W m^{-2} K^{-1}. Therefore, the sheet-pipe absorber design is not qualified for this material. A similar graph is shown in the up-

per right diagram illustrating the dependency on the thickness of the absorber sheet. Both parameters contribute to the sheet's performance and demonstrate the importance of a highly conductive material and/or sheet thickness. Absorber manufacturers are aiming at lower costs, hence, are substituting the copper sheet by an aluminium sheet. Further cost reduction by the use of steel is not reasonable as the loss in the collector efficiency factor cannot be compensated by the sheet thickness like in case with aluminium.

The fin width represents another possibility for efficiency improvement and cost reduction respectively. However, as illustrated in the lower left diagram of Figure 2.22, the collector efficiency factor is significantly decreased with increasing fin width. Therefore, this is not a suitable method for further cost reduction while maintaining high collector efficiency. The overall collector heat loss coefficient U_L has also a strong impact on the collector efficiency factor. However, the heat loss coefficient is not only based on the collector casing, but also defined by the emittance of the selective coating. The lower right diagram of Figure 2.22 shows the graph with a typical heat loss coefficient of state-of-the-art absorbers as mentioned in Appendix D / Table D.1.

Table 2.5: Overview of Collector Efficiency Factors for Various Absorber Designs (Rockendorf et al 1996)

No	Design	Fin			Pipe			Volume Flow per Fin [l h^{-1}]	k_{int} [W m^{-2} K^{-1}]	F' with k_{v1}=3.8 W m^{-2}K^{-1} [–]
		Width [mm]	Thickness [mm]	Material [–]	OD [mm]	Wall Thickness [mm]	Material [–]			
1	Clamping  *)	137	1.5	Al	12	1	Cu	14	28	0.881
2	Clamping 	137	0.3	Cu	8	0.6	Cu	20	40	0.913
3	Clamping 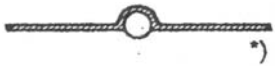 *)	86	0.1	Cu	10	1	Cu	80	47	0.925
4	Folded Seam Connection 	132	0.3	Cu	10	0.5	Cu	25 60 110 200	46 56 67 71	0.924 0.936 0.946 0.949
5	Joint 	98	0.5	Cu	10	0.5	Cu	60 110	122 148	0.970 0.975
6	Ultrasonic Welding 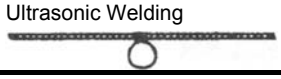	113	0.3	Cu	10	0.75	Cu	22	50	0.929

*) Insufficient Thermal Contact

Table 2.4 in section 2.4.2 illustrates current manufacturing processes for the connection between sheet and pipe. The appropriate collector efficiency factors for some fin designs are given in Table 2.5 and represent measured values by Rockendorf et al (1996). The

F'-factor varies from 0.88 to 0.975, however, care has to be taken when different values are compared due to varying parameters. For example, the efficiency factor of number 5 (soldered absorber) is achieved by a high copper sheet thickness of 0.5 mm and an outer diameter of 10 mm for the riser pipe. Yet, these conditions raise costs and complexity of the absorber and collector. Current header-riser absorbers normally consist of a copper or aluminium sheet with a thickness of 0.2 mm or 0.5 mm and risers with an outer diameter of 8 mm. According to Eisenmann et al (2004) a collector efficiency factor of at least 0.90 is necessary to be competitive on the market.

Manufacturing Process

The manifold of a sheet-pipe absorber is composed of various components that have to be prepared, processed and handled. Finally, the header-riser or meander piping has to be attached to the selectively coated sheet. The connection of the circular piping and the plane selectively coated sheet is laborious and was done manually by soft soldering in the beginning of solar absorber manufacturing. As shown in Table 2.4 it was meant to achieve improved and automated processes, however, the basic weaknesses in manufacturing and in collector operation remain almost the same. Table 2.6 characterises the production processes presented in Table 2.4.

Collector Operation

The improvement of collector components like selective coatings or anti-reflective glasses intensified the temperature problems in solar thermal systems. The stagnation temperature rises as heat losses are reduced. Table 2.6 states the difficulties of high stagnation temperatures, the separation of pipe and sheet or the fumigation of flux residues (Epp 2002). While separation makes a proper function of the absorber impossible, flux residues reduce the transmission of the transparent cover by deposits or can even damage the selective coating (Epp 2002).

High Manufacturing Costs

As shown in Figure 1.1 approximately half of the manufacturing costs of a collector are connected with the absorber (Mangold 1996, 2004). The collector in turn amounts approximately 25% to 30% of the total costs of a solar-assisted heating or hot water system (Remmers 1999b). In order to make solar thermal collectors more attractive the total

costs have to be decreased. Possibilities exist in the re-design of the absorber layout and in the application of different materials with lower costs.

Table 2.6: Deficiencies of Current Manufacturing Processes of Sheet-Pipe Absorbers

Production Process	Deficiencies	
Bonding	• Low processing temperatures → Operating temperatures ↓ → Risk of detached piping and sheet during operation • Thermal conductivity of connection ↓	Non Substance-to-Substance Bonds
Clamped or Pressed Connections in Different Designs	• Thermal conductivity of connection ↓ • Complex bending or pressing tools	
Soldering	• Low process temperature → Operating temperatures ↓ → Risk of detached piping and sheet during operation • Fumigation of flux residues → Depositions on absorber surface	Substance-to-Substance Bonds
Ultrasonic Welding	• Complex identification of welding parameters → Risk of detached piping and sheet during operation • Damage of selective coating along welding seam	
Plasma Welding	• Complex identification of welding parameters → Risk of detached piping and sheet during operation → High energy density during welding (deformation, …) • High thermal stresses or deformations • Damage of selective coating along welding seam	
Laser Welding	• Complex identification of welding parameters → Risk of detached piping and sheet during operation → High energy density during welding (deformation, …) • Risk of microcracks in welding spots • Interrupted welding seam	

2.4.4 Analysis of Sheet-Pipe Connections

In this section the various sheet-pipe manufacturing processes presented in Table 2.4 are investigated regarding structure and condition by SEM micrographs produced at the University of Applied Sciences Ingolstadt.

Soldered Connection

Two different soldering connections are presented in a cross section to the pipes´ longitudinal axis. Figure 2.23 shows a flow-soldered absorber with a homogenous joint as well as a large joint surface between pipe and sheet. Consequently, a large area for heat conduction is available. The furnace-soldered absorber in Figure 2.24, however, provides a smaller heat transition surface due to less solder. During the manufacturing process,

some flux residues concentrated on the right side of the pipe that are responsible for disadvantageous fumigations.

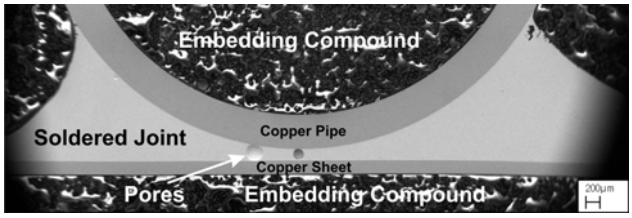

Figure 2.23: Micrograph of a Flow-Soldered Connection

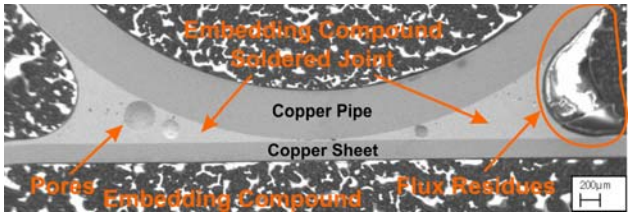

Figure 2.24: Micrograph of a Furnace-Soldered Connection

Ultrasonic Welded Connection

Figure 2.25 shows the micrograph of a homogenous ultrasonic welded absorber. However, a deep knurl is created by the sonotrode. The sheet thickness is reduced in the welding area accompanied by an increase of the thermal resistance. Moreover, the connection provides a width of only about 1 mm for the energy transport to the heat carrier pipe. Despite the small area for heat conduction as shown in Figure 2.25, Eisenmann (2003) did not observe a decrease in comparative efficiency calculations.

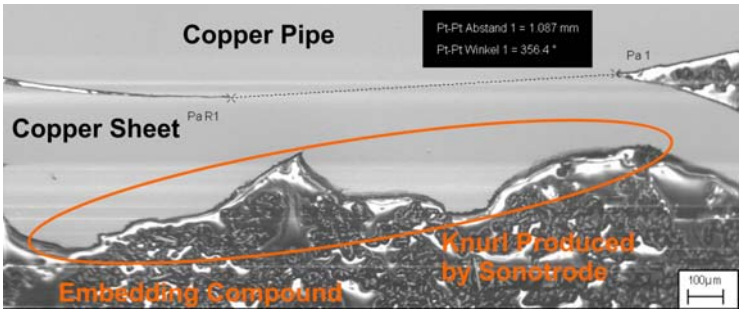

Figure 2.25: Micrograph of a Ultrasonic Welded Connection

Laser Welded Connection

Laser Welded absorbers are processed on the reverse side. Therefore, the laser beam pulses from both sides on the sheet and pipe and partially smelts these areas without reaching the vertex of the pipe. Gaps on both sides are the consequence as illustrated in Figure 2.26. In Figure 2.27 the length of the welding spot is less than 1.5 mm (dashed line) and Figure 2.28 shows a distance between the welding spots of about 2.5 mm. Hence, just 40% of a straight riser pipe length is welded with a spot width in the flow direction of about 1 mm.

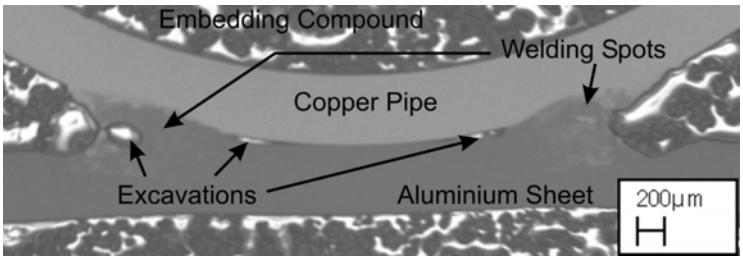

Figure 2.26: Micrograph of a Laser Welded Connection

Furthermore, intermetallic phases occur when two different materials are welded. They are characterised by extremely high hardness and low ductility as Figure 2.29 exemplifies

by an unused absorber with microcracks due to the welding process. Damage to the connection is not inevitable but crack propagation can occur as shown by tests of Heck (2005).

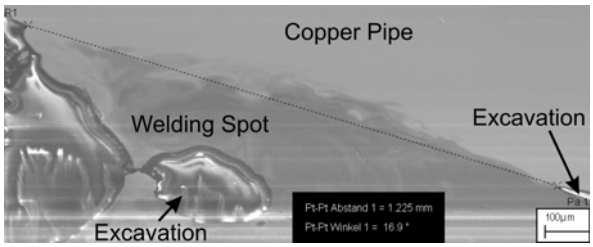

Figure 2.27: Welding Spot – Micrograph Perpendicular to Axis of Pipe

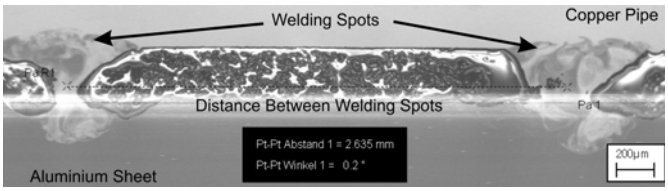

Figure 2.28: Welding Spots – Micrograph Along Axis of Pipe

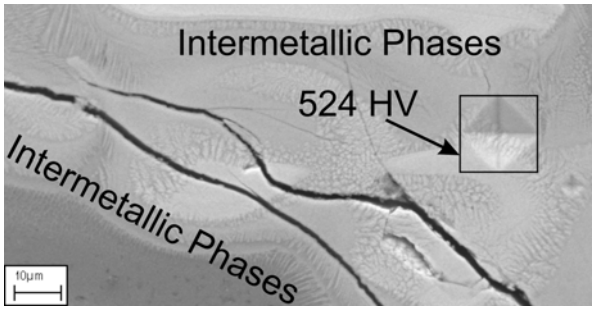

Figure 2.29: Microcrack in a Laser Welded Spot

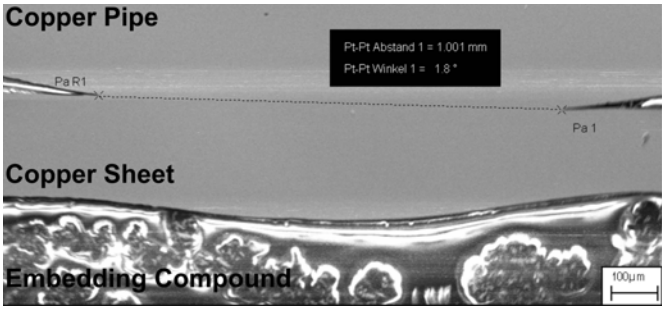

Figure 2.30: Micrograph of a Plasma Welded Connection

Plasma Welded Connection

The plasma welded seam is continuously produced and the micrograph reveals a homogenous welding spot with a constant sheet thickness. However, the thermal bridge between sheet and pipe is about 1 mm only as Figure 2.30 shows.

3 Concept Development

3.1 Definition of Design Specifications

The definition of design specifications by means of a requirements list forms the basis of the solar thermal absorber development. According to functional aspects the requirements list is divided into several sections, while each requirement is classified as a demand being compulsory or a wish being desirable but not essential. The detailed specifications arise from the boundary conditions set by the solar system, the collector frame, of internal and external physical conditions as well as inputs from absorber manufacturers. The latest version of the complete requirements list can be found in Appendix B.

3.2 Function Structure

The definition of requirements is followed by an analysis of the absorber's functions. The overall function of the absorber as shown in the top box of Figure 3.1 is broken down into sub-functions leading to the function structure in the lower box of Figure 3.1. In a systematic investigation solutions for every function have to be derived and finally integrated into a whole concept. The proceeding follows a systematic design approach as proposed by Pahl et al (1996), aiming at the definition of a most promising design solution.

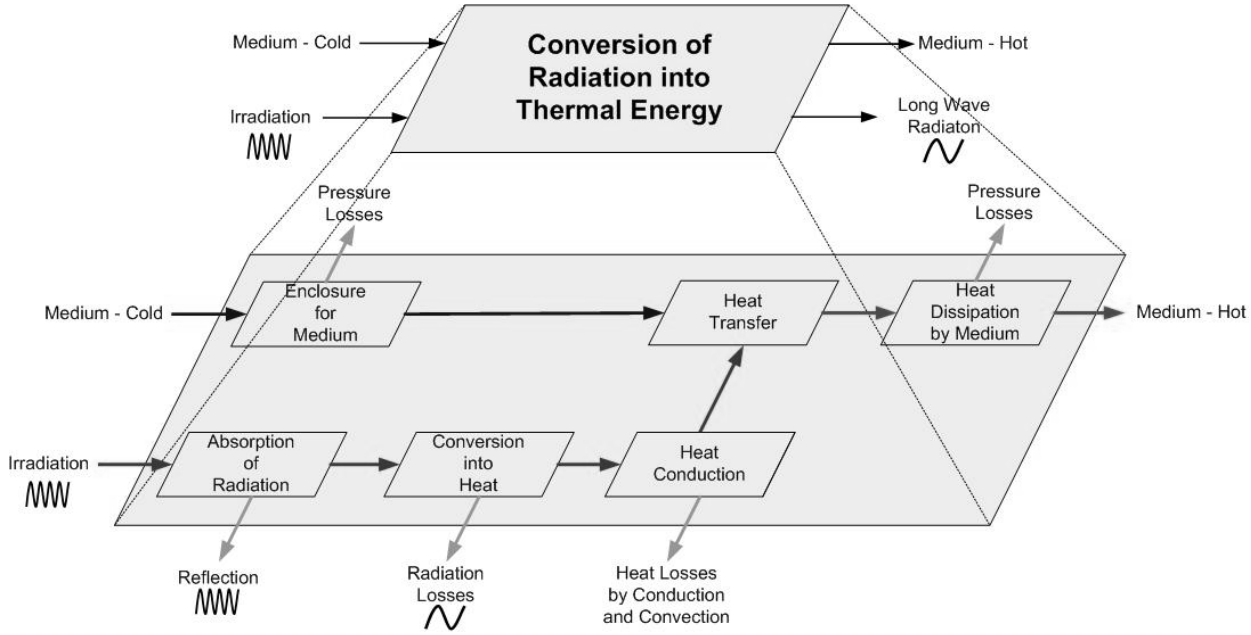

Figure 3.1: Function Structure of the Absorber of a Solar Thermal Flat-Plate Absorber

In the detailed lower box of Figure 3.1 two main inputs are given – a mass flow through the irradiation absorbing structure and an energy flow onto the structure. The latter is absorbed by the structure and converted into heat. Furthermore, the heat is conducted within the structure and transferred to the mass flow, which in turn is guided by the structure itself.

3.3 Concept Designs

After the definition of the function structure, it is possible to search for physical effects as well as suitable technical implementations. Solutions for the optimum flow of the medium within the structure and an ideal transport of the incident solar energy to the fluid are the most important operations in this development phase. Therefore, solutions to both problems are presented in the following sections.

3.3.1 Materials

The new absorber concepts are aimed at improved manufacturing processes and higher efficiencies for the whole product. Thereby, it has to be considered what kinds of materials are suited regarding desired properties as low weight, high thermal conductivity or temperature stability. Figure 3.2 shows three different categories of absorber materials.

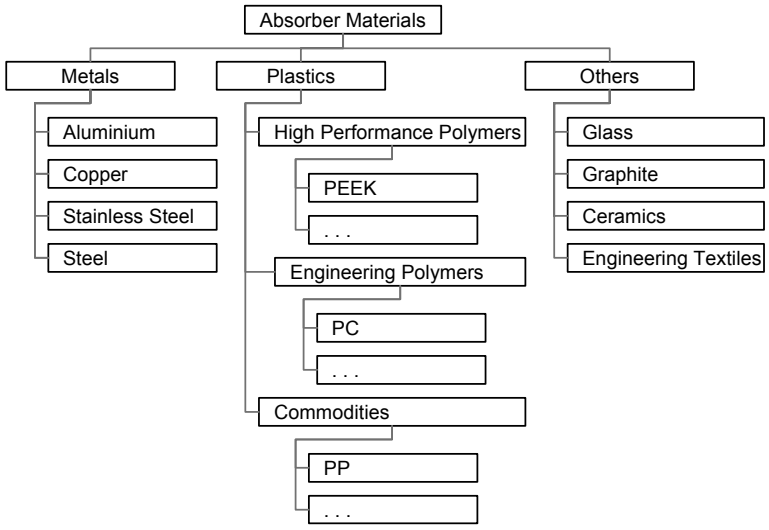

Figure 3.2: Overview of Applicable Materials

Metals are typically used materials for solar thermal absorbers as they provide high temperature stability and thermal conductivity: however, they have an unfavourable density and a high material cost in general.

Plastics as a second category offer very low densities and can have advantageous material costs. In this context, requirements for the absorber material have to be chosen carefully as they make a tremendous impact on the costs. Hence, plastics have to be subdivided into high performance polymers, engineering polymers and commodities with a descend-

ing order of costs and material properties, e.g. strength at high temperatures and pressures. At the moment, high temperatures cannot be completely avoided, especially during summer times and systems for solar space heating. Figure 3.3 shows the yearly temperature loading time in different temperature ranges for a SDHW system with 6 m^2 collector area (flat-plate collectors) and 400 l storage. The framed temperature ranges on the lower right side of the diagram are critical for all of the commodity polymers and most of the engineering polymers. Additionally, further loads have to be taken into account like the operating pressure or UV radiation which intensifies the requirements as the loads have influences on several material properties at the same time.

In order to meet the requirements with polymer materials and to find adequate design and manufacturing solutions for polymer based absorbers Task 39 “Polymeric Materials for Solar Thermal Applications” was founded at the end of 2006 within the Solar Heating and Cooling Programme of the International Energy Agency (IEA-SHC).

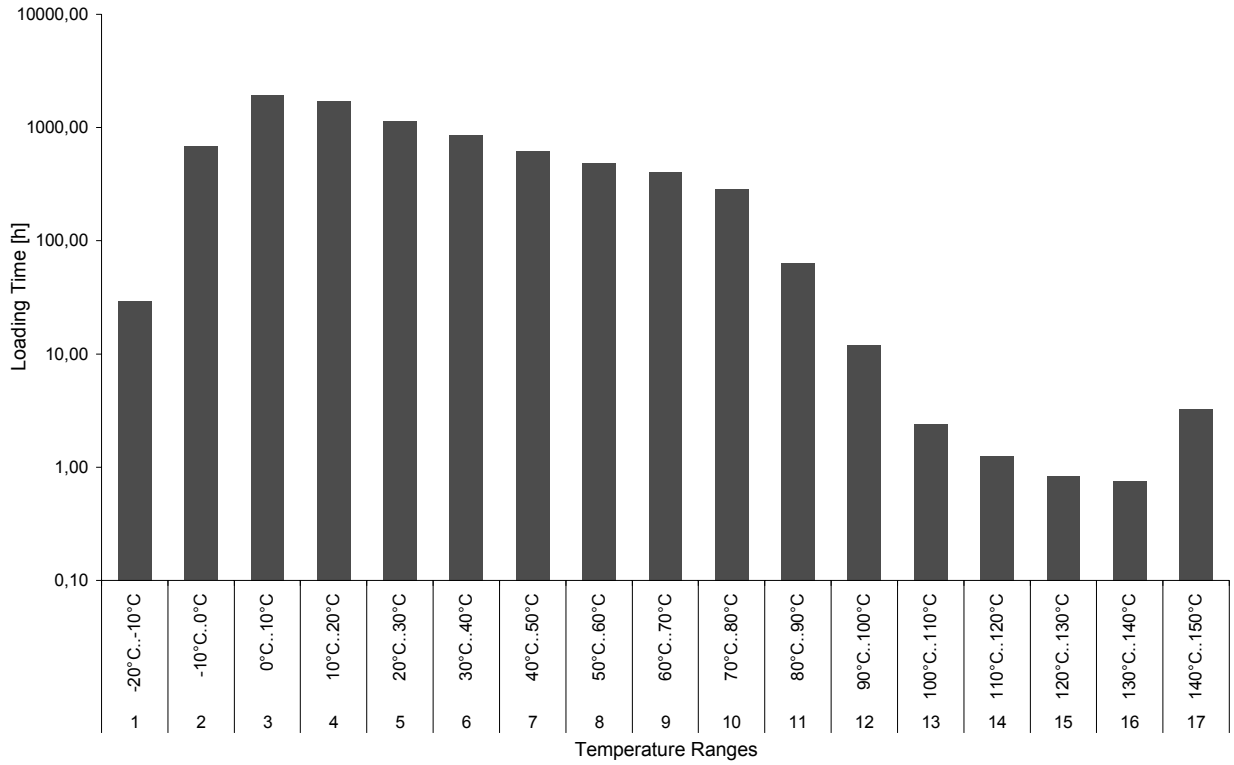

Figure 3.3: Yearly Temperature Loading Time in a Typical SDHW System

Finally, special materials are applied when particular demands are made on the absorber. Hermann et al (2002) for example, designed an all glass absorber to avoid corrosion damage of the absorber used in a seawater desalination systems. Pressed graphite

as highly conducting material with an embedded header-riser or meander absorber was tested by the company SGL Group. Arnold et al (1993) and Bäckmann (2001) reported about engineering textiles used in solar thermal absorbers. Ceramics are also used in high temperature applications as material for absorbers in volumetric receivers of solar thermal power systems (Karni et al 1998).

3.3.2 Absorber Structure

The analysis of the function structure of Figure 3.1 provides the basis for solutions to the absorber design problem. The basics to be fulfilled according to the subfunctions are:

- an irradiation absorbing surface with the ability for heat conduction into the absorbing structure,
- a flow distribution within the absorbing structure enabling heat transfer to the fluid.

Figure 3.4 shows three different categories with solutions

1) controlling the flow of the fluid within the structure,
2) for heat conduction,
3) enabling both, flow control and heat conduction.

Category 3) is subdivided into two further possibilities. Integrable structures are elements that can be implemented in a channel for enhanced flow distribution and heat conduction. Flow conditions can be improved by creating higher Nusselt numbers and thus better heat transfer conditions. Integral structures, however, provide solutions to absorb radiation, distribute the flow and transfer the heat in one part without further additions of 1) or 2). Therefore, an absorber concept can be composed of a solution from 1) and 2) and eventually of 3) with integrable structures, while 3) provides stand-alone solutions also. A state-of-the-art absorber, for example, consists of 1) with pipe fluid passages and a sheet for absorption of irradiation and heat conduction from category 2). The final absorber concepts are categorised in the following sections.

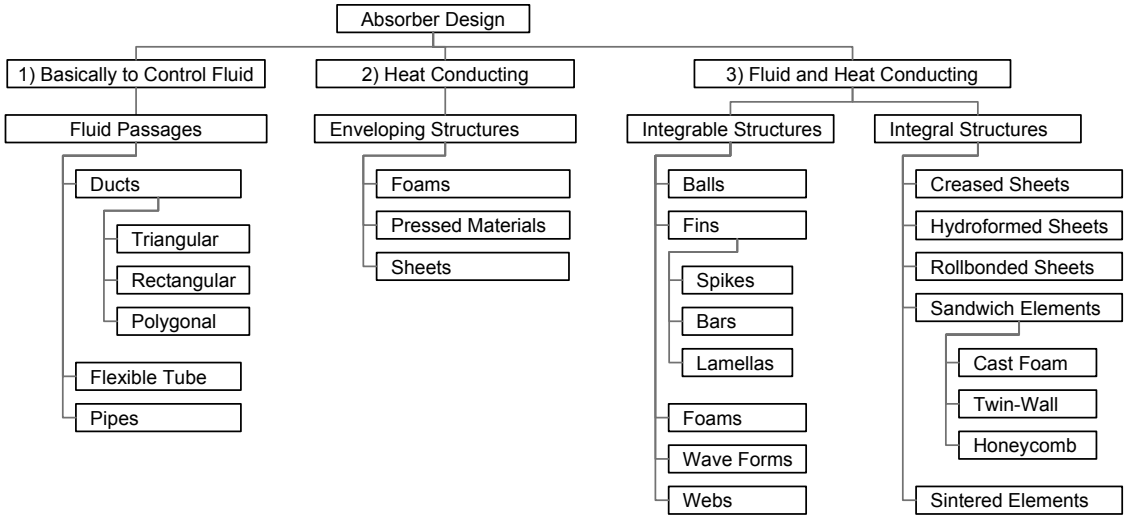

Figure 3.4: Overview of Possible Absorber Layouts

3.3.3 Overview of Concepts

In the course of concept development based on the solution diagram in Figure 3.4, several concepts were developed. The concepts presented in the following sections result from a first evaluation regarding feasibility and cost-effectiveness.

Absorber with Corrugated Pattern

The absorber with corrugated pattern consists of two sheets. While one sheet is creased to form the corrugated pattern the other one is smooth as shown in Figure 3.5. According to the morphological diagram of Figure 3.4 this concept is based on an integral structure within category 3) and one enveloping structure of category 2). Furthermore, the concept has to be joined and sealed at the circumference, which can be done by manufacturing processes like TIG welding, seam welding or fric-

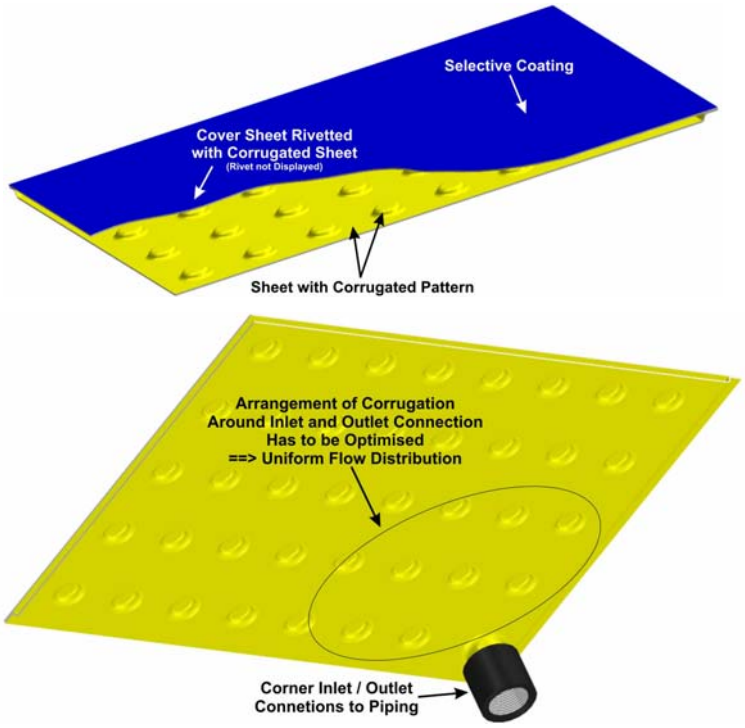

Figure 3.5: Absorber with Corrugated Patterns and Corner Inlet / Outlet Connections

tion stir welding. The advantage of the last two processes, however, is their ability for automation and mass production without further costs, for example, for filler material. In order to avoid any deformation of the absorber under pressure the creased sheet has to be joined with the plane sheet at the deformed points as illustrated in Figure 3.5. Again two different production processes can be applied for this step – spot welding or clinching. In contrast to seam welding, spot welding is less applicable with aluminium due to higher welding currents and the necessity of cleaning and etching the surfaces. Clinching provides more advantages for such a connection as it

- does not damage an applied selective coating
- is a low-cost process with low energy demand,
- needs no consumables,
- is a fast manufacturing process,
- provides a long tool life.

Therefore, the manufacturing processes of choice are friction stir welding for the circumferential and clinching for the internal joints. The fluid supply of this absorber can be realised either by headers or by corner inlet / outlet connections with a modification of the corrugations to ensure a uniform flow distribution (Figure 3.5).

Corrugated Sheet Absorber

The corrugated sheet absorber is based on an integral structure for fluid and heat conduction 3) as well as an integrable structure by wave forms for improved rigidity of the concept under pressure (Figure 3.4). The design uses a sandwich plate which is normally used in lightweight applications in automobile or railway industry when large, rigid surfaces are needed. In this case, however, the plate is used as a heat exchanger. Two cover sheets are bonded by hot-melt glue with a corrugated sheet that forms the fluid ducts as illustrated in Figure 3.6. According to the datasheet the maximum operating temperature of the hot-melt glue is 100°C (Metawell 2008). However, temperatures above 100°C can occur in solar thermal absorbers especially in the case of stagnation. Although modification would be possible and adhesives with enhanced temperature resistances exist, the sandwich panel manufacturer was not ready for changes in manufacturing. Both supply pipes and the side-fed end strips are connected by bonding with a structural adhesive.

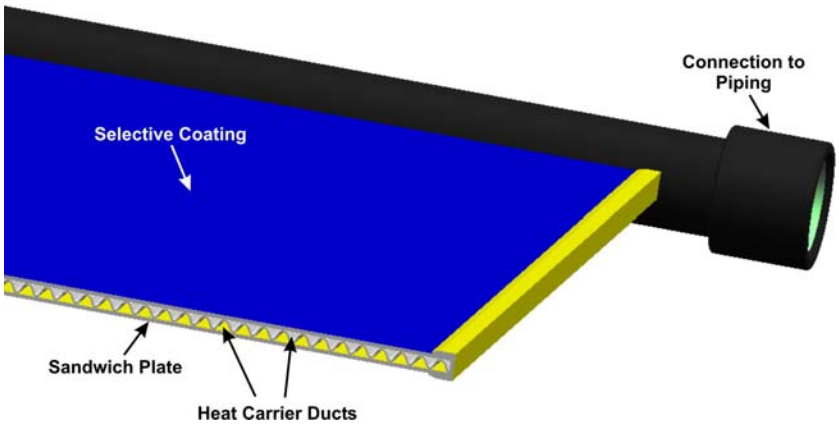

Figure 3.6: Corrugated Sheet Absorber with Defined Fluid Channels

Rollbond Absorber

In the morphological diagram of Figure 3.4 the rollbond absorber is based on an integral structure 3) with rollbonded sheets and polygonal ducts. This design is aiming at integrating several risers with an enhanced riser width for reduced thermal resistance of the absorber panel. Two headers are diverging/converging the flow to/from the risers. Figure 3.7 shows the concept with connecting pipes.

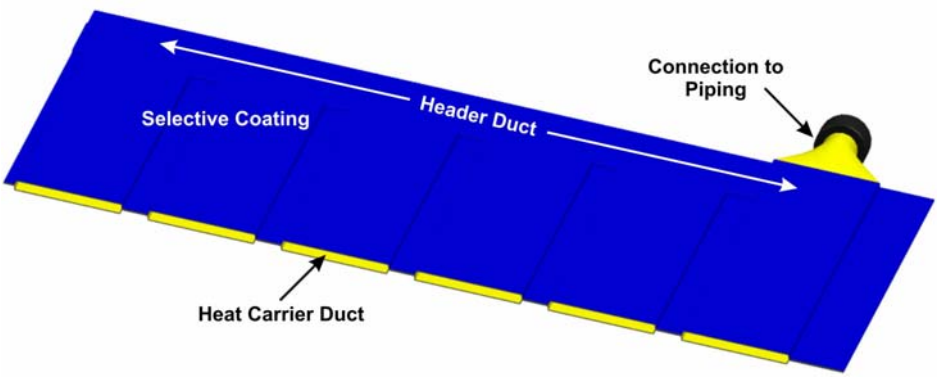

Figure 3.7: Rollbond Absorber with Extensive Fluid Channels

Rollbonding is widely-used in refrigerators as manufacturing process for evaporator panels. It provides a low-cost manufacturing process that is independent of the number of channels integrated into the panel as the material used remains the same. Although rollbonding provides some flexibility in channel arrangement, several limitations have to be accepted as explained in section 4.2.6 when going into detailed design. The rollbond panel consists of two aluminium sheets. One sheet is coated with a pressure resistant ink according to the shrinked channel structure. Then the second aluminium sheet is put on top of the other and both sheets are joined and stretched to the final length by one or more rolling mills. Along the coated areas the sheets remain separated and are inflated

by air in a subsequent step. Finally, pipes have to be TIG welded at both open ends of the panel.

Metal-Matrix Absorber

The metal-matrix absorber can be associated with an encasing structure for heat conduction 2) and an integrable structure for fluid/heat conduction 3) as illustrated in Figure 3.4. The foam is attached to a selectively coated sheet by welding or soldering (Degischer & Kriszt 2002) and then inserted into a U-shaped sheet profile which is finally closed by welding. However, open foams can also be produced with solid areas (Wagner et al 2000) as shown in Figure 3.8. Therefore, a design according to Figure 3.4 with an integral structure for fluid and heat conduction 3) would be possible. In both cases the open foam improves the flow distribution in the absorber channel accompanied by increased heat transfer properties due to the foam structure. Figure 3.9 shows the concept with open foam stripes as integrable structure attached to a selectively coated sheet. The foam sandwich is supported with the heat carrier fluid by a diverging and a converging header.

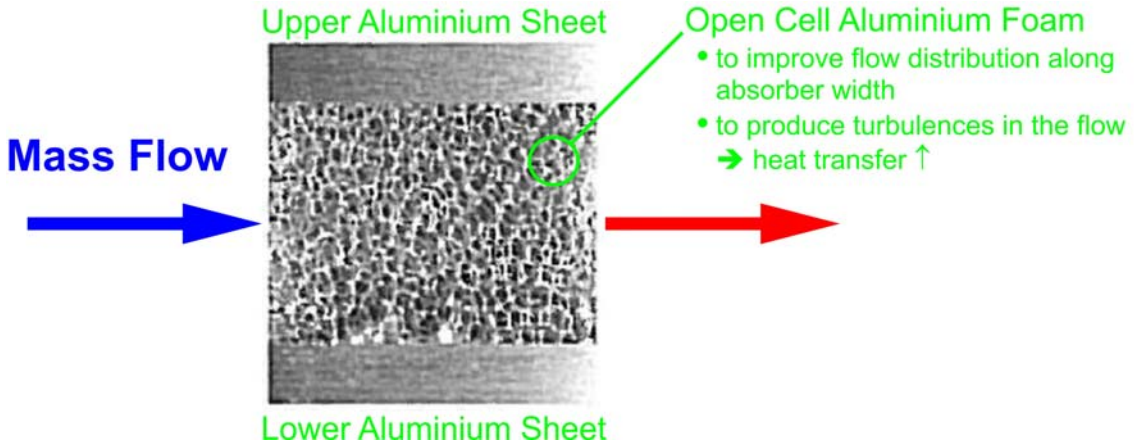

Figure 3.8: Open Foam Design Possibilities for Heat Exchanger Applications (Wagner et al 2000)

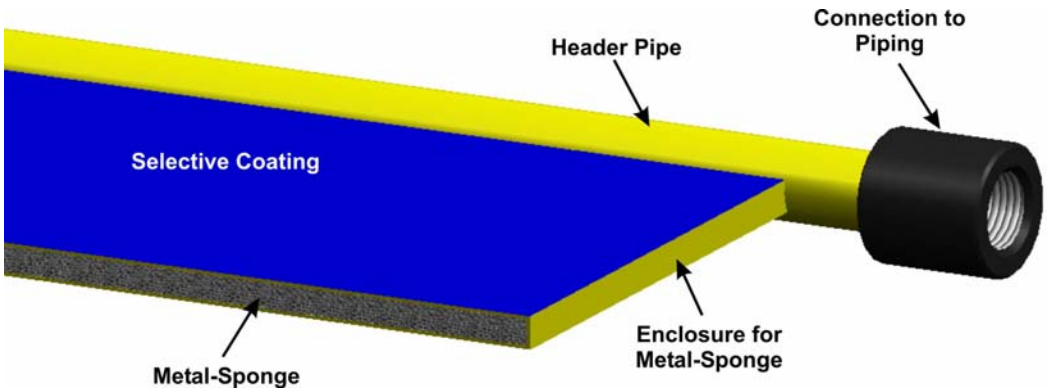

Figure 3.9: Absorber with Foam Matrix Stripes

3.4 Identification of Concept Properties

For the concepts presented in section 3.3 technical and economic properties were calculated in order to gather further information for the concept evaluation.

3.4.1 Technical Properties

The technical properties are derived from the requirements list given in Appendix B, with a focus on the following aspects:

- Design attributes of the absorber geometry,
- Basic thermodynamic attributes,
- Basic fluid dynamic attributes.

Table 3.1 shows the objectives defined in the requirements list in Appendix B.

Table 3.1: Target Values Defined for Concept Phase

Content of Heat Carrier Fluid [l]	Net Weight of Absorber [kg]	Heat Capacity [kJ K^{-1}]	Collector Efficiency Factor [-]	Production Cost [€]
<< 8	< 8	<< 40	> 0.92	≤ 65

Design Characteristics of the Absorber Geometry

With the concept design and the applied materials the design characteristics are defined. Therefore, the content of the heat carrier fluid, the absorber weight and the heat capacity can be calculated. The latter value is determined by the simple approach given in Deutsches Institut für Normung (2006). The results for the concepts of section 3.3 are given in Table 3.2.

Thermodynamic Attributes

The thermodynamic attributes are represented by the collector efficiency factor F', which is explained in detail in section 4.4. Subject to the concept design either the sheet-pipe absorber approach (Duffie & Beckman 2006) or the volumetric approach (Bliss 1959) is used. The parameters referring to the design are taken from the concepts, while general parameters are taken from Table D.1 in Appendix D. Table 3.2 shows the results of the preliminary efficiency calculations for each concept.

Fluid Dynamic Attributes

The considerations within the fluid dynamic attributes are restricted to pressure drop calculations. Due to the various and complex channel structures the determination of the flow distribution with its strong dependence on the design was carried out by numerical simulation with a further optimisation process for selected concepts. The calculation of the pressure loss of the discussed concepts is applied according to Martin et al (2002), Idelchik et al (1996) and Wagner (2001). The results are shown in Table 3.2 with a range for the state-of-the-art absorber as the lower value corresponds to the header-riser design and the upper one to the meander absorber.

Table 3.2: Comparison of Concepts with State-of-the-Art Absorbers

	State-of-the-Art Header-Riser Absorber	**Absorber with Corrugated Pattern**	**Corrugated Sheet Absorber**	**Metal-Matrix-Absorber**	**Roll-bond-Absorber**
Design Properties					
Quantity of Heat Carrier [l]	1.0 - 1.5	4.8	6.3	5.8	2.1
Absorber Net Weight [kg]	6.8	4.7	4.0	5.8	4.7
Heat Capacity [kJ K^{-1}]	8.8	23.7	22.0	29.4	10.7
Thermodynamic Attributes					
Collector Efficiency Factor F' [-]	0.88 - 0.95	0.98 - 0.99	0.98 - 0.99	0.98 - 0.99	~ 0.97
Fluid Mechanic Attributes					
Pressure Loss [mbar] at 60 l h^{-1}	2 - 210	21	12	23	23

3.4.2 Cost Analysis

The technical analysis is accompanied by an economic evaluation to provide a complete overview of the characteristics of the concepts. Today collector manufacturers try to achieve improvements in the collector efficiency of about 0.1% with absorbers based on the sheet-pipe design. However, a switch to volumetric absorbers promises much higher efficiency gains and even cost savings by the application of new, less expensive materials with suitable manufacturing processes.

Table 3.3 can only provide a rough estimation of costs in the stage of concept development.

The cost analysis was separated into two items:

- Material costs – depending on quantity and type of material used in the concepts,
- Manufacturing costs – depending on quantity and type of applied manufacturing processes used in the concepts.

Machine costs resulting from relevant investments were not included in the analysis at this stage because

- manufacturing process optimisation is only feasible when detailed design information is available,
- production quantity influences manufacturing process selection, hence machine costs significantly,
- machine costs are influenced considerably by the level of potential automation.

Table 3.3: Cost Analysis for Absorber Concepts

	State-of-the-Art Header-Riser & Meander Absorber	Absorber with Corrugated Pattern	Corrugated Sheet Absorber	Metal-Matrix-Absorber	Rollbond-Absorber
Material Costs [€/unit]	41	30	50	60	25
Production Costs [€/unit]	34	20	5	25	20
Total Costs [€/unit]	**75**	**50**	**55**	**85**	**45**

3.5 Concept Evaluation

The concepts presented in the previous sections were evaluated in order to select the best concepts for further optimisation. The evaluation process is based on a systematic approach (Pahl et al 1996), which was already started in section 3.4 by the calculation of characteristic technical and economical properties. These parameters are used to identify criteria for evaluation. Table 3.4 describes the evaluation criteria with an explanation of the influence on the absorber as well as the objectives towards an optimum concept.

Weighting factors were introduced in Appendix C / Table C.1 to define the importance of each criterion on the whole concept solution. The weighting factors are copied in the rating matrix in Appendix C / Table C.3 and are multiplied by the points assigned to each criterion and concept. The points itself represent the quality of each concept in respect to the evaluation criteria and are based on the analysis of Table 3.2, Table 3.3 and Table 3.4. Appendix C / Table C.2 shows the points for each concept and criteria.

Table 3.4: Description of Evaluation Criteria

Technical Assessment Criteria		
Fluiddynamic and Thermodynamic Criteria	Pressure Drop	Influence on the ● overall energy gain of a solar heating system, ● dimensioning of the pump in the collector loop, ● collector array configuration, ● aim ➔ pressure drop ↓.
	Thermal Resistances & Collector Efficiency Factor	Influence on the ● thermal transfer from the irradiation absorbing surface to the heat carrier fluid, ● aim ➔ thermal resistances ↓ ➔ collector efficiency factor ↑.
	Heat Capacity	Influence on the ● collector response time (e.g. warm-up, clouds,…), ● aim ➔ collector heat capacity ↓.
Operating Criteria	Operating Pressure	Influence on the ● application flexibility when the absorber is used in different systems with high or low operating pressures (structural rigidity, …), ● aim ➔ applicable operating pressures ↑.
	Operating Temperature	Influence on the stability of ● absorber material, ● manufacturing processes, ● aim ➔ applicable operating temperature ↑.
	Corrosion Resistance	Influence on the durability of ● applied materials in the absorber design, ● aim ➔ corrosion resistance ↑.
	Weight	Influence on the efforts necessary ● in the absorber / collector manufacturing, ● during roof mounting, ● aim ➔ weight ↓
Production Criteria	Number of Components	Influence on ● logistics, ● manufacturing simplicity, ● aim ➔ number of components ↓.
	Number of Steps in Production Process	Influence on the ● manufacturing simplicity, ● complexity of the manufacturing process, ● level of automation, ● aim ➔ number of steps in production process ↓.
Economic Assessment Criteria		
	Material Costs	Influenced by ● quantity of used material and consumables, ● type of used materials, ● aim ➔ material costs ↓
	Production Costs	Influenced by costs for ● processes, ● assembly effort, ● aim ➔ production costs ↓

Figure 3.10 illustrates the results taken from the rating matrix of Appendix C / Table C.3 in order to get an optimum solution for both criteria, technical as well as economic. Figure 3.10 shows the weak economic and technical performance of the sheet-pipe absorber. The metal-matrix absorber has also a low economic and technical rating due to high material costs and challenges in integrating the metal foam. The other three concepts, however, range close to the optimum line and represent solutions with good technical and economic properties. In accordance with Figure 3.10 these concepts will be analysed in detail, while the metal-matrix absorber is discarded.

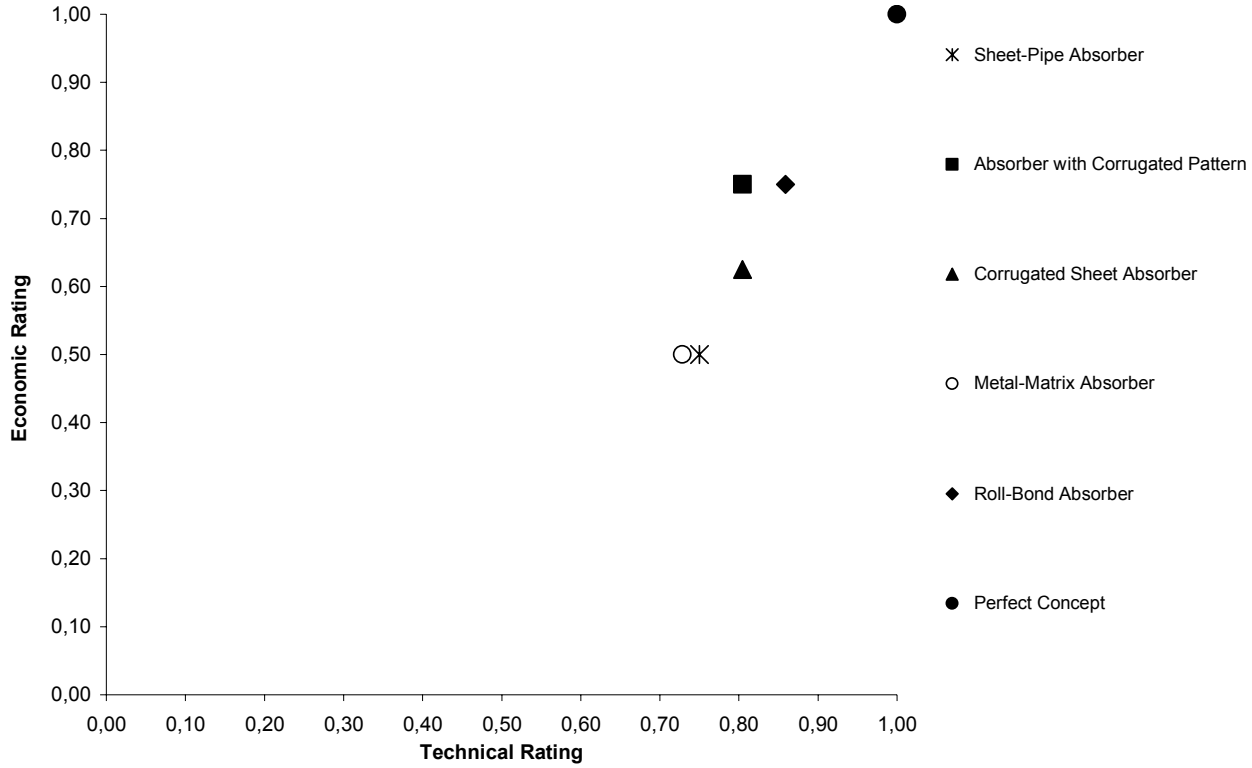

Figure 3.10: Technical and Economic Ranking of Concepts

3.6 Detail Engineering of Concepts

Corrugated Sheet Absorber

As already mentioned in section 3.3.3, the structural adhesive for connecting the corrugated sheet with the upper and lower cover sheet could not resist temperatures above 100°C. It was planned with the sandwich manufacturer to set up a research programme for optimisation of this absorber concept, i.e. to develop alternatives of the sheet connections and to integrate headers into the sandwich stucture. At the beginning of the optimisation process and the detail engineering phase the sandwich manufacturer, however,

decided not to enhance the portfolio with solar thermal absorbers and restricted the products to structural sandwich elements and ceiling elements for cooling.

Nevertheless, the corrugated sheet absorber was considered as a promising concept. Therefore, it was optimised in the theoretical analysis of chapter 3 and a simple prototype was built in an earlier stage. This prototype was also tested, however, suffered from difficulties to bleed the absorber structure when filled with water. Furthermore, the connection of the headers to the sandwich element was problematic and leaked in several areas. Due to these circumstances the corrugated sheet absorber was optimised and tested regarding flow distribution by infrared images, however, pressure drop and efficiency tests could not be carried out.

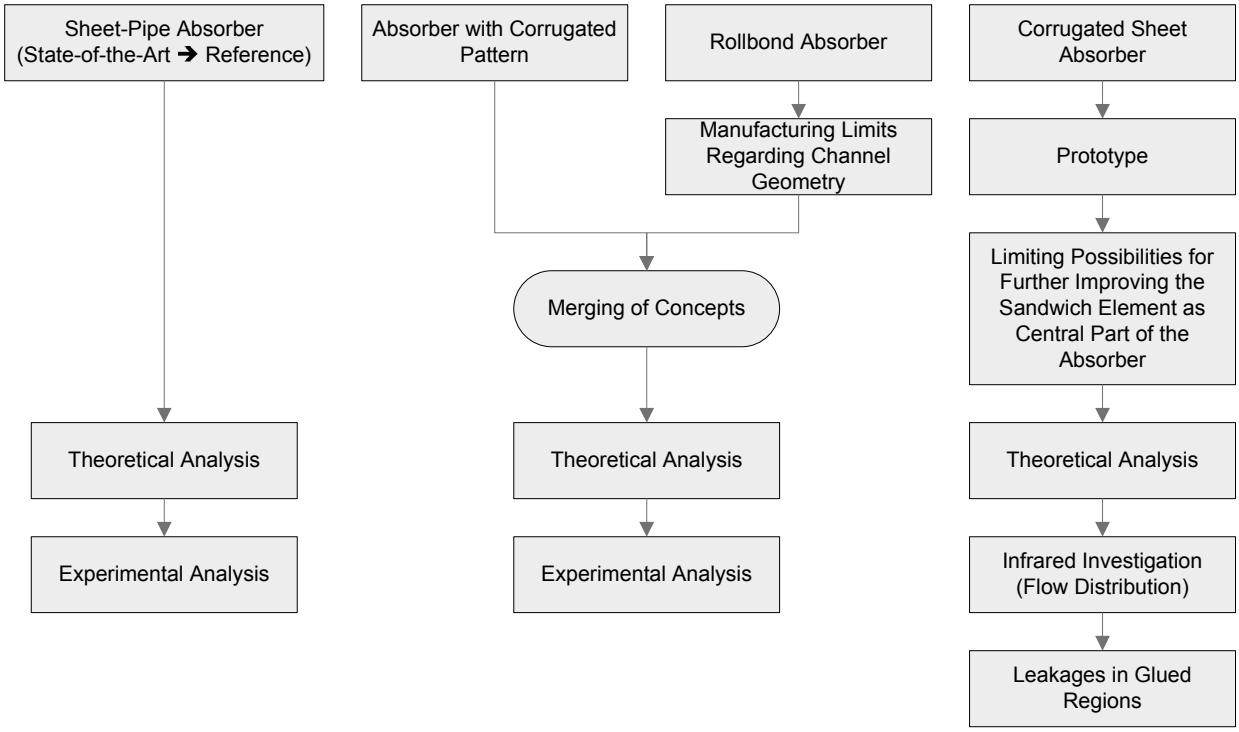

Figure 3.11: Further Development of Concepts

Rollbond Absorber

In the course of the detail engineering of the rollbond absorber concept and meetings with manufacturing companies (Macia 2007) it arose that the channel structure can be designed flexibly, but that the channel geometry is restricted by manufacturing conditions. Details on the manufacturing parameters of the rollbond process are given in section 4.2.6 and Table 4.7. These manufacturing preconditions made the rollbond absorber with extensive fluid channels impossible. By re-arrangement of the channel structure and adaption to the limits given by the rollbond manufacturing process it is possible to design

a solar thermal absorber. However, the channel structure of the re-arranged rollbond absorber and the absorber with corrugated pattern proved to be nearly equal. It was therefore decided to combine both concepts and use the channel structure of the absorber with corrugated pattern produced by the rollbond manufacturing process. In the following chapters, this approach is applied, optimised and tested.

Figure 3.11 shows the further development of the concepts and the tests carried out on the realised prototypes.

4 Theoretical Analysis

It is very important to carry out a thorough theoretical analysis of absorber geometries as efficiency can be increased without any further material costs. Rotz (2002) mentions an increase in efficiency between 5% and 10% by well optimised absorber geometry. This statement is related to well-investigated sheet-pipe absorbers, however, the significance for volumetric or quasi-volumetric absorbers is even higher. An equal flow distribution has great effects on the efficiency of solar thermal absorbers; therefore, this chapter starts with flow investigations of different absorber types. In the second part, thermodynamic calculations are carried out to verify the absorbers' efficiency. The calculations are partly based on the results of the flow simulations.

4.1 Project Related Application of CFD

Computational Fluid Dynamics simulations are increasingly applied in the automobile and chemical industry as well as many other aspects of fluid flow incorporating multi-phase flow, chemical reactions, moving meshes and force interaction. The progress in computing power and storage capacity made this possible. However, huge effort is necessary when the model has to be meshed, especially in more complicated areas or simply in high aspect ratios of the model itself. Therefore, section 6.2 is in largely dedicated to mesh generation, but also to particular design properties of the absorber geometries under consideration. The better these preparatory steps are carried out, the better the results of the simulations will be.

CFD simulations are an important step from CAD design to model testing in a pre-experimental phase, to save money and time by testing and optimising the geometry in a virtual way (Pahl et al 1996). Considering solar thermal absorbers the following properties are of great interest:

- Equal flow distribution in each riser channel
  An equal flow distribution is important for a homogenous heat removal and transport from the irradiation absorbing surface to the heat transfer medium and towards the outlet of the absorber respectively.

- Low pressure loss

  A low pressure loss is beneficial as pumps with reduced energy consumption can be used. Manufacturers already provide energy-saving pumps as energy consumptions in system operation get more and more important. In case of very large collector arrays, a low pressure loss is also advantageous as more collectors can be connected in series.

The analytical calculation of flow distribution in a multi-channel system is not possible without knowing the friction factors of the diverging and converging bifurcations of the system. Therefore, the pressure loss of each path through the system has to be calculated by an iterative method before a flow distribution can be presented. The flow rates in solar absorbers, however, are quite low compared to flow rates in heat exchangers. Reasons are the flow distribution into several riser ducts, the necessity of lower pressure losses and higher temperatures at the absorber outlet. Hence, laminar flow is dominant, but laminar flow in bifurcations, especially with uncommon geometries, is not very well investigated and applicable friction factors are hard to find (Hermann 2005; Martin et al 2002). Therefore, CFD simulations were applied to investigate and optimise the absorber geometries proposed. CFD provides the possibility to simulate even complex geometries without knowing friction factors of discrete bifurcation points at special flow conditions. Under these circumstances a positive effect of the laminar flow is that no complex turbulence models have to be tested and applied during the CFD simulation process.

CFD simulations, however, are not easy to carry out. On the one hand the costs of purchase are rather high and on the other hand a lot of time is necessary by the user to get to know the simulation environment and features as well as the appropriate meshing process. These obstacles could be responsible for the cautious use of CFD in the field of solar thermal absorbers. Furthermore, state-of-the-art absorbers with pipes and standard bifurcations like 90°-tees can be calculated without difficulty by establishing a network and solving the equations in an iterative way and by using the well understood friction factors for these geometries.

Fan et al (2007) investigated a typical header-riser absorber in U-configuration by CFD simulations. The objective was to study the flow and temperature distribution in the absorber by modelling manifolds and riser tubes, while heat flux and heat losses were cal-

culated by the linear form of the efficiency equation of the collector under consideration. Apart from flow simulations, simulations with heat transfer and buoyancy effects were carried out. The effect of flow distribution quality on the collector efficiency was not investigated.

CFD simulations were only carried out for particular cases, when analytical methods or simpler approaches are not applicable. As an example, Hermann (2005) applied CFD simulations to calculate friction factors for his bionic bifurcations. Due to the complicated bifurcation geometries with different angles, diameters and flow conditions it was impossible to find any suitable friction factors in the literature.

4.2 Modelling of Absorber Designs

4.2.1 CAD Design

The CAD design process is based on the specifications given in the requirements list as explained in detail in section 3.1. The prototypes have to fit into a typical collector casing for testing, therefore all models are defined by a common absorber size. A uniform number of connections was also fixed in the specification according to header-riser absorbers in Figure 4.1 (a) and absorber models in Figure 4.1 (c), respectively. In a discussion with the project partner, however, the number was changed from four to two connections during the simulation phase. A typical state-of-the-art header-riser absorber with two connections is shown in Figure 4.1 (b) and Figure 4.1 (d) shows the corresponding scheme of a quasi-volumetric absorber. Due to this circumstance the designs discussed and illustrated until section 4.2.5 consist of four possible connections, while section 4.2.6 describes the absorber with two connections. The project partner favoured the absorber illustrated in Figure 4.1 (b), because of increased sales with a high margin. The arrangement of absorber connections is an issue as a lot of different positions among the products of different collector manufacturers exist, for example regarding cost-efficient connection techniques and unique selling points.

In case of stagnation of a solar thermal system, the best position, in case of two connections, would be on the lower side of the absorber as suggested by Hausner and Fink (2002). However, this configuration could be difficult to purge of air. In case of the simula-

tion it does not make any difference if the absorber is used as in Figure 4.1 (a/c) or (b/d) or if the models are turned by 180° degrees. Gravity acts perpendicular to the flow direction, which means the absorbers are oriented horizontally and air pockets at exposed positions can not occur. Moreover, neither heat transfer is simulated, nor two phase flows of air and water during the filling process are applied.

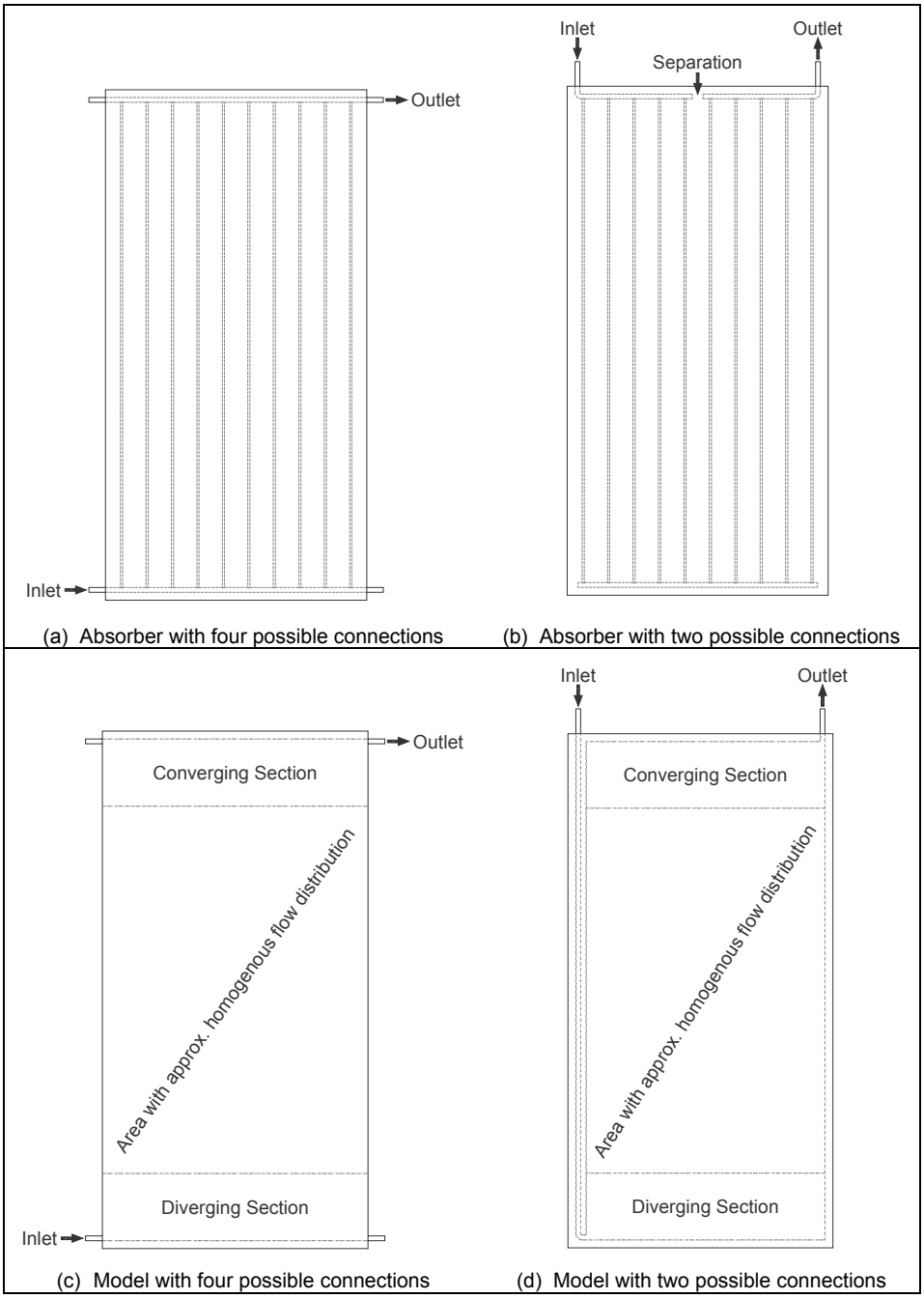

Figure 4.1: Different Absorber Connection Configurations

During the design process the absorber has to be divided into different sections as shown in Figure 4.1 (c) and (d). On the inlet side a diverging section has to provide a uni-

form flow distribution along the following channel structure, while the converging section has to collect all mass flows to the outlet. The section between both should be as long as possible and provide as much area as possible for heat transfer with a uniform flow distribution in these channels.

A lot of research has been carried out since the 1930s to understand the flow distribution in header systems. The investigations were not only restricted to solar thermal absorbers but also focused on common header configurations in heating systems or the process industry. The first investigations by Keller (1949) dealt with several different header systems either with a single diverging or converging header. McNown (1982) made a comparison of several experiments carried out during this time and had a closer look at the procedures at branching points. Acrivos et al (1959) focused on single header systems like flow from a diverging header into risers and flow from risers into a converging header, respectively. They all aimed at finding out more about the physics in a branch connection and the interaction between the header and the risers. Wagner (2001) gives a general suggestion for the dimensions of both headers in a header-riser system in order to reach an approximate homogenous flow distribution:

$$A_H = f_{HT} \sum_{j=1}^{n} A_{Rj} \qquad (4\text{-}1)$$

therefore

$$d_H = \sqrt{f_{HT} \sum_{j=1}^{n} d_{Rj}^2} \qquad (4\text{-}2)$$

with $A_{Rj} = A_{Rj+1} = A_{Rj+2} = ... = A_R$ and $d_{Rj} = d_{Rj+1} = d_{Rj+2} = ... = d_R$ respectively

if follows that

$$d_H = \sqrt{f_{HT}\ n}\ \ d_R \qquad (4\text{-}3)$$

diverging headers: $f_{HT} = 2$ (Wagner 2001)

converging headers: $f_{HT} = 4$ (Wagner 2001)

with

A_H	Cross sectional area of header (either diverging or converging)	[m²]
A_{Rj}	Cross sectional area of riser j	[m²]
d_H	Header diameter (either diverging or converging)	[m]
d_{Rj}	Diameter of riser j	[m]
f_{HT}	Factor for header types	[m]
n	Number of risers	[-]

As can be seen from the equations suggested by Wagner (2001) it is common practice to design the cross-sections of diverging and converging headers much greater than those of the riser channels. Bassiouny (1985) and Martin (1988), however, showed another possibility to gain equal flow distribution in the risers with a smaller area ratio of both headers. By solving the diverging and converging header problem analytically and neglecting friction losses in both headers (compared to the change in momentum) an equal flow distribution can be reached when equation (4-4) is satisfied.

$$\frac{A_{DH}}{A_{CH}} \approx 0.58 \ldots 0.7 \qquad \text{(Martin 1988)}$$

$$d_{CH} \approx (1.2 \ldots 1.3)\, d_{DH} \qquad (4\text{-}4)$$

with

A_{CH}	Cross sectional area of converging header	[m²]
A_{DH}	Cross sectional area of diverging header	[m²]
d_{CH}	Diameter of converging header	[m]
d_{DH}	Diameter of diverging header	[m]

The following sections (4.2.4 et seq.) show in detail the dimensioning of the headers of state-of-the-art absorbers and proposed designs. The length of the uniform flow section is determined by both header sections and depends on the design and the degree of optimisation.

4.2.2 Meshing Strategies

Depending on the complexity of the absorber design, different meshing processes are possible. Hence, the whole model or different parts have to be designed. SolidEdge (Siemens 2008), a commercial CAD software package, was used for creating the absorber models by 3D geometries. Fast and easy changes are possible by the user due to parametric dimensioning, which is very convenient during the optimisation runs where every step needs changes in channel size or position.

After the design process, the final body is exported from the CAD software to the simulation environment where it is prepared for simulation. The file format used for transfer is the IGES-standard which destroys the 3D body by creating a volume based on surfaces.

The simulations are carried out by StarCD (Cdadapco 2005a, 2005b, 2005c), a CFD software package of the CD-adapco Group. Table 4.1 shows the different programs of the package, which are necessary for pre-processing, solving and post-processing.

Table 4.1: Programme Modules of the CFD Software Package

	pro-SURF	**pro-STAR**	**pro-AM**	**star**
Description	Program for: ● CAD import ● Geometry repair ● Surface meshing ● Database export	General program for pre-processing ● Meshing ● Application of BCs ● Simulation parameters, etc. and post processing ● Generation of results ● Viewing of results, etc.	Automatic meshing module used in combination with pro-star (meshing only)	CFD-solver

After exporting the IGES geometry from the CAD software, the repair process is done within the pro-surf module. By an automatic, iterative process, the geometry is checked for failures, mainly caused by converting to the exchange format. Geometry errors can be:

- merging of endpoints / curves,
- join / split curves,
- removal of duplicate or zero-area surfaces.

The resulting precise CAD model is the basis for following meshing processes (Cdadapco 2005a). The repaired geometry was meshed by an automatic surface meshing tool implemented in pro-SURF. This surface mesher generates a grid of triangles on the surface of the geometry, which are necessary only for following mesh generation purposes (Cdadapco 2005b). Finally, the mesh has to be exported to a binary coded StarCD database file, which can be imported in pro-AM for fluid mesh generation. Figure 4.2 shows the steps from the absorber design to the surface repair and meshing in pro-SURF.

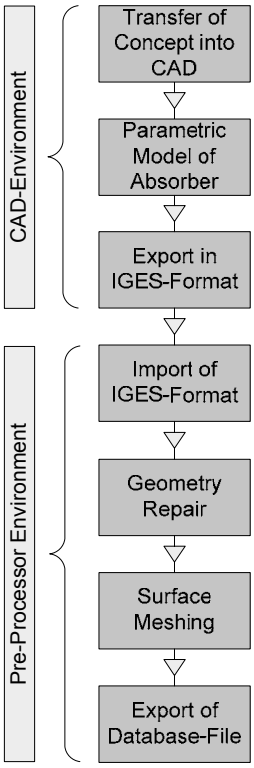

Figure 4.2: CAD Design and Surface Processing

The database is imported in pro-am where the automatic meshing is carried out. The meshing process starts with the creation of a subsurface that is smaller than the original surface imported. The gap between both surfaces represents the boundary layer in the following fluid mesh. It is an important region for flow resistance and heat transfer and has great influence on the results in simulations with turbulent flows (Cdadapco 2005c). However, even in laminar simulations without heat transfer, the use of this boundary layer is recommended to improve the mesh quality as the core mesh (green cells in Figure 4.5) consists of trimmed cells at its outer area (Cdadapco 2005b). Figure 4.3 shows the section of the shells of the surface and subsurface of a branch connection.

The template mesh is the first volume mesh and consists of equally formed hexahedra and virtually covers the whole surface mesh. However, the template mesh can be refined in regions where refinement parameters were applied to the surface mesh. A refined region in the template mesh is shown in Figure 4.4, based on the surface and subsurface shells of Figure 4.3.

In the following step, the core fluid mesh is produced from the template mesh by calculating its intersection with the subsurface shells. Finally a new shell layer is generated on the surface of the core fluid mesh, which has to be extruded to surface shells. These layer cells represent the boundary layer of the meshed fluid domain and fluid particles in this area would be in contact with the channel material in real operation. Figure 4.5 shows the final fluid mesh created by the automatic mesh module.

Based on a pre-meshed model, further meshing operations can be carried out to describe the whole absorber geometry by cells in the CFD simulation. Figure 4.6 shows the two possible methods applicable for the final mesh creation. However, it depends on the geometry whether the left or right path in Figure 4.6 makes more sense in order to save time for meshing and producing an adequate mesh quality in particular. The advantage of the left path is a constant mesh quality due to simple geometries, extrusion of pre-meshed sections and several copies of a high-quality mesh.

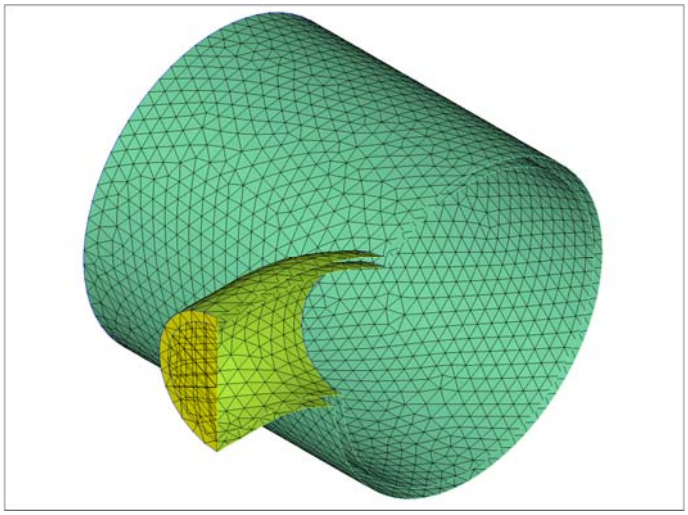

Figure 4.3: Sectioned Surface and Subsurface

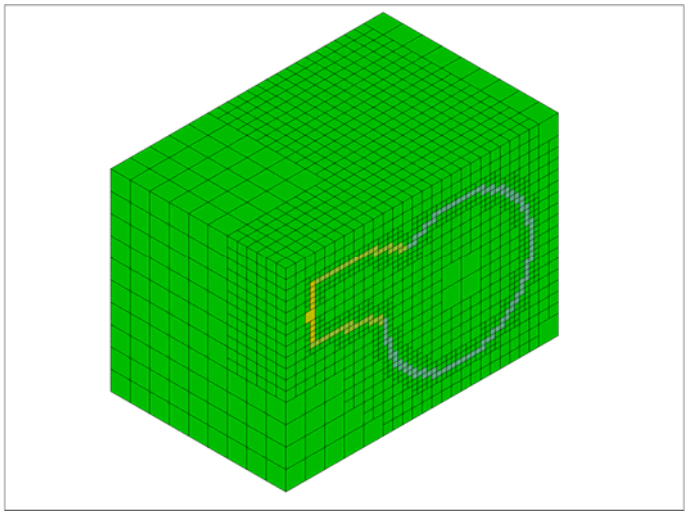

Figure 4.4: Sectioned Template Mesh

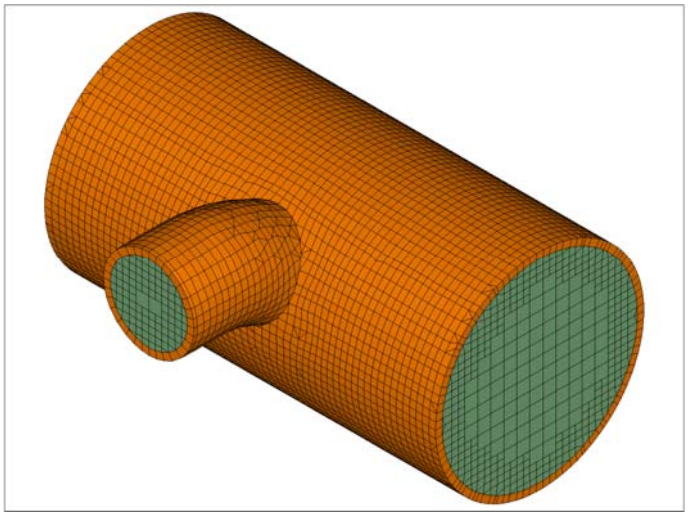

Figure 4.5: Fluid Mesh with Core and Boundary Layer Cells

However, if a lot of different periodic patterns exist the right-hand path is more suitable as changes in geometry can be carried out faster which is quite important during optimisation as explained in section 4.3.4.

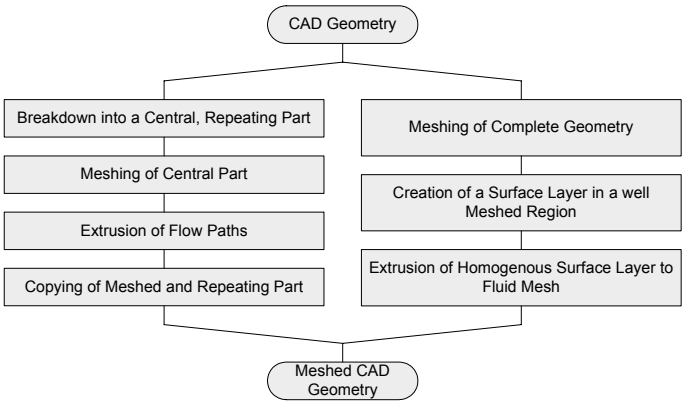

Figure 4.6: Absorber Meshing Possibilities

In case of less complex absorber designs with periodic patterns, only simple but central parts of the model are designed, processed in pro-surf and meshed in pro-am. The remaining parts of the absorber are created by mesh extrusion processes and copies of the periodic structures of the absorber. This meshing process is demonstrated for the header-riser absorber as shown in Figure 4.7.

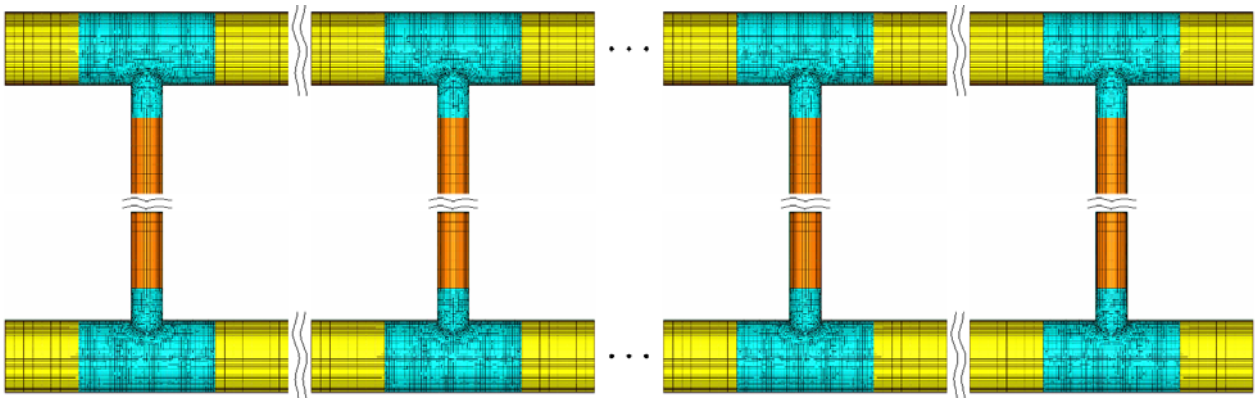

Figure 4.7: Mesh Generation for Geometries with Periodic Pattern

More complex geometries which consist of a lot of different periodic patterns and geometries that have to be changed quite often in the optimisation phase are not suited to be meshed as shown in Figure 4.7. It would cost a lot of time to re-mesh the periodic bodies and to reassemble them to the final mesh. Even when scripts are used for these processes it takes a lot of time to adjust them to the conditions in the changed geometry or the changing cell structures of the pre-meshed periodic parts. Therefore, the whole geometry is designed in the CAD software and exported to the meshing environment where it is meshed by use of the automatic meshing tool. However, the very large aspect ratio of the absorber length or width to the absorber height causes problems in the automatic meshing tool. Therefore, it is taken care of by a suitable mesh quality in the plane of the absorber width to absorber length, while the cell quality in the absorber height is of lower

interest as it will be re-meshed manually in a subsequent step. By this approach good results are reached for the cells in the edge regions of the absorber due to a high quality mesh in the plane section and as a second step by extrusion of these cells in the direction of the absorber height. Figure 4.8 shows cells produced by this process viewed from the top and shows also manually produced cells along the absorber height.

A disadvantage of the latter meshing processes is the restriction to rectangular channels only. As the cells forming the absorber height are produced by extrusion, no special channel section shapes like rhomboid or elliptical shapes are possible. However, in some manufacturing processes shapes like these are produced. Figure 4.9 shows real absorber channel shapes and modelled shapes. The amount of cells necessary to describe the real channel shape is far greater than in case of rectangular channels as hexahedra cells have to be generated in arc-formed regions with sharp corners. To achieve an acceptable cell quality, the size of the cells has to be reduced, while the number of cells is increased. Complex absorber models, however, have cell numbers of about 3 million, hence already make high demands on the computer equipment. An adjustment of the cell size for smaller models is possible, but absorber sizes of 985mm x 1925 mm x 3 mm (see Appendix B) cannot be modelled in the same scale.

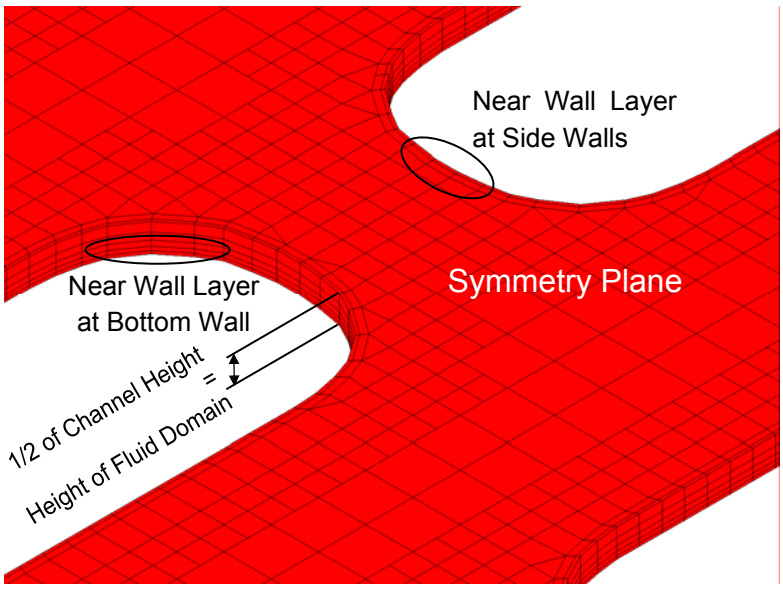

Figure 4.8: Mesh Generation for Fluid Domain of Complex Absorber Geometries

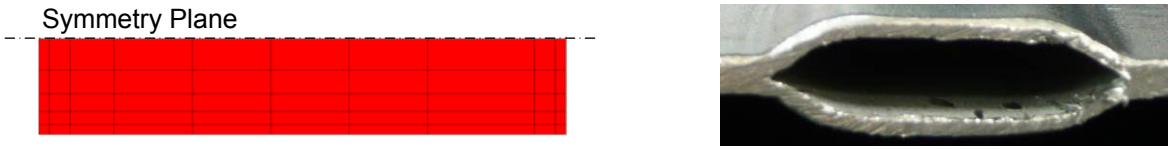

Figure 4.9: Channel Section Shapes of Model and Real Part

4.2.3 Boundary Conditions

The final step in pre-processing is the application of boundary conditions. Boundary conditions specify special regions on the fluid mesh and have to be placed to describe the real flow situation as closely as possible. Table 4.2 shows the different boundary conditions used in these flow simulations.

Table 4.2: Applied Boundary Conditions

Boundary Condition	Description
Inlet	The inlet boundary condition specifies the section for the flow into the absorber. The flow velocity in [m s^{-1}] has to be specified at the inlet.
Outlet	The outlet boundary condition specifies the section for the flow out of the absorber. The flow split in [%] can be defined at the outlet. Due to the continuity equation and just one outlet at the absorber model, 100% have to pass through the outlet boundary.
Internal Boundary	Internal boundaries can be placed in sections where additional flow data are of interest. The data is calculated during simulation and saved in an UTF-8 text file for further processing.
Symmetry Plain	If absorber geometry provides regions where the flow is symmetric only one half of the region has to be meshed. On the remaining cut section a symmetry plane has to be applied.
Wall	The wall boundary condition is applied to all cell surfaces which would provide the contact to the pipe or duct wall. The flow velocity is forced to zero at those surfaces according to the no-slip condition.

On the inlet boundary condition, different flow velocities are applied. Solar collectors and solar systems respectively are split into low-flow and high-flow types according to the flow rates in operation (Remmers 1999a). It depends for instance on the desired temperature output of the solar system as well as the system configuration and operating costs. Hausner and Fechner (1998) investigated a flat-plate collector under different flow conditions. He showed that the absorber fluid flow is in the transition area from laminar to turbulent flow at a flow rate of more than 120 l h^{-1} in case of typical conditions like ambient temperature and insulation. The typical flow rate for one collector (header-riser design) in operation, however, is about 80 l h^{-1} (SPF 2005) and therefore far below the transition area.

Remmers (1999a) recommends for low-flow systems a specific flow rate of 10-15 [l $h^{-1}m^{-2}$] and for high-flow systems 25-40 [l $h^{-1}m^{-2}$]. Table 4.3 shows the defined flow rates starting at the proposed flow rate for low-flow systems. The higher values

cover the flow rates for typical pressure loss measurements of state-of-the-art absorbers. Different flow rates were used in the simulation to investigate their influence on flow distribution and pressure loss.

Table 4.3: Inlet-Flow Rates

Flow Rate [l h^{-1}]	Comment		
19.0	Based on a specific flow rate of 10 [l $h^{-1}m^{-2}$] (low-flow systems) and an absorber area according to the specification in Appendix B.	Common operational flow rate range	Flow rates to investigate flow distribution and pressure loss
30.0			
60.0			
76.0	Based on a specific flow rate of 40 [l $h^{-1}m^{-2}$] (high-flow systems) and an absorber area according to the specification in Appendix B.		
120.0			
180.0			
240.0	Rounded up recommendation according to Deutsches Institut für Normung (2006) and Appendix B for highest flow rate, 0.03 kg $s^{-1}m^{-2}$		

Weitbrecht et al (2002) have investigated the flow and the flow distribution in header-riser absorbers at constant temperature and showed that the Reynolds Numbers are below the critical Reynolds Number ($Re < Re_{krit} = 2{,}320$) in the risers and most parts of the manifolds. Only at high inlet flow rates and just at the inlet and outlet area of the headers transitional or slightly turbulent flow occurred.

If Reynolds Numbers of state-of-the-art absorbers are compared with those of volumetric or quasi-volumetric absorbers it can be seen, that Reynolds Numbers of the latter are even lower in most of the channels. Therefore, laminar flow condition is defined for all flow simulations.

The fluid temperature for the flow simulations is fixed to 293.15 K. Therefore, effects of changing fluid properties at increasing temperatures are not considered, hence the Reynolds Number depends on velocity only. Moreover, it is more comfortable to work at ambient temperature as the flow remains in most flow domain areas in the laminar condition (e.g. chapter 5.4 / Figure 5.15) and no complex turbulence model has to be applied.

In contrast to real absorber and collector operation respectively, the absorber models and the simulations are based upon the assumptions and specifications given in Table 4.4.

Table 4.4: Simulation and Model Characteristics vs. Real Operation Characteristics

Simulation	**Experimental Investigation / Operation**
Laminar flow simulation	All flow regimes can occur
No heat transfer is considered, hence • no buoyancy effects can occur (see next item)	Heat transfer occurs, herewith • buoyancy effects can occur • fluid properties change according to operating conditions
Horizontal absorber model: • no static heights • no buoyancy effects can occur (due to a constant fluid temperature no buoyancy effects can occur at all)	Absorber is fixed e.g. at 45° (or arbitrary angle in normal operation) to the gravitational force of the earth • static heights act on the flow • buoyancy effects can occur
Perfectly formed geometry and channels • no manufacturing tolerances • channel shapes depend on manufacturing process and thereby on specific parameters (see Table 4.7)	Real channel shapes with • manufacturing tolerances (channel height, width, shape, etc.) • sharp edges, etc.

4.2.4 State-of-the-Art: Header-Riser Absorber

The header-riser absorber geometry used for the simulations is derived from the existing absorber of the project partner. The absorber consists of ten riser pipes which are on one side connected to a diverging header pipe and on the other side to a converging header pipe. The principle layout can be seen in Figure 4.1 (a). Table 4.5 shows the geometry details from a CitrinSolar absorber (case 5) as well as modified absorber models. Case 1 in Table 4.5 is identical to case 5: except that the riser pipes do not extend into the header pipes. Due to a simpler design and mesh creation process, the absorber of case 1 is defined as the reference. Case 2 is based on case 1, but consists of 15 riser pipes. In case 3 and case 4, the headers are calculated according to equation (4-4) by Holger Martin (1988) and equation (4-3) by Walter Wagner (2001), respectively. Consequences regarding flow distribution between real and calculated header dimensions are discussed in section 4.3.2.

The inlet of the absorber is on the lower left side while the outlet is on the upper right side of the absorber. All riser pipes are passed through in parallel. The meshing is set up by

the automatic meshing of one branch connection and the extrusion of its surface sections. Finally, a block set, consisting of the branch connection, riser and header pipe meshes, is created and copied according to the number of riser pipes.

Table 4.5: Header-Riser Absorber Geometry Values

			Case 1	Case 2	Case 3	Case 4	Case 5
Diverging Header Pipe	d_{DH}	[mm]	16	16	16	31	16
Riser Pipe	d_R	[mm]	7 (in all cases)				
Riser Pipe Length	L_R	[mm]	1818	1818	1809.4	1763.6	1818
Riser Pipe Distance	ΔL_R	[mm]	96	64.1	96	96	96
Number of Risers	n_R	[-]	10	15	10	10	10
Converging Header	d_{CH}	[mm]	16	16	21	44	16
Header Length	L_H	[mm]	1026	1026	1026	1026	1026

4.2.5 Concept 1: Corrugated Sheet Absorber

The corrugated sheet absorber is based on the concept as shown in Figure 3.6 in section 3.3.3 and the layout in Figure 4.1 (c), respectively. Figure 4.10 shows the section of the sandwich plate with an upper and a lower cover sheet attached to a corrugated core by hot-melt glue.

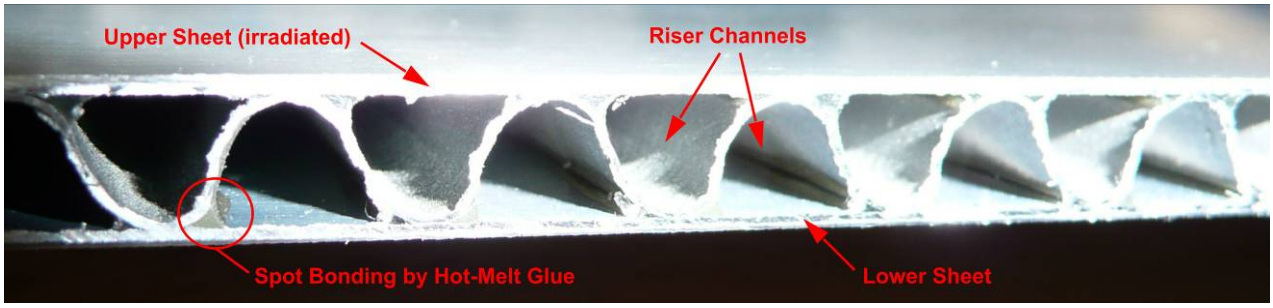

Figure 4.10: Sandwich Plate with Riser Channels

The simulation model is created by two circular manifolds, one diverging manifold and one converging manifold. In between, the riser channels are designed according to the specifications given by the sandwich plate, which are presented in detail in Metawell (2008). However, the glue at the bonding surface is not modelled in contrast to Figure 4.10 showing a real sandwich plate. The dimensions of the manifolds are shown in Table 4.6. Case 1 is based on the typical standard headers used in solar thermal ab-

sorbers while cases 2 and 3 are defined by equations (4-4) and (4-3), respectively. Case 4 is derived from case 3 by reducing the header diameters by a factor of four. It was originally designed to reduce the absorber volume (Table 4.8). Case 5 was modelled according to a prototype which was built and tested at the university and is discussed in detail in section 5.1 and 4.3.3 with regard to geometry and simulation results.

Table 4.6: Characteristics of the Corrugated Sheet Absorber

			Case 1	**Case 2**	**Case 3**	**Case 4**	**Case 5**
Diverging Header Diameter	d_{DH}	[mm]	16	16	96	24	21
Riser Width	b_{RW}	[mm]	5 (in all cases)				
Riser Top Radius	R_{RT}	[mm]	1.5 (in all cases)				
Riser Height	h_R	[mm]	4 (in all cases)				
Riser Duct Distance	ΔL_R	[mm]	5 (in all cases)				
Riser Duct Length	L_R	[mm]	1832.6	1830.1	1732.7	1819.4	999.4
Number of Risers	n_R	[-]	258	258	258	258	526
Converging Header Diameter	d_{CH}	[mm]	16	21	135	34	21
Header Length	L_H	[mm]	1110	1110	1110	1110	2100

4.2.6 Concept 2: Absorber with Corrugated Pattern

The absorber with corrugated pattern is derived from concepts shown in sections 3.3.3 and 3.6, which are partly based on the rollbond manufacturing process. Due to the great flexibility in designing and arranging channels, rollbonding seems to be a unique production process. However, a number of restrictions exist when going into details.

Table 4.7 lists the most important rules as they show the limits within the concept of section 3.3.3 and the difficulties in the current design. The parameter list is valid for a working pressure of up to 3 bar_e (Collenz 2007b), however, the test pressure is required to be 4.5 bar_e according to the German standard DIN EN 12975 2 (Deutsches Institut für Normung 2006) and standards of other European countries.

Based on the design rules given in Table 4.7, an initial model was established with an overall channel width of 14 mm. The distance between the islands in the flow direction is 14 mm for all models. Furthermore, the model was designed according to the require-

ments given in the specification, for example the supply for the heat carrier fluid (arrangement and dimensions) or the general dimensions of the absorber.

Table 4.7: Basic Design Rules of the Rollbond Process (Anon 1999; Collenz 2007a, 2007b; Macia 2007)

Rule	Limits	Note
Inlet and Outlet Channel Width	28 mm	Short, extended channels as adapting area for the welded inlet and outlet pipe. Greater channel heights in these sections are required to fit the (circular) connection pipe.
Universal Channel Width	6.5 mm – 14 mm	Large channel width and working pressures cause absorber deformations, hence limits are necessary.
Channel Height	3 mm	The given range for the universal channel width would result in a constant channel height according to Collenz (2007b). Beyond this range the channel height strongly depends on the channel width. The smaller the channel width the lower the channel height.
Minimum Radius	6.5 mm	A minimum radius must be maintained to avoid areas with high stresses and high local velocities.
Minimum Island Width	$b_I = \frac{b_{left} + b_{right}}{2}$	The island width depends on the surrounding channels and contributes in combination with the channel width to the rigidity of the rollbond panel.
Top and Bottom Margins *Left and Right Margins*	minimum 30 mm minimum 60 mm	Margins must have a minimum width for rigidity and manufacturing reasons.

The absorber model is partitioned into three areas as in Figure 4.1 (d), as the flow has to be equally distributed in all channels along the absorber width. The approach to equalising the flow distribution applied to the concepts in section 4.2.4 and 4.2.5 cannot be used with rollbond panels due to the restrictions of the channel size. Therefore, the diverging section is in turn subdivided into areas with increasing channel numbers in the flow direction while the converging section has decreasing channel numbers in flow direction. Each section is arranged in three channel areas with alternating channel numbers. Figure 4.11 illustrates the layout of the absorber models based on the rollbond manufacturing process.

In between the two sections a straight channel system with 40 channels in parallel and a constant channel width of 10 mm is arranged. These straight channels are the central part of the absorber and therefore should be as long as possible, provided a satisfactory flow distribution can be reached. In between the straight channels are lateral channels in alternating distances and quantity along the absorber width. Due to huge deformations of

rollbond absorbers tested at higher pressures (Figure 4.12) and with greater channel width, lateral channels were introduced. The deformed absorber as shown in Figure 4.12 had a constant channel width of 20 mm and was tested up to a working pressure of 6 bar_e (Collenz 2007a). Its maximum deformation of 105 mm occurred along centreline of the absorber. Furthermore, the channel height increased by 75% to 5.8 mm at a final pressure of 6 bar_e compared to the initial channel height of 3.3 mm at 1 bar_e.

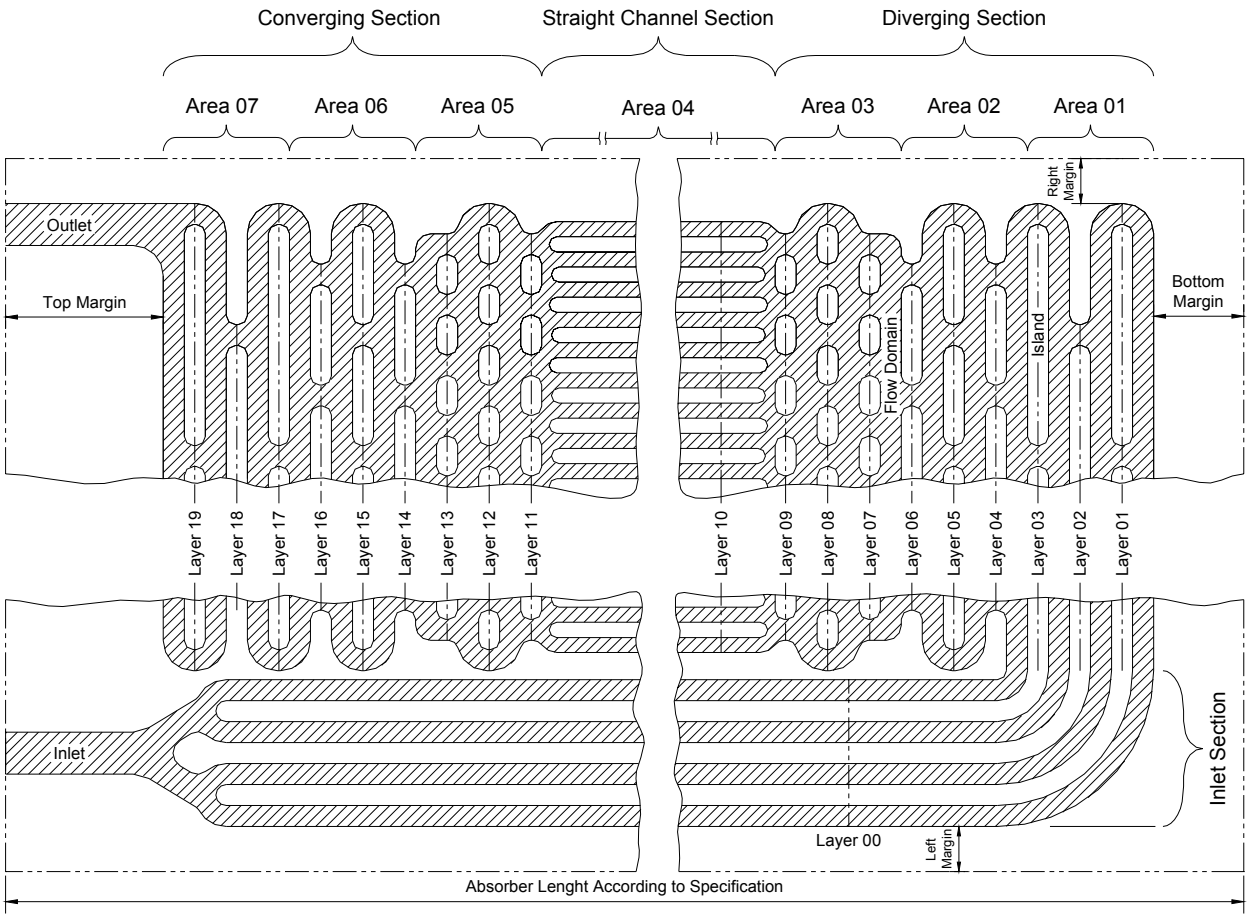

Figure 4.11: Definition and Layout of the Absorber with Corrugated Pattern

The initial model was designed in 3D CAD software and provides the basis for further optimisation regarding equal flow distribution. However, because of the great number of parameters, namely the channel width in the layer sections (Figure 4.11), a more convenient way of changing values

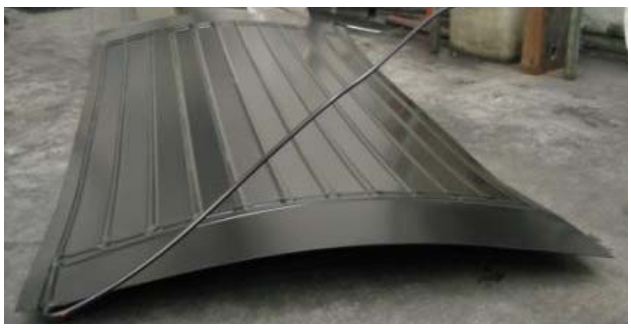

Figure 4.12: Deformed Rollbond Absorber with Extensive Fluid Channels (Collenz 2007a)

had to be used. For this reason, the CAD model was linked to a spreadsheet programme where the model dimensions were calculated according to the initial model and the rules given by the manufacturing process. As the evaluation of the simulation runs was also carried out in the spreadsheet programme the new width values could be transferred to the CAD model by the linked spreadsheet. The optimisation algorithm applied is explained in section 4.3.4. In compliance with section 4.2.2, mesh creation was carried out by extrusion based on the CAD model. Due to symmetry only one half of the model had to be meshed.

4.3 Simulation Results

4.3.1 Results and Interpretation

The simulation provides on the one hand the velocity data at arbitrary points of the absorber geometry, hence, the flow distribution among channels of interest. On the other hand, the pressure loss of the whole absorber design is obtained.

The velocity data is extracted from the CFD solution file by a VisualBasic for Applications (VBA) programme and then presented in spreadsheets and charts for further processing. The extraction process searches for the last iteration step of the simulation, selects the boundary number of interest and assigns this velocity data to the corresponding channel section. Based on this information, the flow rate is calculated and normalised to the summarised flow rate of the considered section, as documented by equations (4-5) to (4-16).

The flow rate in each pipe or duct is calculated by:

$$\dot{V}_j = v_j \, A_j \qquad (4\text{-}5)$$

$$\dot{V}_j = \frac{\pi}{4} v_j \, d_j^2 \qquad \text{circular section} \qquad (4\text{-}6)$$

$$\dot{V}_j = v_j \, b_j \, h \qquad \text{square section} \qquad (4\text{-}7)$$

with

A_j	Area of pipe or duct j	[m²]
b_j	Width of duct j	[m]

d_j	Diameter of pipe j	[m]
h	Height of duct	[m]
$\dot{V}_j$	Flow rate in pipe or duct j	[m³ s^{-1}]
v_j	Flow velocity in pipe or duct j	[m s^{-1}]

In each layer section the overall flow rate is:

$$\dot{V}_O = \sum_{j=1}^{n} \dot{V}_j = \sum_{j=1}^{n} \left(v_j \; A_j \right) \qquad (4\text{-}8)$$

$$\dot{V}_O = \frac{\pi}{4} \sum_{j=1}^{n} \left(v_j \; d_j^2 \right) \qquad \text{circular section} \qquad (4\text{-}9)$$

$$\dot{V}_O = h \sum_{j=1}^{n} \left(v_j \; b_j \right) \qquad \text{square section} \qquad (4\text{-}10)$$

with

n	Number of pipes or ducts in layer	[-]
$\dot{V}_O$	Flow rate at absorber inlet	[m³ s^{-1}]

In case of homogenous flow distribution the flow rate in every pipe or duct is:

$$\dot{V}_H = \frac{\dot{V}_O}{n} = \frac{1}{n} \sum_{j=1}^{n} \left(v_j \; A_j \right) \qquad (4\text{-}11)$$

$$\dot{V}_H = \frac{\pi}{4} \frac{1}{n} \sum_{j=1}^{n} \left(v_j \; d_j^2 \right) \qquad \text{circular section} \qquad (4\text{-}12)$$

$$\dot{V}_H = \frac{h}{n} \sum_{j=1}^{n} \left(v_j \; b_j \right) \qquad \text{square section} \qquad (4\text{-}13)$$

with

$\dot{V}_H$	Ideal flow rate (homogenous flow distribution in all channels)	[m³ s^{-1}]

Finally, the ratio can be expressed between the flow rate in each pipe or duct to the flow rate that results, if homogenous flow distribution exists:

$$\dot{V}_{nH_j} = \frac{\dot{V}_j}{\dot{V}_H} = \frac{n \; v_j \; A_j}{\sum_{j=1}^{n} \left(v_j \; A_j \right)} \qquad (4\text{-}14)$$

$$\dot{V}_{nH_j} = \frac{n\, v_j\, d_j^2}{\sum_{j=1}^{n}\left(v_j\, d_j^2\right)} \qquad \text{circular section} \qquad (4\text{-}15)$$

$$\dot{V}_{nH_j} = \frac{n\, v_j\, b_j}{\sum_{j=1}^{n}\left(v_j\, b_j\right)} \qquad \text{square section} \qquad (4\text{-}16)$$

with

$\dot{V}_{nH_j}$	Normalised flow rate of channel j	[-]

The absorber concepts described in section 4.2.4 and 4.2.5 all have risers with equal cross sections. Therefore the corresponding equations of the previous outline can be further simplified. In the following sections, all charts showing flow distributions are based on the previous equations.

The pressure loss of the absorber prototypes is measured in horizontal position. Therefore, the simulations are also carried out in horizontal model position. In this case, the acceleration of gravity acts perpendicular to the flow continuum and no other gravity components occur. Furthermore, the z-coordinates of the inlet and outlet region cells are equal and no hydrostatic pressure term appears. Hence, the overall pressure loss is calculated by the static pressure at the inlet and the outlet sections, as shown in equation (4-17).

$$\Delta p = p_{s,in} - p_{s,out} \qquad (4\text{-}17)$$

with

Δp	Pressure loss of absorber	[Pa]
$p_{s,in}$	Static pressure at inlet cross section	[Pa]
$p_{s,out}$	Static pressure at outlet cross section	[Pa]

4.3.2 State-of-the-Art: Header-Riser Absorber

Flow Distribution

The simulation of state-of-the-art absorbers provides a validation of the simulation models with simulations and experiments investigated in the literature. Furthermore, aspects of improvement are shown. The analysis starts with the reference case 1 and its variations case 2 as well as case 5 all having a constant riser header diameter ratio of 0.44.

Due to the configuration of headers and risers in a typical absorber with equal length of each flow path, see Figure 4.1 (a) an equal flow distribution would be expected. Figure 4.13 shows the normalised flow rate $\dot{V}_{nH_j}$ (see equation (4-14) and (4-11)) for three different cases plotted against the normalised riser position $\frac{x}{W_A}$. In contrast to an equal distribution, however, Figure 4.13 / case 1 shows an absolute maximum deviation from homogenous flow distribution of about 22%. For connecting collectors in parallel this design is also used in solar thermal systems, known as a Tichelmann configuration (Peuser et al 2002).

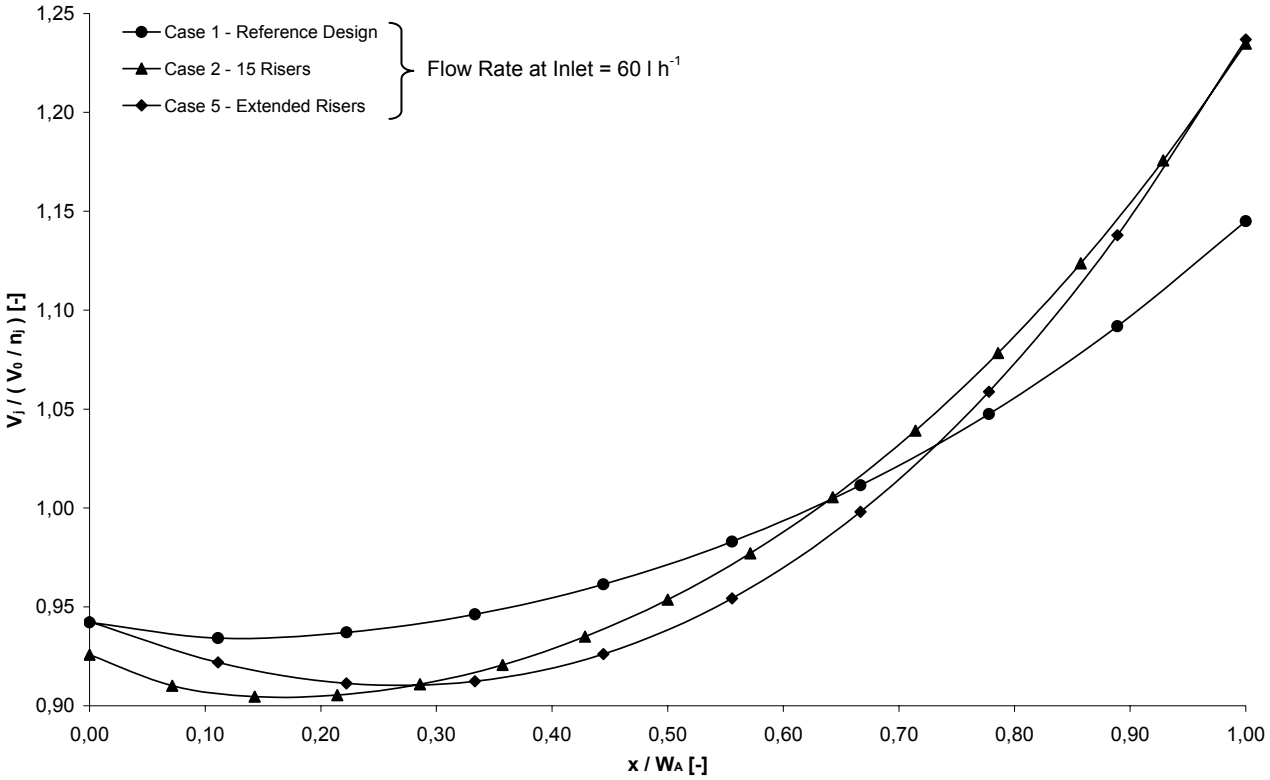

Figure 4.13: Flow-Distribution of Header-Riser Absorbers with Constant Riser Header Diameter Ratio of 0.44

Investigations of solar thermal absorbers by Weitbrecht et al (2002) and Jones and Lior (1994) showed similar results for a parallel-flow absorber. Figure 4.14 shows the experiment and the simulations carried out by Weitbrecht et al (2002). As can be seen the graphs of 'Experiment' and simulation 'Case 1' (of Figure 4.14) are in good agreement with the results in Figure 4.13 of the CFD simulations. Both graphs belong to an absorber geometry similar to the one mentioned in Table 4.5 (Case 1). Due to the special flow conditions in a solar thermal absorber, Weitbrecht et al (2002) shows by graph 'Case 2' the flow distribution for the same geometrical configurations as in 'Case 1' but simulated with loss coefficients for turbulent pipe flow. 'Case 3' neglects all energy losses in the risers and the manifolds and leads to a homogenous flow distribution similar to 'Case 4' where the risers are extended from 1.8 m to 10 m. The geometry of 'Case 5' is based on a riser distance of 1 m and leads to a parabolic graph.

Weitbrecht et al (2002) divides the graphs into three different categories:

- Velocities in the risers increasing from the first to the last riser,
- Uniform velocities in all risers (segment),
- Velocities high in the outer risers and decreasing to the central risers (symmetric parabola).

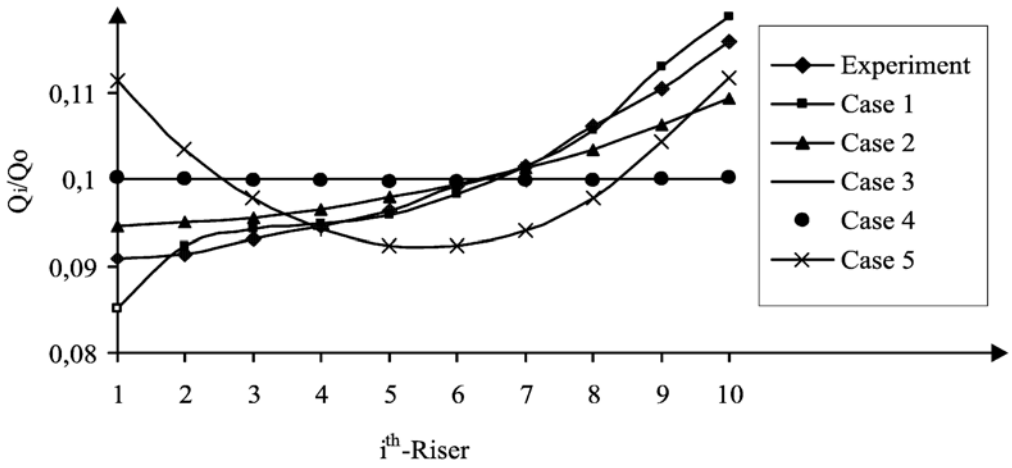

Figure 4.14: Flow Distribution of Header-Riser Absorber (Weitbrecht et al 2002)

Weitbrecht et al (2002) as well as Jones and Lior (1994) explain the different flow distribution graphs by the losses in the different parts of the absorber. If the overall pressure loss is dominated by the pressure losses in the riser pipes, a flow distribution close to uniformity can be reached. However, if the overall pressure loss is controlled by momen-

tum and frictional pressure changes in both manifolds, a flow distribution similar to that in Figure 4.15 (Z-configuration) will occur or even like the graph shown in Figure 4.14 / 'Case 5'. This approach is not only restricted to header-riser systems but can also be applied to collector arrays. Wang and Wu (1990) for example, measured a collector system connected in parallel and got a parabolic flow distribution in their system due to an unfavourable connection arrangement. If neither the pressure loss in the risers nor the inertial and frictional pressure changes in the manifolds are dominant, an increasing graph for the flow distribution will occur between the first and the last riser. This case is typical for state-of-the-art header-riser absorbers as can be seen from Figure 4.13.

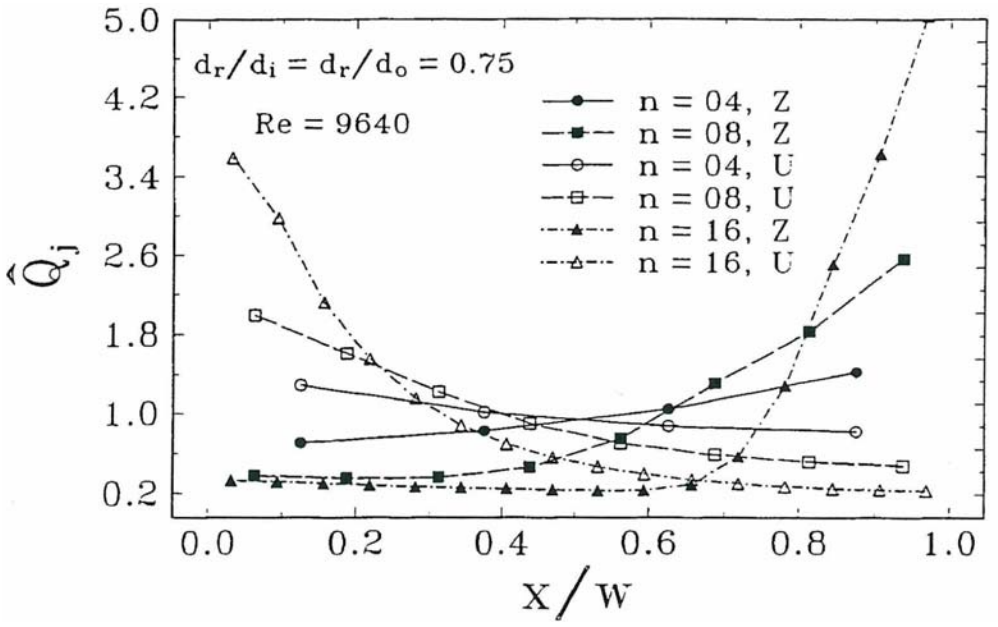

Figure 4.15: Flow Distribution of Absorbers in Z- and U-Configuration (Jones & Lior 1994)

Figure 4.15 shows the normalised flow rate of each riser, if homogenous flow distribution occurred in all risers. This normalised flow rate $\hat{Q}_j$ is plotted against the ratio of each riser position to the width of the absorber $\frac{x}{W}$. The riser-header diameter ratio is kept constant at 0.75 while the number of risers varies. The configuration type considered is the Z-configuration. A comparison of these graphs reveals an increasing maldistribution with a growing number of risers. Furthermore, with a constant number of risers the quality of flow distribution decreases when the riser header diameter ratio is increased. Case 2 (ratio 0.44 / 15 risers) in Figure 4.13 and the graph with 16 risers in Figure 4.15 (ratio 0.75) show this trend. Consequently, both the number of risers and the riser header di-

ameter ratio have an important impact on the flow distribution. The formulae given in equations (4-1) to (4-4) consider this influence.

However, an increased number of risers significantly improves the collector efficiency as outlined in section 4.4.1. Two important criteria of a high quality collector do not support this way of efficiency improvement. More risers represent higher collector costs, as more material has to be integrated into the absorber configuration. Considering Figure 1.1 this is not a promising approach. In addition, with an increased number of risers hence more material, the collector weight is increased. Apart from a decreased quality in flow-distribution (Figure 4.13 / case 2), absorber costs and weight are increased when implementing more risers.

Finally, Figure 4.13 illustrates the flow distribution for case 5 with extended risers, as in real absorbers. The riser endings located in the header pipes cause an increasing change of momentum as well as friction loss in the headers, thus the headers become more dominant. As a result, maldistribution is increased and approaches the graph of case 2 with 15 riser pipes. An improvement of the manufacturing process for connecting pipes and headers could result in an enhanced flow distribution of up to 10% without causing any further material costs.

Figure 4.16 illustrates the flow distribution for the optimised header geometries of case 3 and case 4 as well as the reference geometry case 1. Case 3 is calculated by the equation (4-4) of Martin (1988) while case 4 is based on equation (4-3) of Wagner (2001). Both absorber designs show a low deviation to homogenous flow distribution. However, case 3 has more favourable header diameters as case 4 at negligible differences in the results.

Figure 4.17 gives an overview of the flow distribution for header-riser case 1 with different inlet flow rates as recommended by Peusser et al (2002) for different system types and configurations. As can be seen from the graphs, the deviation to homogenous flow distribution is increasing with the flow rate.

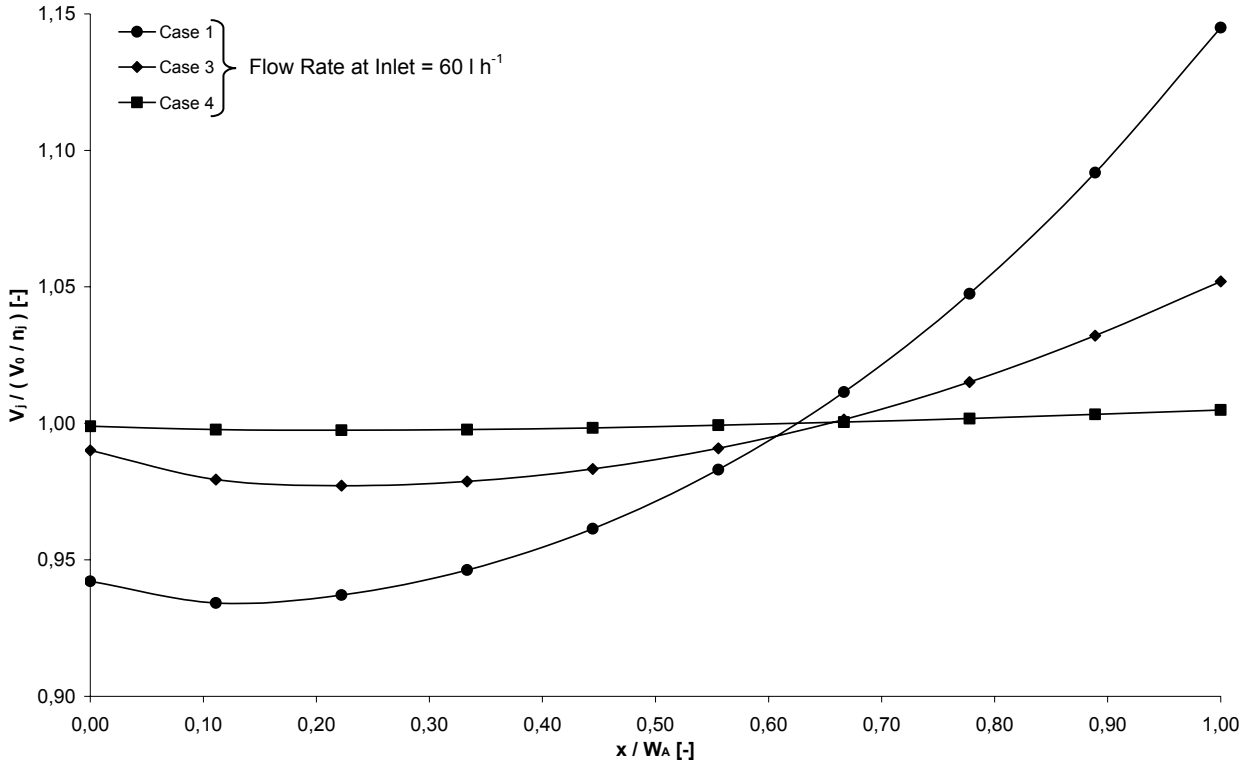

Figure 4.16: Flow Distributions of Header-Riser Absorber Case 1, 3 and 4 with Different Header Diameters

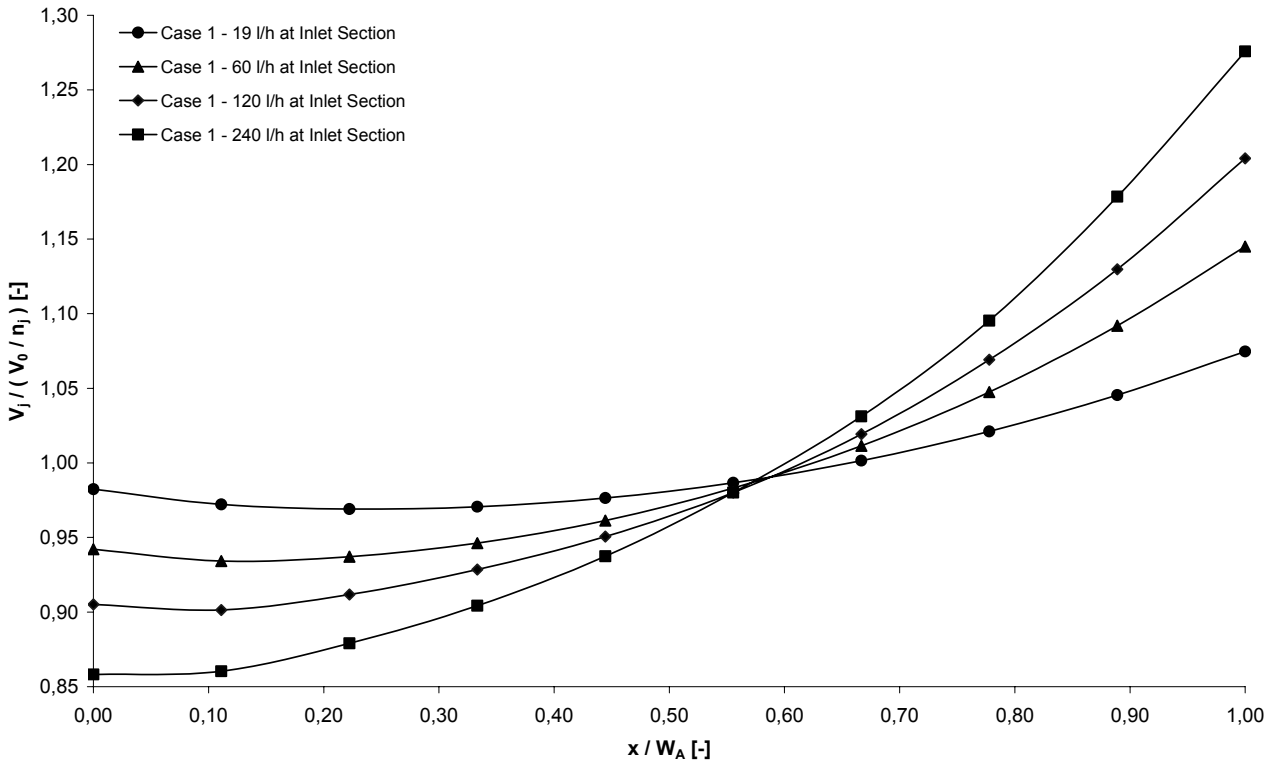

Figure 4.17: Flow Distributions of Header-Riser Absorber Case 1 with Different Inlet Flow Rates

Pressure Loss

An important factor for the pump supporting the collector array is the overall pressure loss of the array and thereby the pressure loss of a single absorber. Figure 4.18 shows the simulated pressure loss curves for header-riser absorber case 1 and case 5. As a result of the extended riser pipes the pressure drop is 54% higher for case 5 at 240 l h^{-1}.

In Figure 4.19 the pressure loss of the absorber designs presented in Table 4.5 is shown for an inlet flow rate of 60 l h^{-1}. By comparing the reference case 1 with case 3 and case 4, a similarity with the flow distribution in Figure 4.16 can be found. The pressure loss decreases with an increasing uniformity in flow distribution. At higher flow rates the advantage of case 3 and case 4 regarding pressure loss is even stronger. However, even case 2 shows a lower pressure drop compared to case 1 and even case 5, whilst the flow distribution is comparatively bad. This is because, due to more risers in case 2, the flow velocity in each riser is decreased compared to case 1, hence, a lower pressure loss is generated.

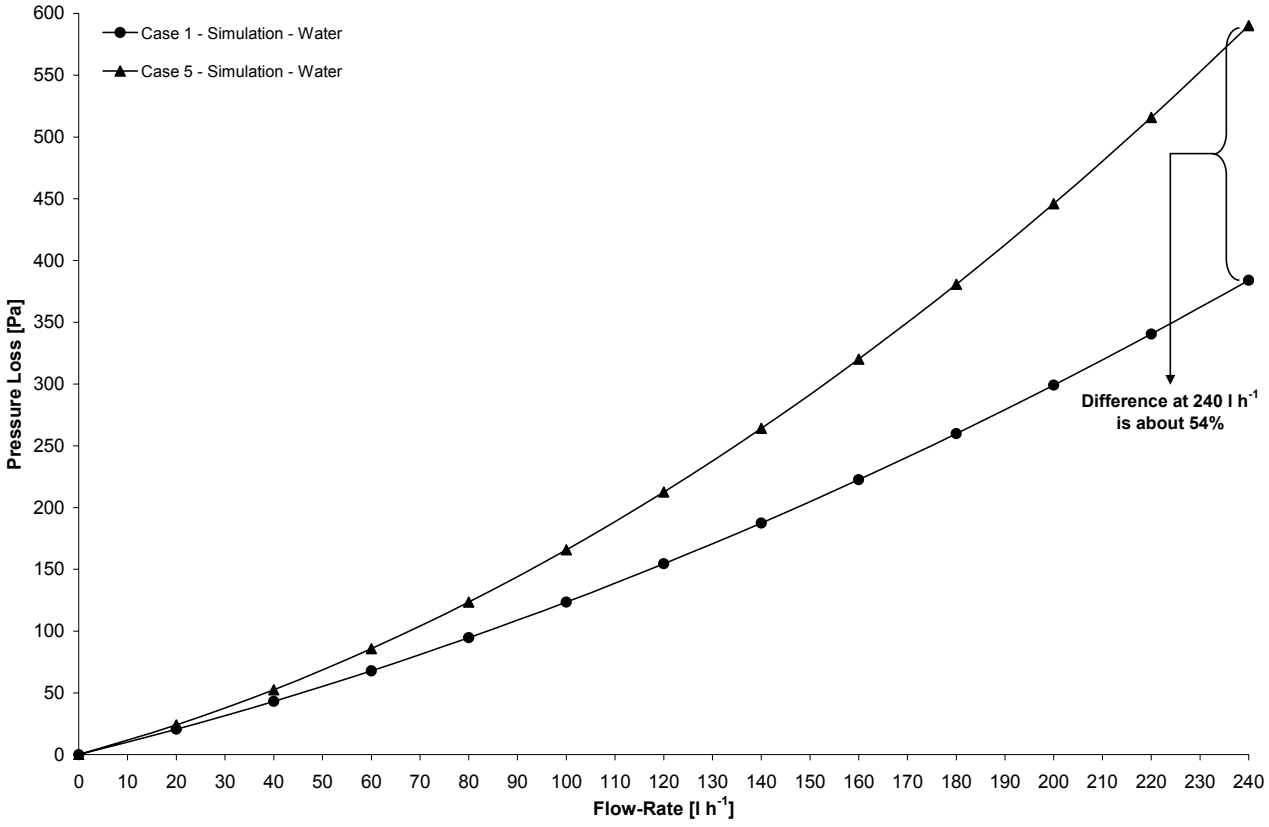

Figure 4.18: Simulated Pressure Loss of Header-Riser Absorber Designs

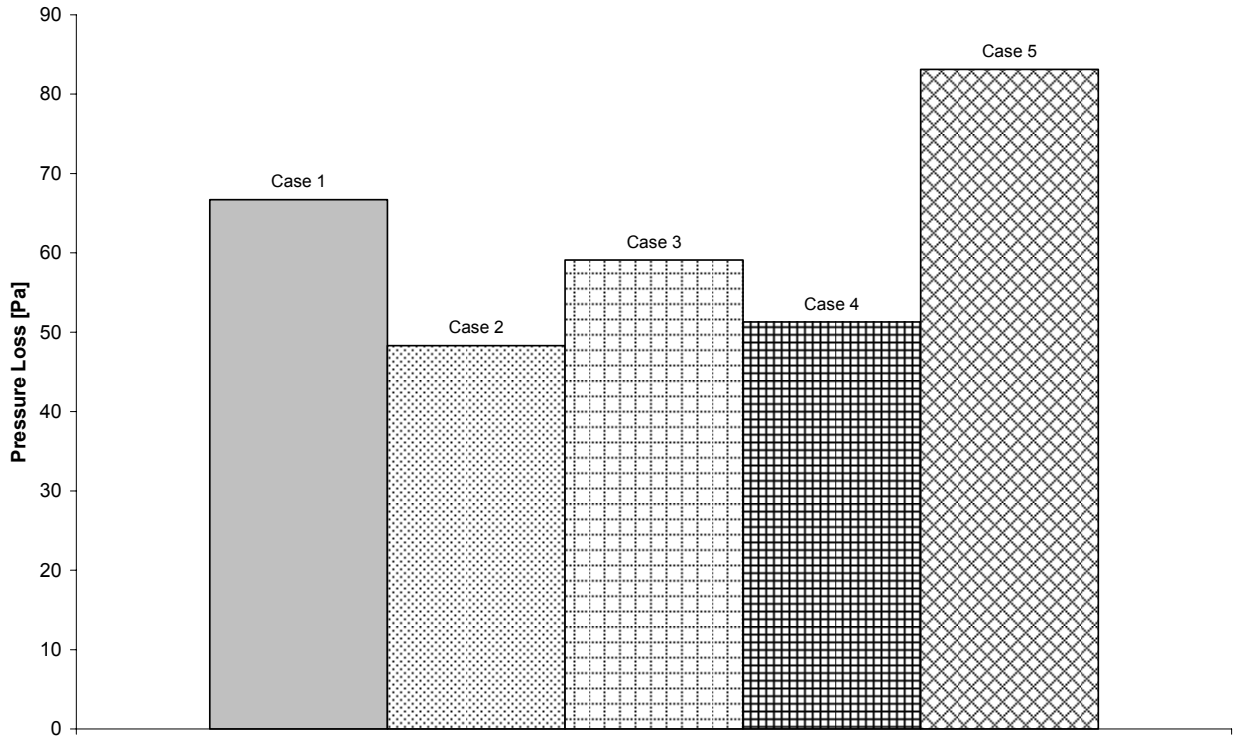

Figure 4.19: Pressure Losses for Header-Riser Designs for 60 l h^{-1}

4.3.3 Concept 1: Corrugated Sheet Absorber

Flow Distribution

The starting case within the corrugated sheet absorbers is case 1 as specified in Table 4.6. The header dimensions used in this model are transferred from typical headers in today's header riser absorbers. However, in contrast to the latter, case 1 has 25.8 times more risers in its configuration. After considering the evaluations in the preceding section, a stronger deviation in all risers is expected compared to the header-riser absorber designs. Figure 4.20 presents the flow distribution for case 1 with a minimum deviation of 25% and a maximum deviation of 70% relating to homogenous flow distribution.

Due to the fixed geometry of the sandwich plate the risers cannot be modified. The approach is in line with the header variations carried out in section 4.2.4 and 4.2.5, respectively. Graph case 2 refers to the header calculation with equation (4-4) and shows a minimum deviation of -11% and a maximum of 25% again relating to homogenous flow distribution. Compared to the reference header-riser absorber case 1, the maximum deviation is about 67 percentage points higher, hence, representing an unsatisfactory result.

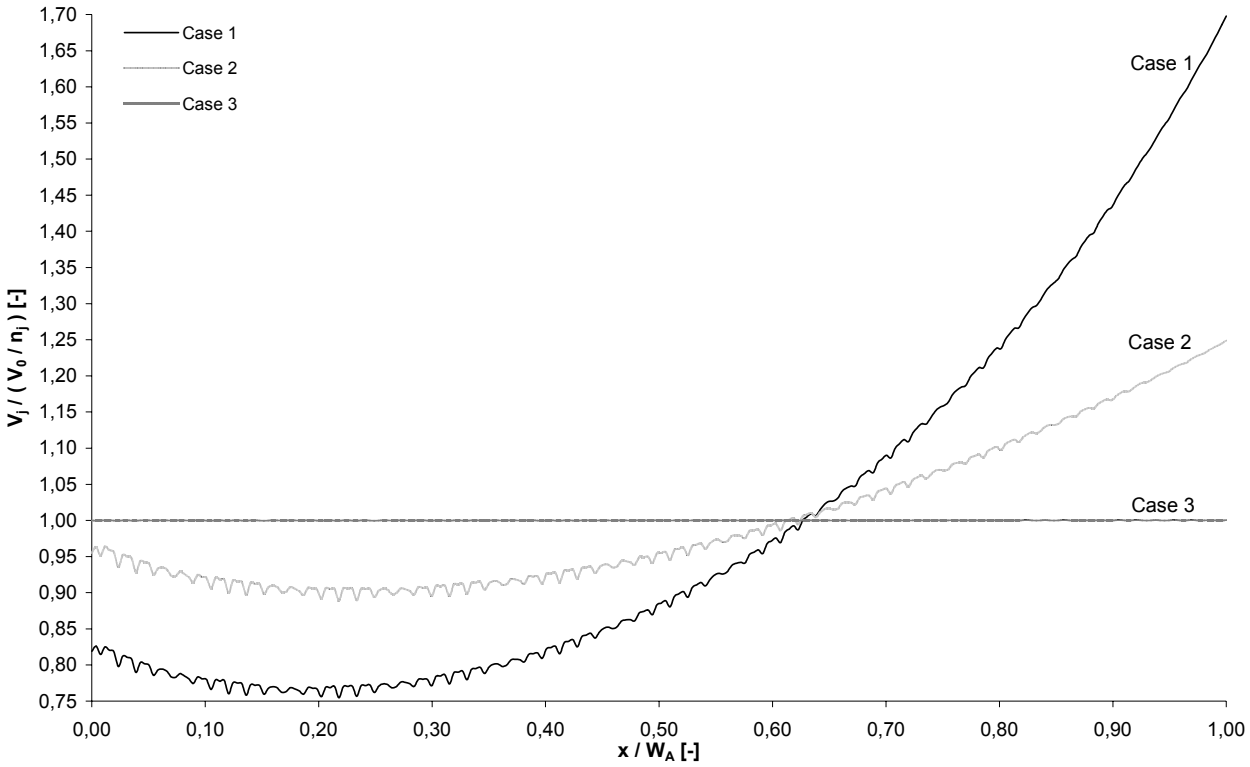

Figure 4.20: Flow Distribution of Corrugated Sheet Absorber Cases 1, 2 and 3

The absorber with corrugated pattern case 3, however, shows an acceptable flow distribution in Figure 4.20. Actually, there is no deviation to homogenous flow distribution in this configuration. Yet, this design has a big disadvantage considering the header dimensions as shown in Table 4.6 versus current collector heights. Therefore, a further simulation was carried out with resized headers. Figure 4.21 illustrates the graph of this case 4 in comparison with case 1 of the header-riser absorber and the previously discussed case 3. Case 4 also has a very homogenous flow distribution with a minimum deviation of -2.2% and a maximum of 3.9%, although both headers are only a quarter of those used in case 3. The header-riser curve of case 1 shows in contrast a worse flow distribution. Nevertheless, Figure 4.21 shows that an absorber in the design of a multi-channel sandwich plate with customised headers can have an equal flow distribution.

Table 4.8 presents the fluid volume for the absorbers with corrugated pattern. Compared to the capacity of header-riser absorbers, the general drawback of volumetric absorbers becomes evident. Due to the huge area for direct contact between radiation absorbing surface and heat transfer fluid, a bigger fluid capacity, hence, a higher heat capacity for the whole absorber is implied. In Table 4.8 the unfavourable absorber design of case 3 is

obvious again. Case 4 has just 14% percent more volume than case 1 but still about 7 times more than the header-riser case 1.

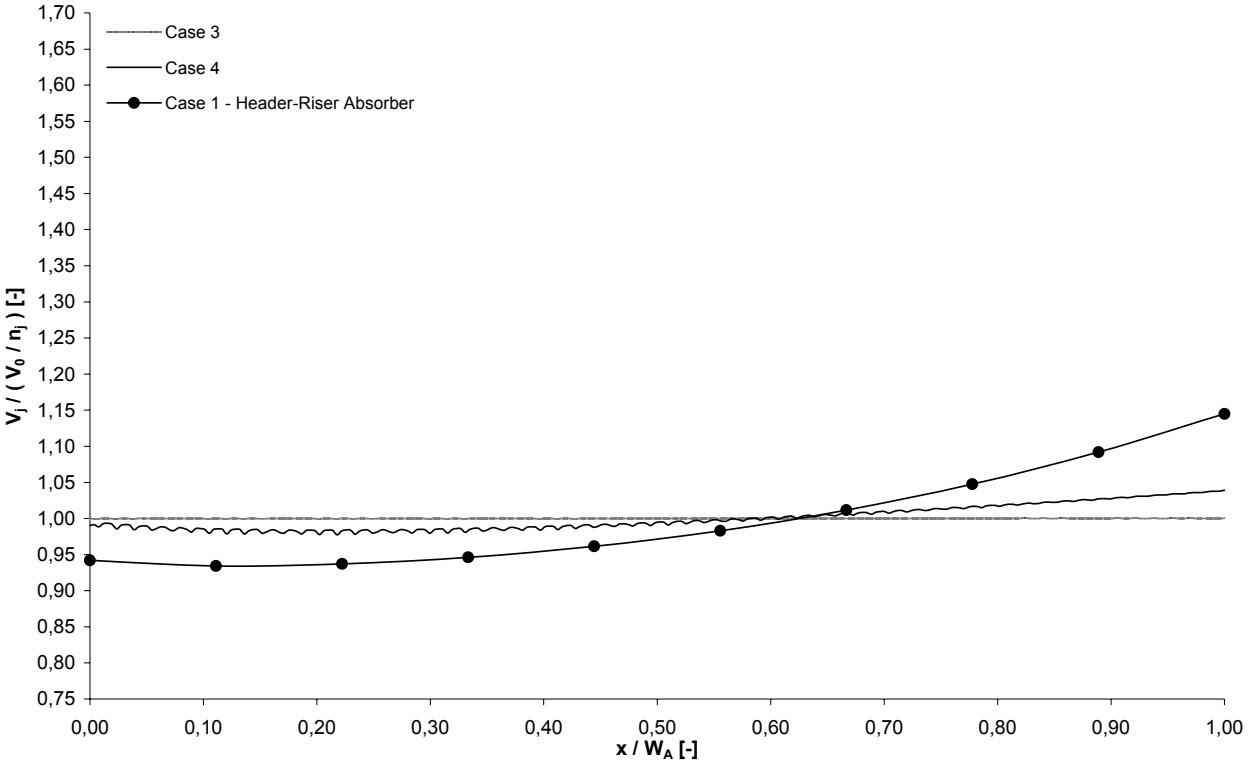

Figure 4.21: Flow Distribution of Case 3 and 4 from Concept 2 as well as Header-Riser Absorber Case 1

Table 4.8: Fluid Volume of the Corrugated Sheet Absorber

		Case 1	Case 2	Case 3	Case 4	Header-Riser Case 1 (SPF 2005)
Fluid Volume	V_F [l]	6.9	7.1	29.4	7.9	1.1

Pressure Loss

The pressure loss for these absorbers is shown in Figure 4.22. As mentioned in section 4.2.5, all models incorporate smooth surfaces, especially in the riser channels. The lower pressure loss of all corrugated sheet absorber configurations is particularly caused by lower flow velocities in the riser channels due to a high number of risers. Within the corrugated sheet absorbers those with a higher quality of flow distribution also show lower pressure loss. The same trend was found with the header-riser absorbers (section 4.3.2) and can be attributed to lower friction losses as well as equal flow velocities without any extrema causing corresponding pressure losses.

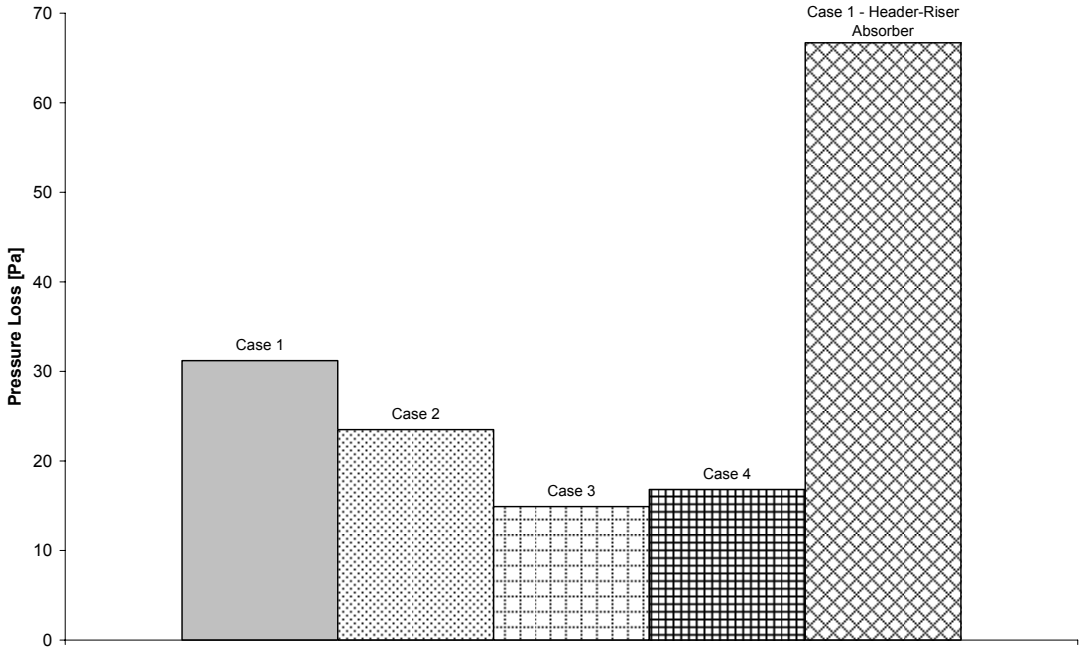

Figure 4.22: Pressure Loss of Corrugated Sheet Absorbers for 60 l h^{-1}

Finally, Figure 4.23 shows the very low pressure loss of the absorber with corrugated pattern. It was already mentioned in section 4.2.5 that the real sandwich plate contains a glue to connect the upper and lower sheet with the corrugated sheet. Similar to varnish tears, the glue agglomerates where it is applied. However, these tears were not modelled and the pressure loss is significantly smaller than in real operation. Compared to case 1 in header-riser design, the pressure loss of case 4 is more than 5.5times lower at 240 l h^{-1}.

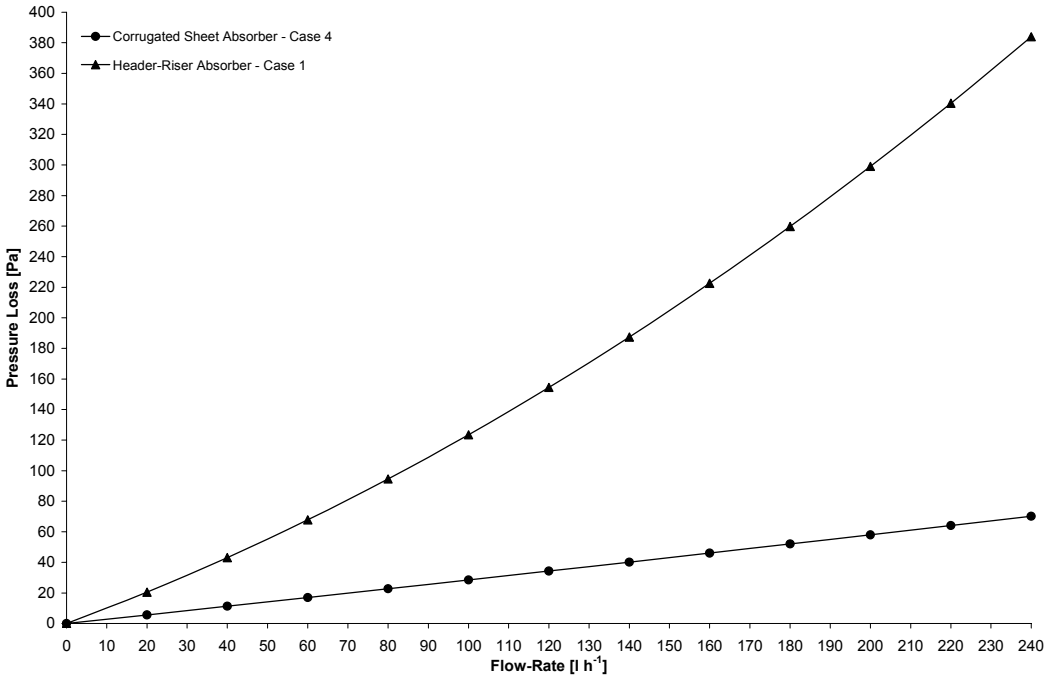

Figure 4.23: Simulated Pressure Loss of Case 4 Compared with Header-Riser Case 1

4.3.4 Concept 2: Absorber with Corrugated Pattern

Flow Distribution

This section describes the results of various optimisation runs of the absorber concept 2 presented in section 4.2.6. Furthermore, the optimisation procedure for homogenous flow distribution is given in detail. All diagrams showing flow distributions start with the diverging section in the lower part (inclusive inlet section), the straight channel section in the central part and the converging section in the upper part. Every section, in turn, includes all channels of the layers as illustrated in Figure 4.11 with their corresponding normalised flow rate $\dot{V}_{nH_j}$. The scaling of the ordinates, however, is different in the three sections, but remain identical when miscellaneous cases are illustrated for better comparison between the figures.

The simulation results for the initial absorber model (case 1) based on an overall channel width of 14 mm are shown in Figure 4.25. As can be seen from the diagram, many channels are beyond the ±10% borderlines in the diverging as well as the converging section. Figure 4.24 presents the frequency distribution of $\dot{V}_{nH}$ for all channels according to their section and their range on the ordinate of Figure 4.25. 48% of all channels in the diverging section are outside the borderlines (range $[\,0\,;\,0.9\,[$ and $]\,1.1\,;\,\infty\,)$ marked in Figure 4.25, while 52% are inside a maximum deviation to equal flow distribution of ±10% (range $[\,0.9\,;\,1.1\,]$). However, the section with straight channels already provides a well distributed flow, as 87% of channels are in the range of ±5% relative to equal flow distribution. In the converging section the frequency distribution is similar to the diverging section; 54% of all channels in this section are outside of and 46% inside of the borderlines. Finally, it can be seen from both figures, that there is a huge potential to improve the flow distribution in the diverging and converging section. An equalised flow distribution avoids local dead water zones accompanied by high temperature which, in turn, causes an increased heat loss coefficient of the collector in this area.

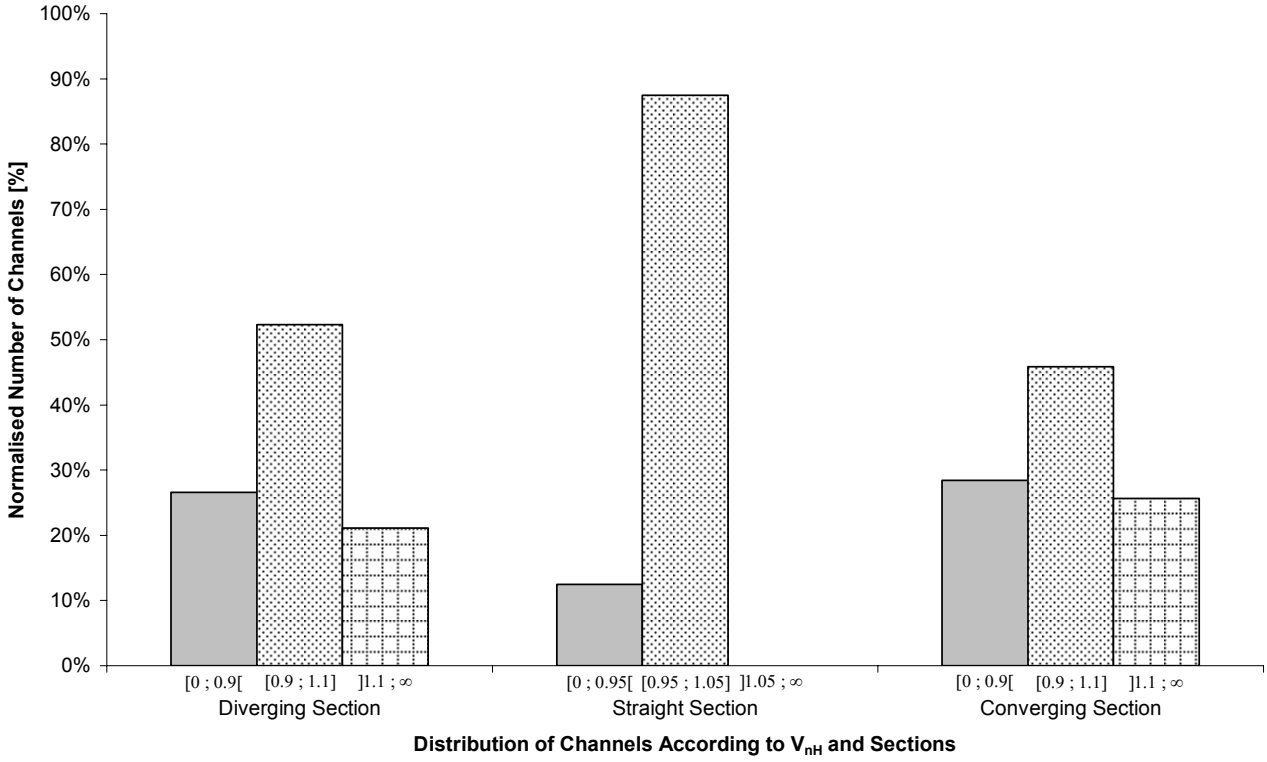

Figure 4.24: Frequency Distribution for Case 1

The optimisation of the diverging and converging channels is based on the information received from the simulation as described in section 4.3.1. In particular, this information is used to optimise the absorber geometry of section 4.2.6 by identifying channels with disproportionate low or high flow rates, as shown in Figure 4.24 and Figure 4.25. Then, these sections are re-calculated according to equation (4-26) by using the simulated velocity values in the flow direction, the expected flow rates for homogenous flow distribution and the deviation to homogenous flow distribution, respectively. The resulting channel widths are applied to the parametric CAD model and then it is exported for the next simulation run.

All equations regarding the optimisation of the channel structure are represented for a single layer only as the number of channels changes from layer to layer along the flow direction.

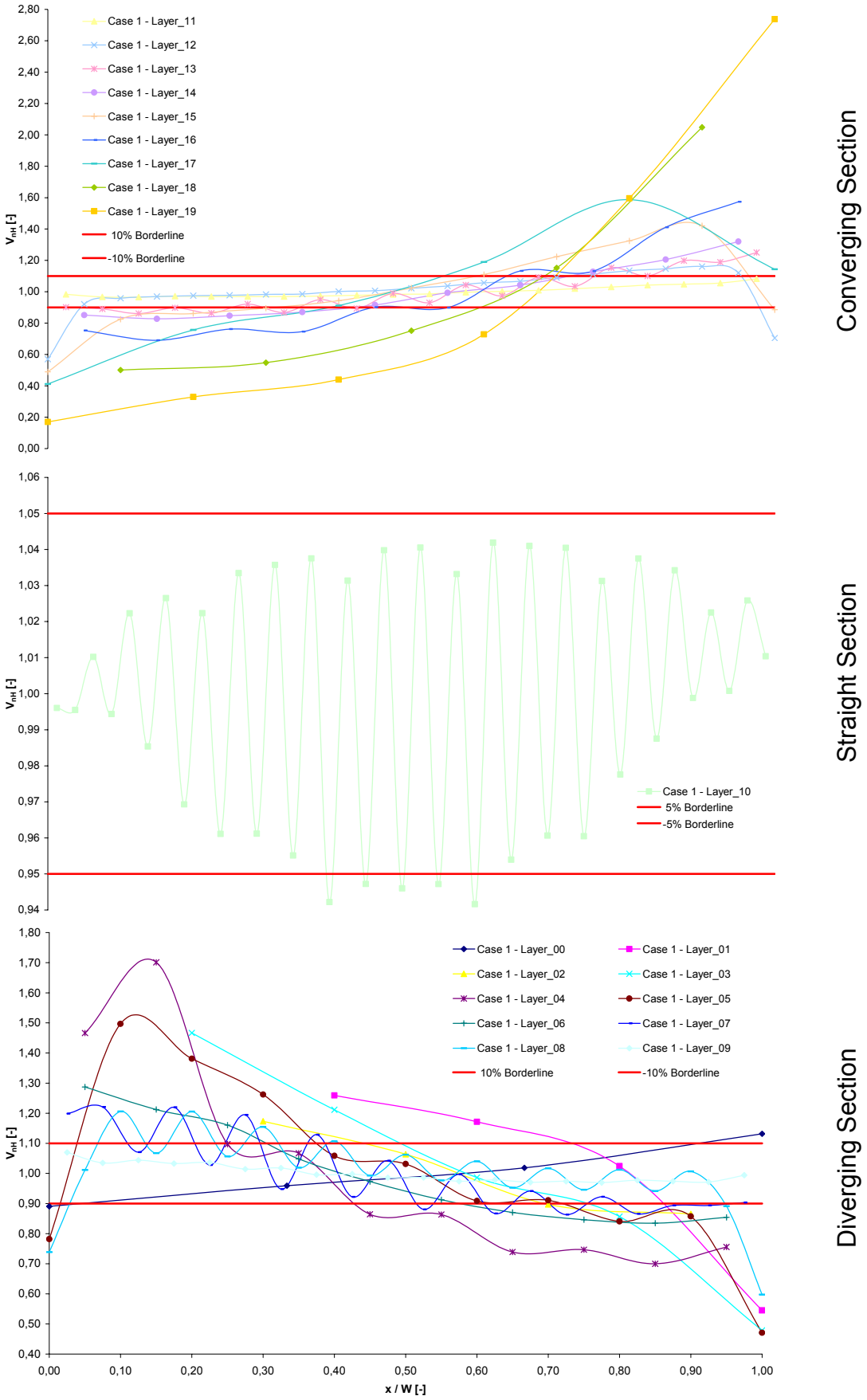

Figure 4.25: Flow Distribution of the Absorber with Corrugated Pattern Case 1

The approximated flow rates in the channels for the successive model (i+1) is based on:

$$\dot{V}_{i+1,j} = v_{i,j}\ A_{i+1,j} = v_{i,j}\ b_{i+1,j}\ h \qquad (4\text{-}18)$$

with

$A_{i+1,j}$	Area of duct j in model i+1	[m²]
$b_{i+1,j}$	Width of duct j in model i+1	[m]
$\dot{V}_{i+1,j}$	Flow rate in duct j in model i+1	[m³ s^{-1}]

Furthermore, the ratio of equation (4-18) and (4-13) represents the normalised flow rates for the channels in model i+1:

$$\dot{V}_{nH_{i+1,j}} = \frac{\dot{V}_{i+1,j}}{\dot{V}_H} = \frac{n\ v_{i,j}\ b_{i+1,j}}{\sum_{j=1}^{n}\left(v_{i,j}\ b_{i,j}\right)} \qquad (4\text{-}19)$$

with

$\dot{V}_{nH_{i+1,j}}$	Normalised flow rate of duct j in model i+1	[-]

The difference between the flow rates from the successive model and the normalised homogenous flow distribution is scaled to the normalised homogenous flow distribution. Consequently, equation (4-20) expresses the order of deviation of the flow rate in channel j in the successive model relative to the homogenous flow distribution in this layer.

$$\Delta\dot{V}_{n_{i+1,j}} = \frac{\dot{V}_{i+1,j} - \dot{V}_{Hn}}{\dot{V}_{Hn}} = \dot{V}_{nH_{i+1,j}} - 1 \qquad (4\text{-}20)$$

with

$$\dot{V}_{Hn} = \frac{\dot{V}_H}{\dot{V}_o} = \frac{1}{n}$$

with

$\dot{V}_{Hn}$	Normalised ideal flow rate	[-]
$\Delta\dot{V}_{n_{i+1,j}}$	Normalised flow rate deviation of channel j in model i+1	[-]

With the aim of reducing the number of iterations, a case differentiation is introduced when calculating the width of the channels for the successive model (i+1). In the first case equation (4-20) should be zero:

$$\Delta\dot{V}_{n_{i+1,j}} \overset{!}{=} 0 \tag{4-21}$$

$$\frac{n\, v_{i,j}\, b_{i+1,j}}{\sum_{j=1}^{n}\left(v_{i,j}\, b_{i,j}\right)} - 1 \overset{!}{=} 0$$

$$b_{i+1,j} \overset{!}{=} \frac{\sum_{j=1}^{n}\left(v_{i,j}\, b_{i,j}\right)}{n\, v_{i,j}} \tag{4-22}$$

In the second case the channel width should be overestimated compared to the previous equations (4-21) and (4-22). The approximation is based on the normalised flow rate deviation $\Delta\dot{V}_{n_{i,j}}$ of the current model (i), which is calculated using $\dot{V}_{nH_{i,j}}$ according to equation (4-16). The derivation is consistent with $\Delta\dot{V}_{n_{i+1,j}}$ of equation (4-20). $\Delta\dot{V}_{n_{i,j}}$ expressed in % represents the deviation of the effective channel flow to homogenous flow-distribution in the corresponding layer.

$$\Delta\dot{V}_{n_{i,j}} = \dot{V}_{nH_{i,j}} - 1 = \frac{n\, v_{i,j}\, b_{i,j}}{\sum_{j=1}^{n}\left(v_{i,j}\, b_{i,j}\right)} - 1 \tag{4-23}$$

With equation (4-23) the absorber width for the second case can be calculated by following equations:

$$\Delta\dot{V}_{n_{i+1,j}} \overset{!}{=} -\Delta\dot{V}_{n_{i,j}}$$

$$\Delta\dot{V}_{n_{i+1,j}} \overset{!}{=} 1 - \dot{V}_{nH_{i,j}} \tag{4-24}$$

$$b_{i+1,j} \overset{!}{=} \frac{2\sum_{j=1}^{n}\left(v_{i,j}\, b_{i,j}\right) - n\, v_{i,j}\, b_{i,j}}{n\, v_{i,j}} \tag{4-25}$$

The first case, here equation (4-22), will be applied when the result of equation (4-23) expressed as percentage is less than or equal to 5%. Equation (4-25) as a second case, however, will be applied when equation (4-23) is more than 5%. The optimisation algorithm can finally be summarised by the following expression:

$$b_{i+1,j} := \begin{cases} \dfrac{\sum_{j=1}^{n}\left(v_{i,j}\ b_{i,j}\right)}{n\ v_{i,j}} & if \quad \dfrac{n\ v_{i,j}\ b_{i,j}}{\sum_{j=1}^{n}\left(v_{i,j}\ b_{i,j}\right)} - 1 \le 0.05 \\ \dfrac{2\sum_{j=1}^{n}\left(v_{i,j}\ b_{i,j}\right) - n\ v_{i,j}\ b_{i,j}}{n\ v_{i,j}} & if \quad \dfrac{n\ v_{i,j}\ b_{i,j}}{\sum_{j=1}^{n}\left(v_{i,j}\ b_{i,j}\right)} - 1 > 0.05 \end{cases} \tag{4-26}$$

with

$b_{i,j}$	Width of duct j in the current model i	[m]
$b_{i+1,j}$	Width of duct j for the successive model i+1	[m]
h	Height of duct	[m]
n	Number of ducts in layer	[-]
$v_{i,j}$	Flow velocity in duct j of model i	[m s^{-1}]

The optimisation process is controlled by the overall normalised flow rate deviation $\Delta\dot{V}_{o_i}$ calculated for the whole model according to equation (4-27).

$$\Delta\dot{V}_{o_i} = \sum_{k=1}^{m}\left(\sum_{j=1}^{n_k}\left(\left|\frac{\dot{V}_{i,k,j} - \dot{V}_{Hn_k}}{\dot{V}_{Hn_k}}\right|\right)\right) = \sum_{k=1}^{m}\left(\sum_{j=1}^{n_k}\left(\left|\dot{V}_{n_{i,k,j}} - 1\right|\right)\right)$$

$$\Delta\dot{V}_{o_i} = \sum_{k=1}^{m}\left(\sum_{j=1}^{n_k}\left(\left|\frac{n_k\ v_{i,k,j}\ b_{i,k,j}}{\sum_{j=1}^{n_k}\left(v_{i,k,j}\ b_{i,k,j}\right)} - 1\right|\right)\right) \tag{4-27}$$

with

$\Delta\dot{V}_{O_i}$	Overall normalised flow rate deviation of model i	[-]

n_k	Maximum number of channels in layer k	[-]
m	Maximum number of layers	[-]

Figure 4.26 shows $\Delta\dot{V}_{o_i}$ for various optimised cases. The possible changes according to Table 4.7 were decreasing, as for example the minimum or maximum channel width was already reached in certain channels. The iterative optimisation process was terminated after case 7 as changes in the overall normalised flow rate deviation were minimal for the last three steps.

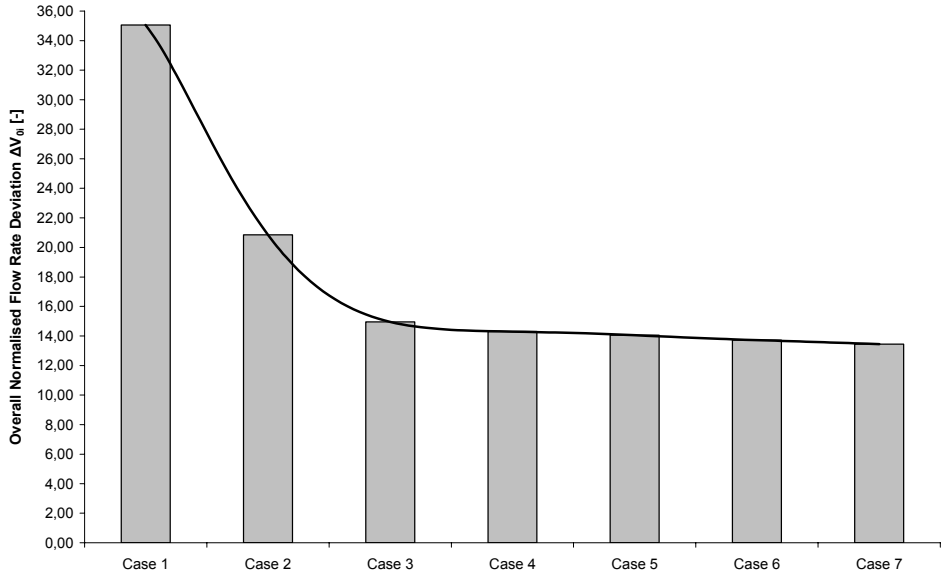

Figure 4.26: Trend of Overall Normalised Flow Rate Deviation $\Delta\dot{V}_{o_i}$ for the Optimisation Steps

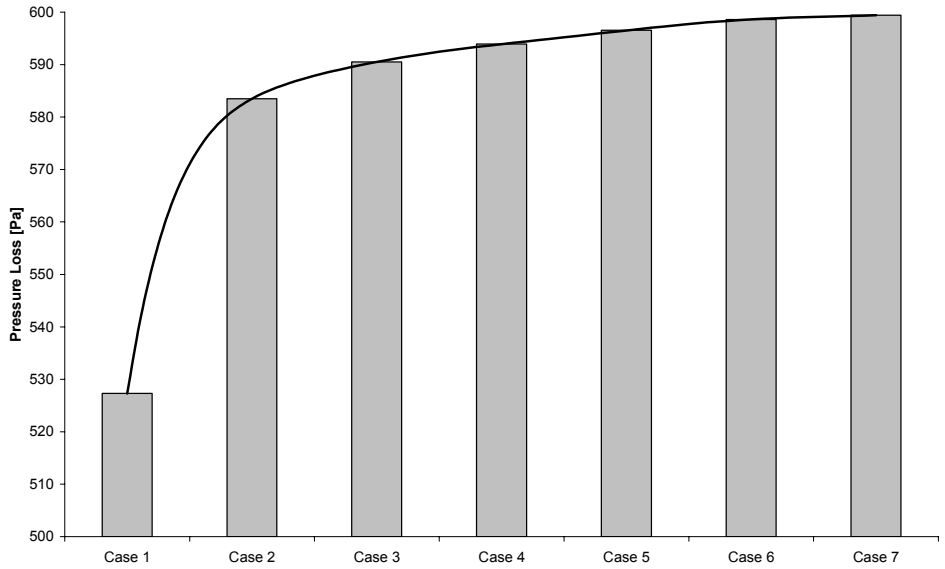

Figure 4.27: Trend of Pressure Loss for Various Optimisation Steps for a Flow Rate of 60 l h^{-1}

In contrast to the overall normalised flow rate deviation, the pressure loss increased from case 1 onwards. However, from case 2 to case 3 the slope is already less than 10 Pa and thus can be neglected in the subsequent cases as illustrated in Figure 4.27.

The following diagrams focus on absorber case 7 as a final iteration. Figure 4.30 shows the flow distribution in every channel of the absorber. Compared to Figure 4.25, the flow rate is much more balanced in all channels due to customised widths. The few channels below the -10% threshold in the diverging and converging section of Figure 4.30 are caused by the given limit of 14 mm channel width of the rollbond process. Above the +10% threshold only ten channels could not be customised because of the width limit of 6.5 mm. The straight channel section shows a more homogenous flow distribution than in the initial simulation, caused by an improved channel structure in the diverging and converging section. Apart from a more homogenous flow distribution another advantage is an increased total length at equalised flow rates as homogeneity starts/ends in the diverging/converging section. Detailed descriptions as well as figures of distinguishing layers between case 1 and case 7 are given in Treikauskas et al (2008).

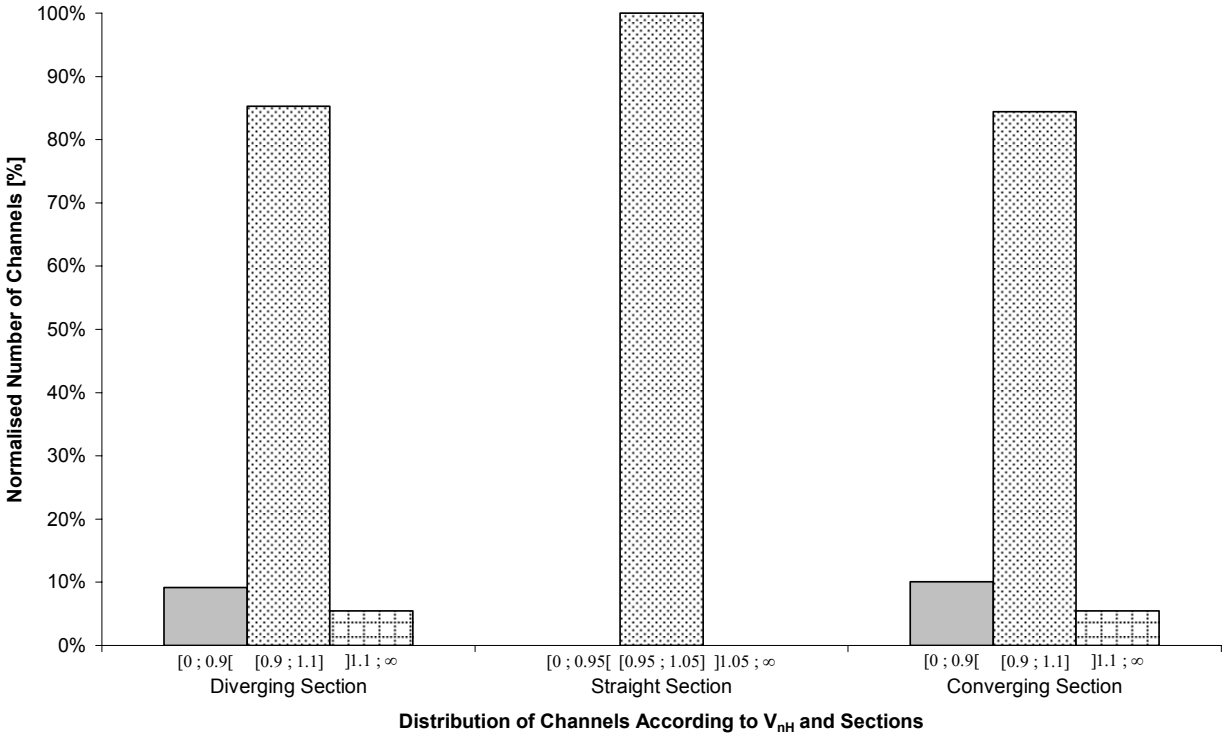

Figure 4.28: Frequency Distribution for Case 7

Figure 4.28 outlines the frequency distribution for case 7. In the diverging section the ratio of the number of channels within the thresholds and the total amount of channels in

this section could be increased to 85%. Hence, an improvement of about 63% was achieved compared to the number of channels within the ±10% borderline in the diverging section of case 1. In the converging section an improvement of 84% was reached versus case 1 and the proportion of channels within the thresholds increased to 84%.

Pressure Loss

While Figure 4.27 shows the trend of the pressure loss during the optimisation for a flow rate of 60 l h^{-1}, Figure 4.29 presents the pressure loss of case 1 and case 7. The graphs below show the pressure loss for the typical flow rate range. Furthermore, the pressure loss of the reference model, namely the header-riser absorber, is shown. As anticipated, it is lower than for the cases of the absorber with corrugated pattern. The difference can be explained by a far larger and complex channel system with a greater area of contact and more changes in directions. Hence, changes in momentum and friction losses are higher. In contrast to the reference absorber, other developments are above the simulated cases as shown in Figure 4.29 for the FracTherm absorber (Hermann 2005). The graphs demonstrate that the simulated curves are in the range of other rollbond manufactured panels while the header-riser absorber proves to have a lower pressure loss.

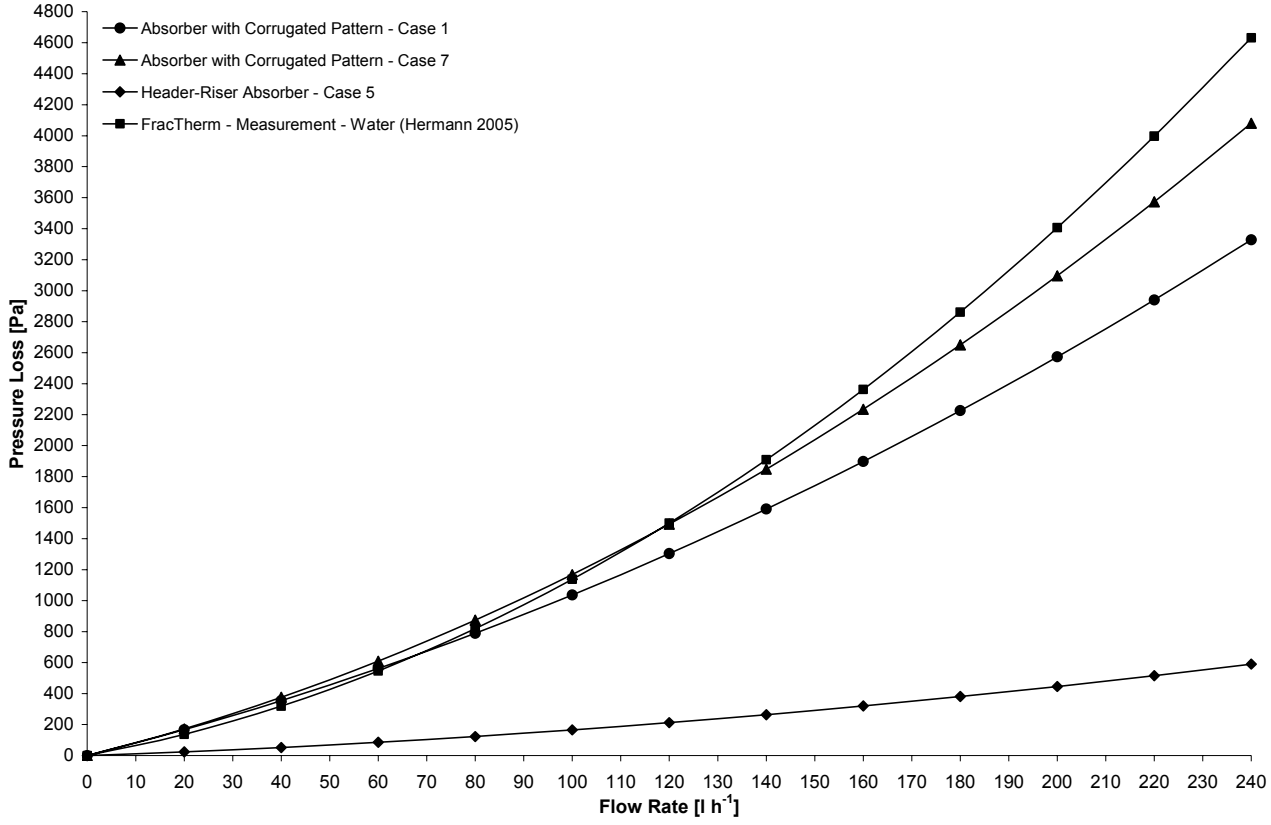

Figure 4.29: Pressure Loss of the Absorbers with Corrugated Pattern in Comparison with Other Absorbers

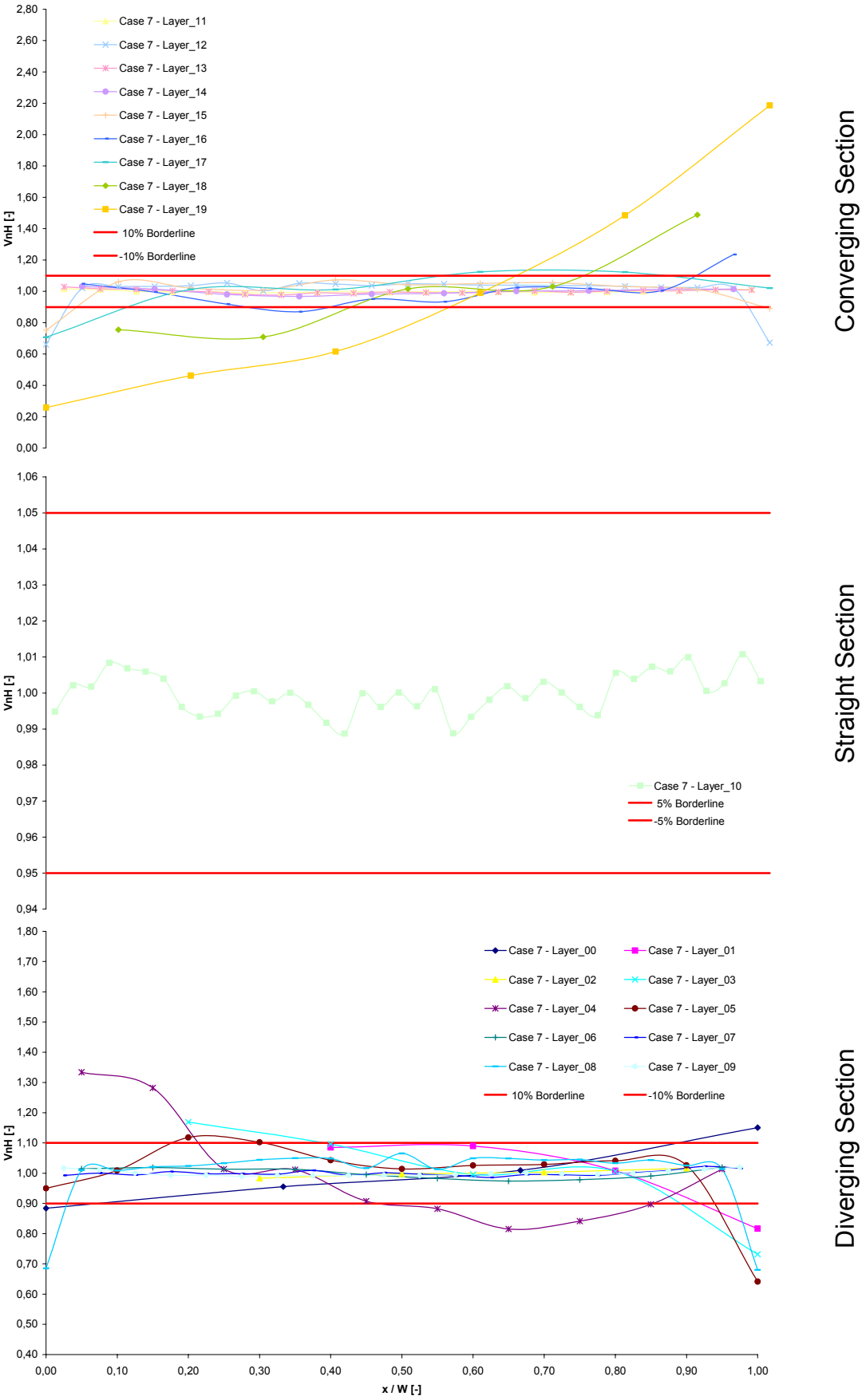

Figure 4.30: Flow Distribution of the Absorber with Corrugated Pattern Case 7

4.3.5 Evaluation and Conclusions

In the course of flow simulations, different absorbers were considered and further optimised. As far as possible, the results were compared with available simulation or measurement results of others for validating the established models. The simulation results may be summarised as follows:

- In the first instance the header-riser absorber was modelled in order to have a reference system for testing the application of CFD in this context, since its configuration has been very well investigated in solar absorber applications and in others. The analysis in the field of header-riser absorbers showed excellent agreement between simulated and measured data.
- As explained in section 3.6 the sandwich absorber cannot be modified to form an effective prototype because of the limited properties of the glue used for connecting the sandwich sheets. Due to the simple and effective design, however, it was considered further. The pressure loss of case 4, for example, is far below the absorber with corrugated pattern concept case 7 (corrugated sheet absorber case 4 is up to 97% lower, see Figure 4.22 and Figure 4.27) and the header-riser absorber case 1 (corrugated sheet absorber case 4 is up to 75% lower, see Figure 4.22). This low pressure loss, however, is attributed to very low flow velocities in the riser channels.

  Furthermore, it is possible to transfer the theory and dimensioning from header designs to the sandwich design and obtain a high quality flow distribution even with a high number of channels. The deviation from homogenous flow distribution of case 4 is well within the range of the improved header-riser case 3 and far better than the state-of-the-art.
- Due to the rollbond manufacturing process, a flexible channel structure can be realised in concept 2, the absorber with corrugated pattern. However, without optimisation an equal flow distribution cannot be reached. In contrast to both other absorber designs modelled, the rollbond manufacturing process does not allow a channel width greater than 14 mm, thus a central diverging and converging header duct cannot be realised. Therefore, these headers are replaced by a diverging and converging area containing many channels with alternating and increasing/decreasing channels from the inlet to the outlet. The CFD simulation provides an important tool for optimising

both areas by an iterative method. However, the pressure loss was increased by about 12% compared to the initial case 1.

4.4 Efficiency Calculations

The efficiency of solar thermal collectors can be calculated as usual by the incoming and outgoing energies or heat flows, respectively. Figure 4.31 shows the incoming solar irradiance diminished by the effective transmittance absorptance product of the glass cover and the absorbers selective surface. This heat flow is decreased by the heat loss flow from the absorber to the environment.

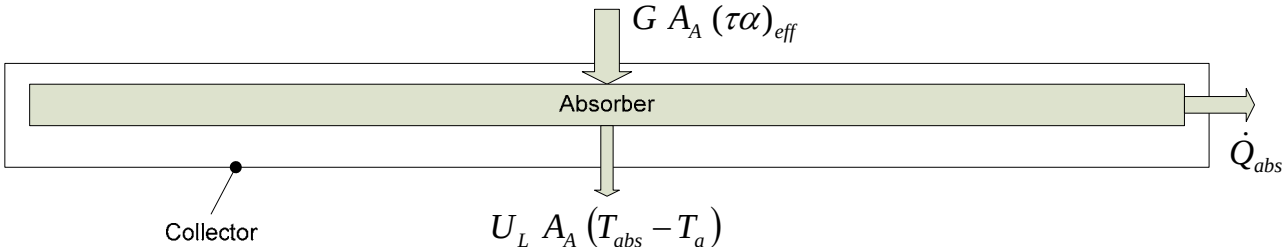

Figure 4.31: Energy Balance of a Solar Thermal Collector

The usable heat flow is given by equation (4-28):

$$\dot{Q}_{abs} = G\ A_A\ (\tau\alpha)_{eff} - U_L\ A_A\ (T_{abs} - T_a) \qquad (4\text{-}28)$$

with

A_A	Absorber area	[m²]
G	Irradiance	[W m^{-2}]
Q_{abs}	Usable heat flow	[W]
T_{abs}	Mean absorber sheet temperature	[K]
T_a	Ambient temperature	[K]
U_L	Collector overall heat loss coefficient (based on T_{abs})	[W m^{-2}K^{-1}]
$(\tau\alpha)_{eff}$	Effective transmittance absorptance product	[-]

The effective transmittance absorptance product $(\tau\alpha)_{eff}$ accounts for the multiple radiation reflections between the absorber and the transparent cover. It can be calculated according to Duffie and Beckman (2006):

$$(\tau\alpha)_{eff} = \frac{\tau\ \alpha}{1-(1-\alpha)\,\rho_c} \qquad (4\text{-}29)$$

with

α	Absorptance of absorber coating – Appendix D	[-]
ρ_c	Reflectance of transparent cover – Appendix D	[-]
τ	Transmittance of transparent cover – Appendix D	[-]

With the overall heat flux on the absorber surface, the collector efficiency can be calculated according to equation (4-31):

$$\eta = \frac{\dot{Q}_{abs}}{A_A\ G} \qquad (4\text{-}30)$$

$$\eta = (\tau\alpha)_{eff} - U_L\ \frac{(T_{abs} - T_a)}{G} \qquad (4\text{-}31)$$

with

η	Collector efficiency	[-]

The average absorber temperature T_{abs} used in equation (4-31) is difficult to measure and to calculate, therefore the efficiency is normally related to the local fluid temperature T_f (Duffie & Beckman 2006; Eicker 2003). At the same time, the collector efficiency factor *F'* is introduced according to equation (4-32) as a factor to account for the fact that the absorber is actually not at local fluid temperature:

$$\eta = F'\,(\tau\alpha)_{eff} - F'\,U_L\ \frac{(T_f - T_a)}{G} \qquad (4\text{-}32)$$

with

F'	Collector efficiency factor	[-]
T_f	Local fluid temperature	[K]

Equation (4-32) can be rewritten by combining the first term to the collector efficiency without irradiation η_0 and by summarising the collector efficiency factor *F'* and the collector overall heat loss coefficient U_L to the measured (in case of a linear curve fitting) heat loss coefficient *U* based on the temperature T_f:

$$\eta = \eta_0 - U \frac{\left(T_f - T_a\right)}{G} \qquad (4\text{-}33)$$

The physical definition of F' is given by Duffie and Beckman (2006):

> *"At a particular location, F' represents the ratio of the actual useful energy gain to the useful gain that would result if the collector absorbing surface had been at the local fluid temperature."*

The collector efficiency factor is used in general to describe the efficiency of an absorber design. In the following sections, several equations of the collector efficiency factor corresponding to different absorber designs are explained. Furthermore, results for the concepts discussed in section 4.2 and 4.3 are presented.

The heat loss of a solar thermal collector consisting of heat conduction, convection and radiation is represented by an overall heat loss coefficient U_L together with a consistent temperature difference between absorber temperature T_{abs} and ambient temperature T_a. It is necessary to mention that the equations shown above are based on linear heat losses from the absorber to the environment. However, heat losses caused by radiation and convection increase non-linearly with absorber temperature, hence, measurement data are approximated by a quadratic function (Deutsches Institut für Normung 2006) as shown in equation (5-1) of section 5.5.1.

4.4.1 State-of-the-Art: Header-Riser Absorber

Much research has been carried out on state-of-the-art collectors with sheet-pipe absorbers. In 1942, Hottel and Woertz (1942) published the first detailed measurements and equations on typical flat-plate collectors which are still used and continually improved. Whillier (1953) also employed this theory and additionally derived equations of the heat removal factor and the collector efficiency factor for further absorber designs. The heat removal factor was primarily used in the past as the collector efficiency was related to the collector fluid inlet temperature (Eisenmann 2003). However, Whillier (1953) already mentioned the importance of the collector efficiency factor for evaluating different absorber designs:

"The coefficient F' is a measure of the effectiveness of the geometry of the fluid flow-circuit in the removal of the energy from the collector."

Today the collector efficiency factor *F'* for sheet-pipe absorbers is well documented in the relevant literature (Duffie & Beckman 2006; Eicker 2003; Eisenmann 2003; Tiwari 2002). In the following, a short overview how to develop the collector efficiency factor is given.

In case of finned absorbers, the temperature distribution on the fin has to be derived first. This leads to a second-order differential equation which can be solved analytically by two boundary conditions. The first boundary condition is shown in Figure 2.21 where at the midpoints between two tubes the maximum temperature is reached and thus the temperature gradient is zero. As second boundary condition the temperature at the fin above the fluid pipe is assumed similar to a typical cooling fin problem with base temperature T_b.

The differential equation for the temperature distribution can be solved by substitution and by introducing the variable *m* for simplification as represented in equation (4-34):

$$m = \sqrt{\frac{U_L}{\lambda_S \, \delta}} \qquad (4\text{-}34)$$

with

δ	Sheet thickness	[m]
λ_S	Thermal conductivity of absorber sheet – Appendix D	[W m^{-1}K^{-1}]

Finally, the collected heat flow from both fin wings can be calculated and the fin efficiency *F* results as follows in equation (4-35):

$$F = \frac{\tanh\left(m \frac{W-D}{2}\right)}{m \frac{W-D}{2}} \qquad (4\text{-}35)$$

with

F	Fin efficiency factor	[-]
D	External diameter of riser pipe	[m]
W	Distance between risers	[m]

The wings' heat flow summed with the directly absorbed heat flow from the area above the fluid pipe must be equal to the heat flow transferred via the tube/sheet connection and by convection to the heat carrier fluid. Now the base temperature T_b can be eliminated and from the resulting heat flow equation the collector efficiency factor *F'* can be defined as shown in equation (4-36):

$$F' = \frac{\frac{1}{U_L}}{W\left[\frac{1}{U_L\left[D+(W-D)F\right]}+\frac{1}{C_b}+\frac{1}{\pi\, d_R\, h_{fi}}\right]} \qquad (4\text{-}36)$$

with

C_b	Bond conductance between riser and sheet – Appendix D	[W m^{-1}K^{-1}]
d_R	Internal diameter of riser pipe	[m]
h_{fi}	Heat transfer coefficient	[W m^{-2}K^{-1}]

Figure 4.32 illustrates the geometry of an absorber fin with mounted risers beneath the radiation absorbing surface as well as the relevant parameters of equations (4-34) to (4-39).

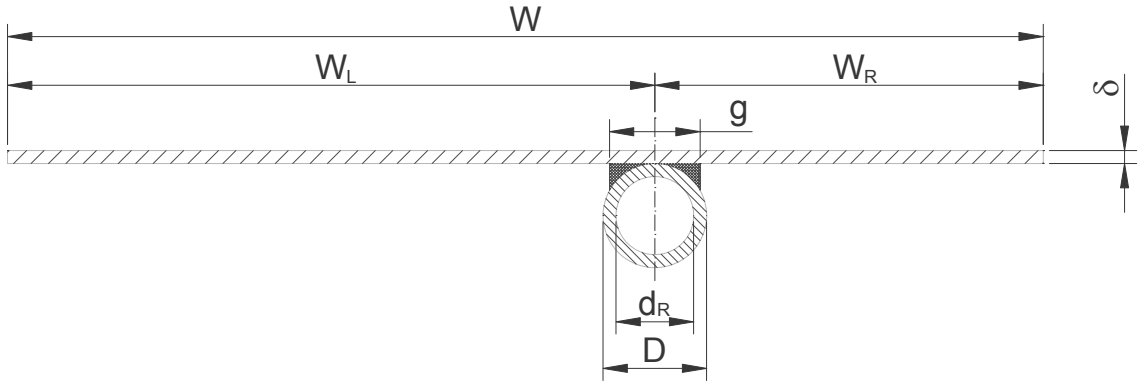

Figure 4.32: Geometry and Notation of an Absorber Fin

Contrary to the assumption (*g* = *D*) made by Duffie and Beckman (2006), the connection between sheet and pipe is not equal to the riser pipes diameter in real absorbers with risers beneath the sheet. Eisenmann (2003) derived a collector efficiency factor and corresponding fin efficiency with a reduced contact area as shown in equation (4-37), where

g represents the contact width (Figure 4.32) and k_{gf} represents the heat conductivity from the sheet to the pipe as well as the heat transfer to the fluid:

$$F' = \frac{1}{W\left[\frac{1}{\left[(W-g)\,F+g\right]}+\frac{U_L}{k_{gF}\;\pi\;d_R}\right]}$$ (Eisenmann 2003) (4-37)

with

g	Bond conductance width	[m]
k_{gF}	Heat transmission coefficient	[W m^{-2}K^{-1}]

In equation (4-37) the contact width is considered by its real value and the heat transfer from the contact area to the fluid is again modelled physically by a circular fin. Despite the enhancement of the collector efficiency factor *F'* it is close to the one given by Duffie and Beckman (2006) and the deviation between both approaches is small in case of highly conductive connections as are normally realised in case of metal-to-metal connections (Eisenmann 2003). Therefore, for further investigations of the header-riser design studies the equations given by Duffie and Beckman (2006) are applied.

As the outer fins of an absorber must not be compulsorily symmetric the following equations are applied instead for the fin efficiency and collector efficiency factor. Due to the complex fin geometries of the bionic absorber of Hermann (2005) a similar approach was applied.

$$F_{as} = \frac{\tanh\left[m\left(W_L-\frac{D}{2}\right)\right]+\tanh\left[m\left(W_R-\frac{D}{2}\right)\right]}{m\left(W_L+W_R-D\right)}$$ (4-38)

$$F'_{as} = \frac{\frac{1}{U_L}}{\left(W_L+W_R\right)\left[\frac{1}{U_L\left[D+\left(W_L+W_R-D\right)F_{as}\right]}+\frac{1}{C_b}+\frac{1}{\pi\;d_R\;h_{fi}}\right]}$$ (4-39)

with

F_{as}	Fin efficiency factor for asymmetric fin	[-]
F'_{as}	Collector efficiency factor for asymmetric fin	[-]

W_L	Left fin width	[m]
W_R	Right fin width	[m]

A mean collector efficiency factor is calculated for the whole absorber by normalising *F'* with the ratio of the corresponding fin area to the overall absorber area; hence the absorber is subdivided into fin stripes. Equation (4-40) shows the correlation while *F'* can also substituted by F'_{as}. Equation (4-41) represents the mean collector efficiency factor for the overall absorber.

$$F'_{FN} = F' \frac{A_{Fin}}{A_A} \tag{4-40}$$

$$F'_m = \sum_{j=1}^{n} F'_{FN_j} \tag{4-41}$$

with

A_{Fin}	Fin area	[m²]
A_A	Absorber area	[m²]
F'_{FN_j}	Normalised collector efficiency factor of fin j	[-]
F'_m	Averaged collector efficiency factor	[-]
n	Number of fins (risers)	[-]

The heat transfer coefficient h_{fi} in equations (4-36) and (4-39) is calculated by the mean Nusselt number based on the simulated velocity for each channel. Laminar flow conditions are assumed as already discussed in section 4.2.3 and the Nusselt number formulae correspond to a constant heat flux boundary condition and hydrodynamic and thermal fully developed flow. The temperature dependent properties of water are taken from Martin et al (2002) as well as the following equations for the mean Nusselt number.

$$Nu_{m,q} = \left[Nu_{m,q,1}^3 + 0.6^3 + \left(Nu_{m,q,2} - 0.6 \right)^3 \right]^{\frac{1}{3}} \tag{4-42}$$

with

$$Nu_{m,q,1} = 4.364 \tag{4-43}$$

$$Nu_{m,q,2} = 1.953\left(\mathrm{Re}\ \mathrm{Pr}\ \frac{d_R}{l}\right)^{\frac{1}{3}} \qquad (4\text{-}44)$$

with

l	Pipe length	[m]
$Nu_{m,q}$	Averaged Nusselt number	[-]
$Nu_{m,q,1}$	First asymptote for the averaged Nusselt number	[-]
$Nu_{m,q,2}$	Second asymptote for the averaged Nusselt number	[-]
Pr	Prandtl number	[-]
Re	Reynolds number	[-]

Now the heat transfer coefficient h_{fi}, used in equations (4-36) and (4-39), is calculated according to equation (4-45):

$$h_{fi} = \frac{\lambda_f}{d_R} Nu_{m,q} \qquad (4\text{-}45)$$

with

λ_f	Thermal conductivity of heat transfer fluid – Appendix D	[W m^{-1}K^{-1}]

Table 4.9 shows the results for the collector efficiency factor *F'* for state-of-the-art absorbers discussed in section 4.2.4 and 4.3.2 based on the assumptions illustrated in Appendix D / Table D.1.

Table 4.9: Calculated Collector Efficiency Factors for Header-Riser Absorber Types

	Case 1	**Case 2**	**Case 3**	**Case 4**	**Case 5**
Collector Efficiency Factor F' [-]	0.94	0.96	0.94	0.94	0.94

Table 4.9 indicates that all absorbers with 10 risers (case 1 and case 3 to 5) show the same collector efficiency factor. These cases differ in the header designs in order to gain equal flow distribution in the risers. However, the flow distribution in the investigated range does not show an impact on the collector efficiency factor.

By contrast, case 2 shows an increased collector efficiency factor, which is only caused by a decreased distance between the risers. The flow distribution quality, however, is

also decreased as illustrated in Figure 4.13 / case 2. The influence of an increased number of risers on the efficiency and material content was investigated by Eisenmann et al (2004). An effective optimisation of a header-riser absorber is restricted to smaller distances between the risers, which in turn result in a higher weight and increased costs. Additional parameters influencing the collector efficiency factor are presented in section 2.4.3. However, the possible modifications are accompanied by growing costs and weight when improving the collector efficiency factor.

F' calculations for header-riser absorbers at higher flow rates yield the same results between the discussed cases, although the flow distribution at higher flow rates is even more inhomogeneous. Due to the assumptions made in the theory of collector efficiency calculation the results for different flow distribution qualities (Table 4.9) and increased inlet velocities are equal. The decisive differences between theory and reality in this case are as follows:

- The assumption that the maximum fin temperature occurs in the centre between two risers is still valid, however, in risers with different flow rates and real operation the maximum temperature moves towards the riser with a lower flow rate.
- The effective flow conditions in the risers depend on flow velocity, local surface and temperature conditions. Therefore, the flow conditions along the riser pipes can change from laminar to turbulent flow and back with increasing and decreasing effects on heat transfer. According to Martin et al (2002) no exact transition point can be specified as it depends on locally prevailing conditions. The calculation procedure, however, is based on constant laminar flow and heat transfer conditions.
- The collector overall heat loss coefficient U_L is constant for each riser and along the riser length. In real operation non homogenous flow distribution causes a lower flow velocity in certain risers with again higher temperatures. In these regions the heat losses are increased due to a higher temperature gradient to the ambient. Although, the influence of the flow maldistribution on the average plate temperature, hence, the overall heat loss coefficient U_L is low, it has to be noted at this point. Moreover, Duffie and Beckman (2006) showed a significant impact on the top loss coefficient of a flat-plate collector at higher plate temperatures changes. Those higher plate temperature changes, for example, can occur in areas with a great flow maldistribution (dead wa-

ter zones), see Figure 2.10. The general influence of the collector overall heat loss coefficient U_L on the collector efficiency factor *F'* is shown in Figure 2.22.

Therefore, the results for the collector efficiency factor for different flow distribution qualities as well as increased inlet velocities are expected to be different in real operation. In case of a more homogenous flow distribution an increased collector efficiency can be assumed.

4.4.2 Volumetric Absorbers

Volumetric absorbers for flat-plate collectors are poorly investigated in contrast to sheet-pipe absorbers whose collector efficiency factors are derived and explained in solar engineering literature. For that reason, the following sections show the derivation of the collector efficiency factor for an overall volumetric absorber.

Figure 4.33 illustrates the heat flux in a volumetric absorber section. The thermal resistance in the irradiance absorber surface is not neglected. Therefore, the useful heat flux is represented by equation (4-46):

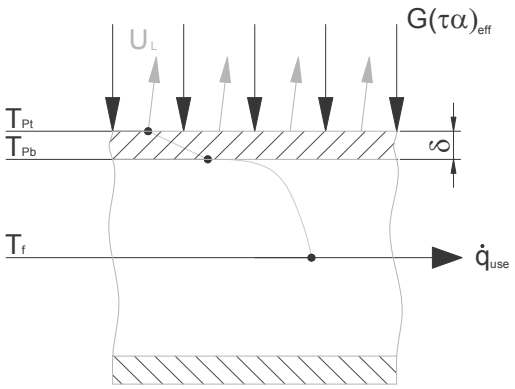

Figure 4.33: Heat Flow in a Volumetric Absorber Section

$$\dot{q}_{use} = \frac{1}{\frac{\delta}{\lambda_S} + \frac{1}{h_{fi}}} \left(T_{Pt} - T_f\right) \qquad (4\text{-}46)$$

with

$\dot{q}_{use}$	Usable heat flux	[W m^{-2}]
T_{Pt}	Local plate temperature	[K]

The unknown plate temperature T_{Pt} (equation (4-48)) is calculated by the usable heat flux $\dot{q}_{use}$ (4-46) and the heat flux from the sun $\dot{q}_{sun}$ (4-47) and then substituted in equation (4-46):

$$\dot{q}_{sun} = G\left(\tau\alpha\right)_{eff} - U_L\left(T_{Pt} - T_a\right) \qquad (4\text{-}47)$$

$$T_{Pt} = \frac{G\left(\tau\alpha\right)_{eff} + U_L\, T_a + \left(\frac{1}{\frac{\delta}{\lambda_S} + \frac{1}{h_{fi}}}\right) T_f}{\left(\frac{1}{\frac{\delta}{\lambda_S} + \frac{1}{h_{fi}}}\right) + U_L} \tag{4-48}$$

$$\dot{q}_{use} = \frac{1}{1 + U_L\left(\frac{\delta}{\lambda_S} + \frac{1}{h_{fi}}\right)} \left[G\left(\tau\alpha\right)_{eff} - U_L\left(T_f - T_a\right) \right] \tag{4-49}$$

From equation (4-49) and the general definition of Duffie and Beckman (2006) the collector efficiency factor for a volumetric absorber with considered plate conductivity is represented by equation (4-50):

$$F' = \frac{1}{1 + U_L\left(\frac{\delta}{\lambda_S} + \frac{1}{h_{fi}}\right)} \tag{4-50}$$

The consideration of heat conductivity is important for plate materials with a low thermal conductivity, e.g. polymers. However, in case of highly conductive materials like aluminium or copper it can be neglected. If λ_S approaches infinity the collector efficiency factor is equal to the result of Bliss (1959) as shown in equation (4-51):

$$\lim_{\lambda_S \to \infty} \frac{1}{1 + U_L\left(\frac{\delta}{\lambda_S} + \frac{1}{h_{fi}}\right)} \to \frac{h_{fi}}{h_{fi} + U_L}$$

$$F' = \frac{h_{fi}}{h_{fi} + U_L} \tag{4-51}$$

In case of the corrugated sheet absorber concept of section 4.2.5 the collector efficiency factor is based on equation (4-51) as the material used for channels and sheets is aluminium. The heat transfer coefficient is calculated according to equations (4-42) - (4-45).

However, the characteristic dimension is changed from the riser diameter d_R to the hydraulic diameter d_h:

$$d_{h_j} = \frac{4\,A_j}{U_j} \tag{4-52}$$

with

A_j	Cross section of duct	[m²]
d_{h_j}	Hydraulic diameter of duct	[m]
U_j	Perimeter of duct	[m]

The mean collector efficiency factor is calculated like in equations (4-40) and (4-41) and results in 0.995 for all cases of Table 4.6. The values for the calculation are given in Appendix D / Table D.1. Although, huge differences in the flow distribution are simulated as presented in Figure 4.20, no difference in the collector efficiency factor can be found.

The reasons for this result are the same as listed in section 4.4.1. Additionally, the flow velocities in all channels are very low due to the very large number of channels. Consequently, the Reynolds and the Nusselt number as well as the heat transfer coefficient are also very low and show no effect on the collector efficiency factor. The calculated Nusselt numbers, in particular, are close to the asymptote given in equation (4-43), hence, changes in the flow velocity cannot further reduce or significantly increase the Nusselt number and F' remains almost constant.

4.4.3 Concept 2: Absorber with Corrugated Pattern

The complex channel structure of the absorber with corrugated pattern requires a partitioning according to Figure 4.11. For the illustrated sections the collector efficiency factor is calculated by the sheet-pipe as well as the volumetric approach as listed in Table 4.10.

Table 4.10: Collector Efficiency Factor Calculation for the Absorber with Corrugated Pattern

Section	Sheet-Pipe Approach	Volumetric Approach
Inlet Channel	•	
Inlet Section	•	
Diverging Section		•
Straight Channel Section	•	
Converging Section		•
Outlet Channel	•	

The volumetric approach chosen for the diverging and the converging section is applied as nearly 60% of the whole absorber surface is in contact with the heat transfer fluid due to the close channel structure. The largest distance between two channels is 14 mm. Furthermore, a comparison of the sheet-pipe approach (using a fin distance of 14 mm) and the volumetric approach showed at equal material properties and heat transfer conditions a difference of less than 0.5%.

The formulae given for the collector efficiency factor *F'* in section 4.4.1 are based on a pipe underneath an absorbing plate as shown in Figure 4.32. The channels in the absorber with corrugated pattern, however, are embedded in the absorber plate like in Figure 4.9. Therefore, the collector efficiency factor equation can be simplified by eliminating the bond heat conductivity term. Another difference is the channel shape, influencing the fin term and the heat transfer term:

$$F' = \frac{1}{\frac{W}{b + (W - b)\,F} + \frac{W\,U_L}{(2b + 2h)\,h_{fi}}} \qquad (4\text{-}53)$$

with

b	Width of duct	[m]
h	Height of duct	[m]

Asymmetric fins and the averaged collector efficiency factor are calculated on the basis of equations (4-38) - (4-41). Finally, for the absorber with corrugated pattern as illustrated in Figure 4.11 the mean collector efficiency factor *F'* is 0.99 based on the values for calculation illustrated in Appendix D / Table D.1. Due to its close channel structure the value is close to the results obtained for the corrugated sheet absorber. With respect to the internal fluid volume the absorber with corrugated pattern is, with 2.1 l, more advantageous than the corrugated sheet absorber designs with more than 7 l (Table 4.8).

Figure 4.34 provides an overview of the investigated collector efficiency factors and underlines the beneficial volumetric and quasi-volumetric absorber designs.

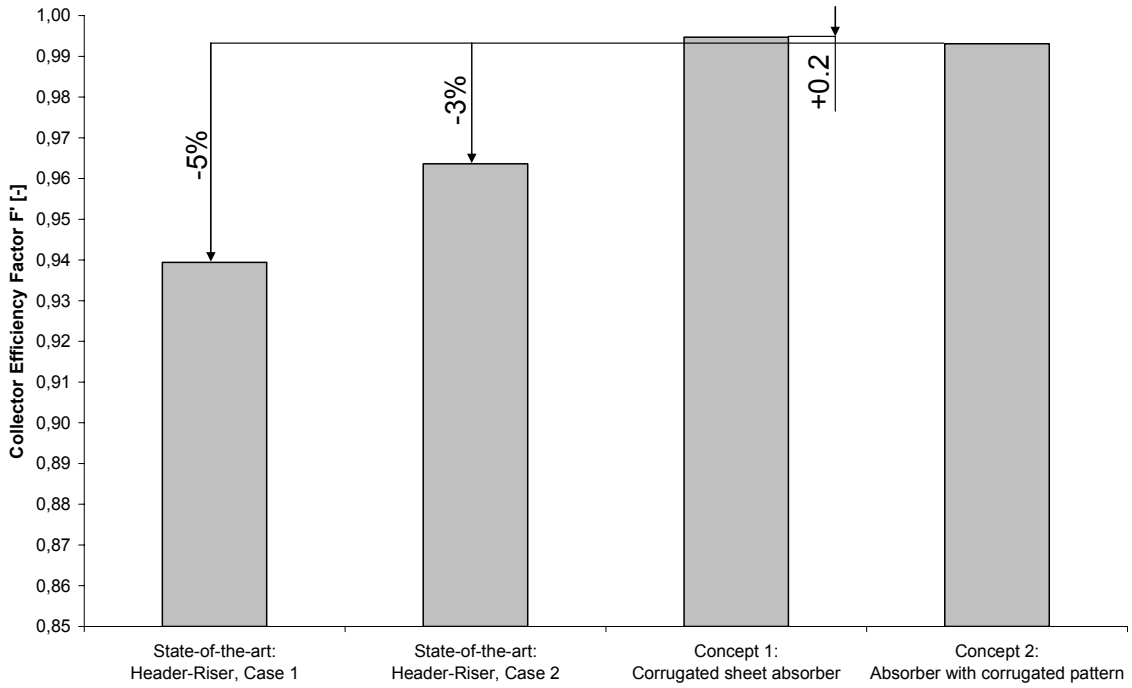

Figure 4.34: Collector Efficiency Factors for Different Absorber Designs

4.4.4 Conclusions

The previous sections show on the one hand different approaches for specifying the thermal efficiency for different absorber designs. On the other hand, the collector efficiency factor for the investigated absorber concepts is calculated showing the following:

- The header-riser absorber design based on the well-investigated formulae given in the literature shows, for this design, typical collector efficiency factors as shown in Table 2.5. Further efficiency improvement is strongly associated with higher material cost and an increased weight.

  At first sight a non-homogenous flow distribution seems to have no impact on the collector efficiency factor as assumptions in the calculation such as a constant overall collector loss coefficient or a constant laminar flow condition cannot provide more detailed analysis. However, it is expected that an absorber with equal flow distribution should show an improved collector efficiency factor in real operation.

- Based on the volumetric approach, the collector efficiency factor for the corrugated sheet absorbers shows a beneficial result. However, in real operation the collector efficiency of case 1 will be decreased due to its unfavourable flow distribution.

- Both approaches are used in the efficiency calculation of the absorber with corrugated pattern. In areas with no bifurcations and straight channels the sheet-pipe approach is applied and in the remaining areas the volumetric efficiency formula is used. As the channels are closely positioned the collector efficiency factor is in the range of the corrugated sheet absorber.
- The thermal efficiency of the corrugated pattern absorber is about 6% superior to the sheet-pipe absorber (case 1) that represents the state-of-the-art.

5 Experimental Analysis

The experimental analysis provided a basis for comparing the results gained from the simulations with results from prototype tests. Furthermore, the experimental outcomes of different absorber designs are compared to each other. As done in the theoretical analysis the experimental analysis considers flow distribution, pressure drop as well as absorber efficiency. The following sections introduce the different absorber prototypes and the measurements carried out at the laboratories of Ingolstadt University.

5.1 Prototypes

State-of-the-Art: Sheet-Pipe Absorber

The sheet-pipe absorber prototypes are of the same size as given in the specification in Appendix B. In contrary to the widespread use of copper sheets in solar thermal absorbers this prototype has attached an aluminium sheet with a thickness of 0.5 mm. Both absorbers, the state-of-the-art header-riser as well as the corrugated pattern absorber should have the same selective coating for the collector efficiency tests. The pipe geometry of headers and risers is the same as presented in section 4.2.4 / case 5, the piping material used is copper. Figure 5.1 shows the sheet-pipe absorber.

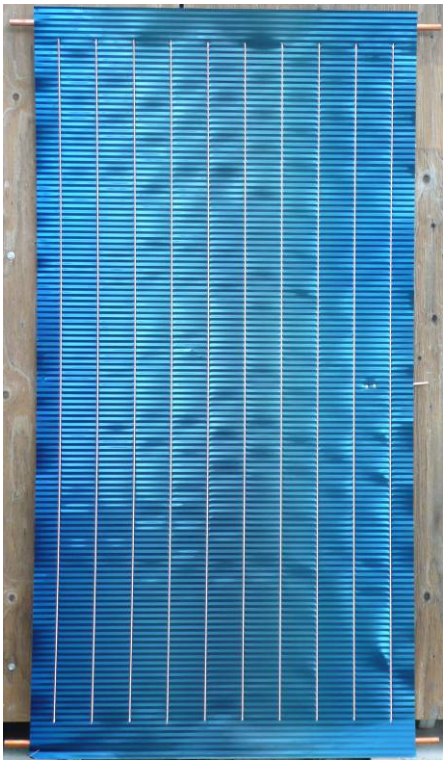

Figure 5.1: Sheet-Pipe Absorber Prototype (Header-Riser Design)

Concept 1: Corrugated Sheet Absorber

In the corrugated sheet absorber prototype as shown in Figure 5.2, the central part is a sandwich plate made from aluminium. The sealing from the sandwich to the headers and the left and right frame is made with a structural adhesive. Welding and other hot processes were not possible due to the low-temperature bonding of the sandwich sheets. During the tests several leakages occurred as the struc-

tural adhesive did not show a high sealing quality in certain locations and could not resist pressures above 0.5 bar_e. Therefore, tests were limited to thermographic investigations.

Another distinguishing point of this prototype is its absorber surface size, which is 2000 mm x 1000 mm like case 5 in Table 4.6, hence, corresponds with an absorber rotated by 90°. The size had to be chosen as standard sandwich plates are only available in sheets of 3000 mm x 1500 mm with riser channels parallel to the width of 1500 mm. For infrared investigations the absorber was painted black.

Figure 5.2: Corrugated Sheet Absorber Prototype

Concept 2: Absorber with Corrugated Pattern

Based on the design rules presented in section 4.2.6 and the results of the optimisation steps a construction drawing was sent to the prototype manufacturing company. The prototype shown in Figure 5.3 has the dimensions given in the specification in Appendix B. The prototype for thermographic investigations is painted black, while a selective coating is applied to the absorber used in the collector efficiency tests.

Figure 5.3: Absorber with Corrugated Pattern Prototype

In contrast to the specified design guidelines of the manufacturing company, the prototype showed different channel heights in case of channel widths smaller then 10.7 mm, as illustrated in Figure 5.4. Furthermore, the number of channels with a decreased channel height is higher in the converging section than in the diverging section as shown in Appendix E / Figures E.1 and E.2. Each channel height was measured (Appendix E / Table E.1) and transferred to a spreadsheet for further investi-

gations of impacts on the CAD model and the simulation. The analysis of these discrepancies is given in detail in section 5.4. The overall channel height of the prototype is 3.2 mm.

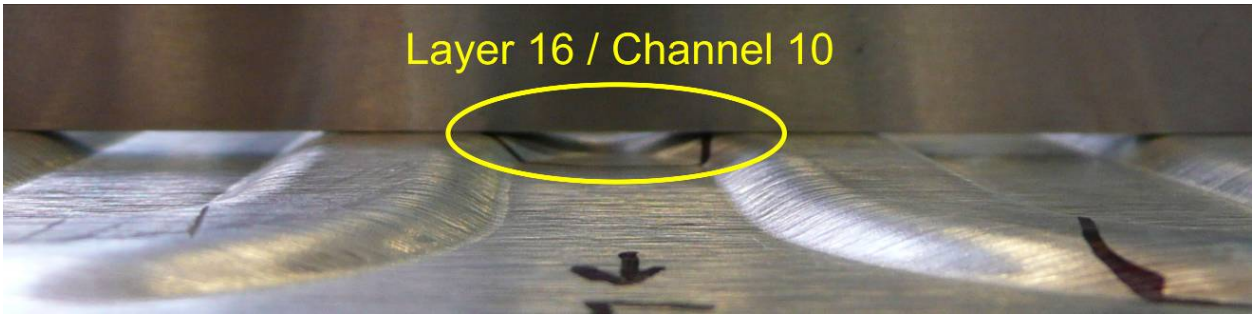

Figure 5.4: Decreased Channel Height in Layer 16 / Channel 10

5.2 Flow Distribution

It is a challenging task to illustrate or even measure the flow and flow distribution in non-transparent channel structures. Hence, in the course of flow distribution investigations an indirect method is chosen. An infrared camera was used to visualise the heat distribution of an absorber which is streamed with hot water. This method reflects the real flow distribution in the absorber channels as the used absorber materials are highly conductive. Thereby, the temperature in adjacent channels also rises quickly, which is again dependent on the distance between the channels. A significant difference exists between the simulated and the investigated flow distribution as the former shows a steady state condition while the latter illustrates a transient condition. In summary the infrared tests can show areas with very low flow-rates or even dead water zones; however, they cannot provide deeper insights into regions with somewhat different flow-rates. Nevertheless, it is used in this context by Peuser et al (1997), Hermann (2005) and Treikauskas et al (2005).

5.2.1 Testing Procedure

The absorber is placed in horizontal position and water at 60°C, controlled by a temperature control unit, enters the absorber at the inlet. According to the flow distribution of the hot water the absorber heats and emits long-wave infrared radiation. This radiation is detected by an infrared camera above the collector and produces an image of the heat distribution that approximately corresponds with the flow distribution in the channels of

the absorber. Finally, the water leaves the absorber at the outlet and returns to the temperature control unit.

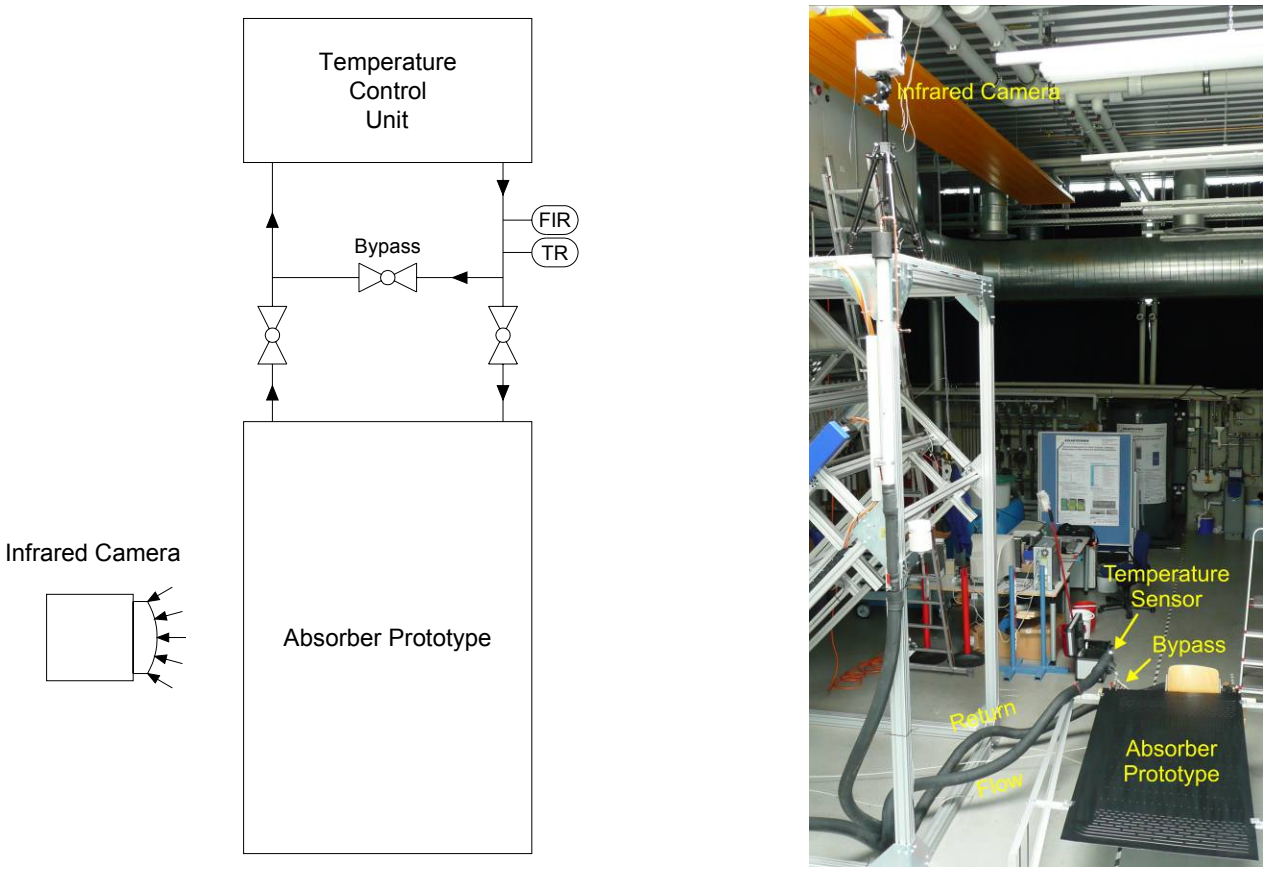

Figure 5.5: Scheme and Experimental Setup for Flow Distribution Tests

During the conditioning phase, the in- and outlet of the absorber is closed and the bypass is opened. At the initial condition the absorber surface is at room temperature and the flow-rate as well as the temperature is set according to sensors in the flow. Figure 5.5 shows the flow chart as well as the experimental setup.

5.2.2 Results

State-of-the-Art: Header-Riser Absorber

In case of the header-riser absorber one infrared image is sufficient to illustrate the temperature distribution as a consequence of the flow distribution, since there is only one diverging and converging header unit. However, a higher inlet flow-rate of 240 l h^{-1} is chosen to better compensate the heat losses along the flow paths and to get a reliable image of the temperature distribution.

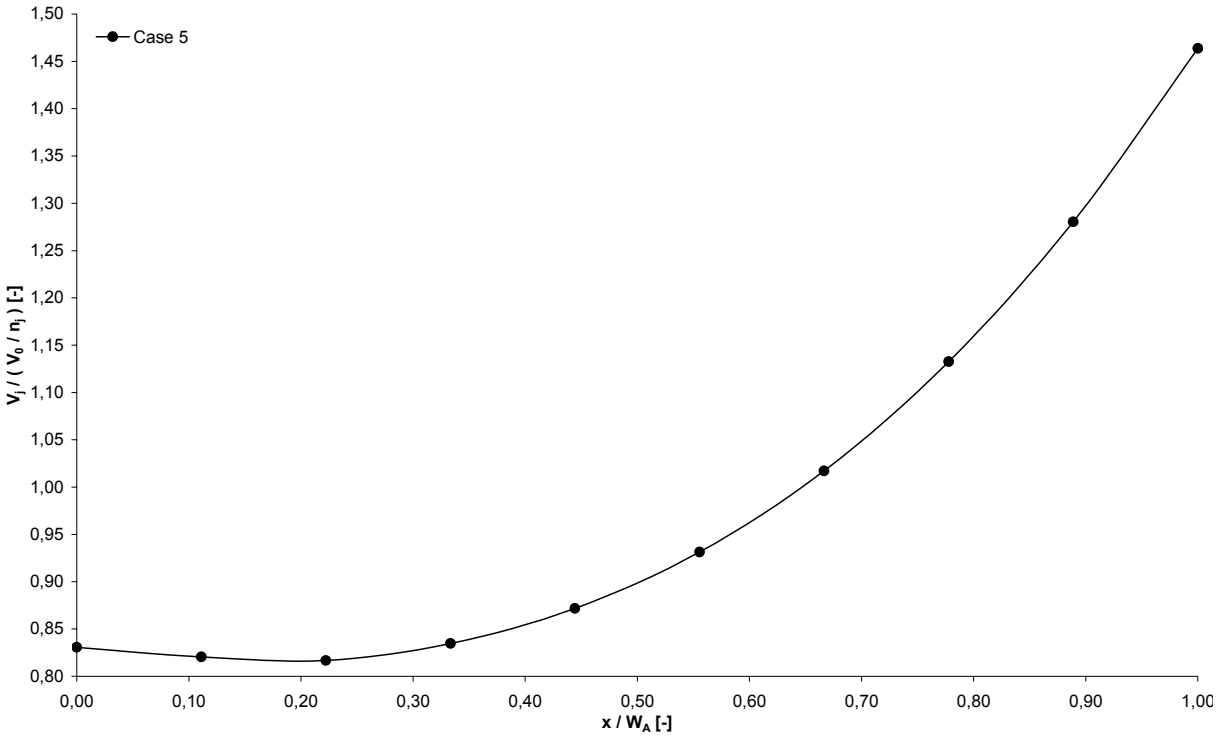

Figure 5.6: Flow Distribution of Header-Riser Absorber Case 5 for 240 l h^{-1}

In addition to the flow distribution diagram of header-riser case 1 (Figure 4.17) the simulated flow distribution for case 5 (geometry similar to prototype) is shown in Figure 5.6. As expected the deviation to the graph of case 1 for 240 l h^{-1} is higher (approximately 25%) due to the extended riser pipes. Figure 5.7 shows the infrared image of the header-riser absorber prototype. In compliance with the graph of Figure 5.6 an increasing flow-rate occurs from the first riser at the inlet region to the last riser. Differences only occur in the first and last riser pipes that can be attributed to the higher heat losses in both areas.

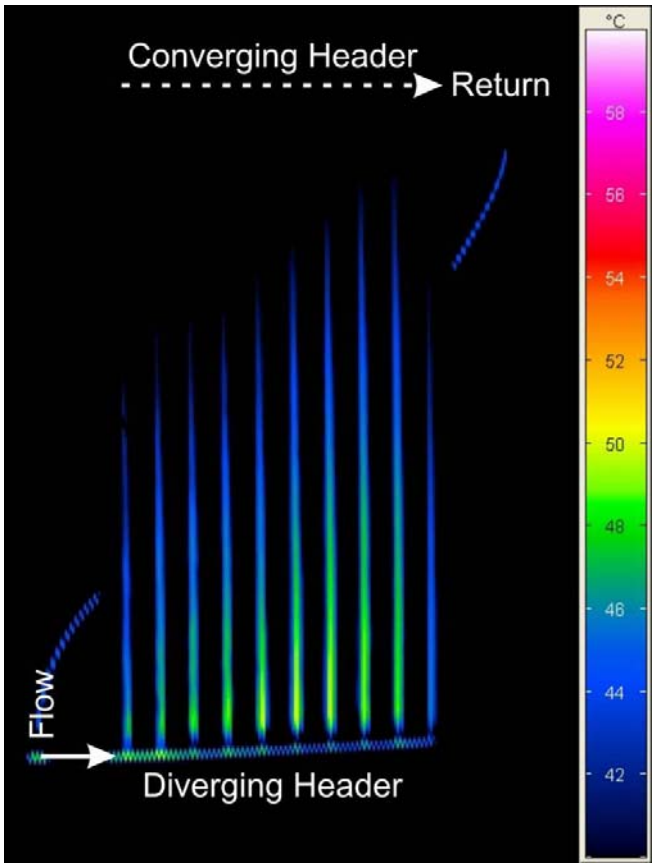

Figure 5.7: Infrared Image of the Header-Riser Absorber (Time from starting the test = 11 s)

Concept 1: Corrugated Sheet Absorber

Case 5 of the corrugated sheet absorber flow simulations is discussed in this section due to the difference in geometry to the cases 1 to 4 of section 4.3.3. Moreover, the infrared experimental test could only be carried out with the geometry according to case 5. Figure 5.8 shows the steady state flow distribution results of the simulation run with a higher flow-rate in the outer risers ranging from +5% on the left risers to +95% on the right risers. In the central risers the flow-rate is reduced up to 25%. The shape of the curve is similar to those presented in Figure 4.20.

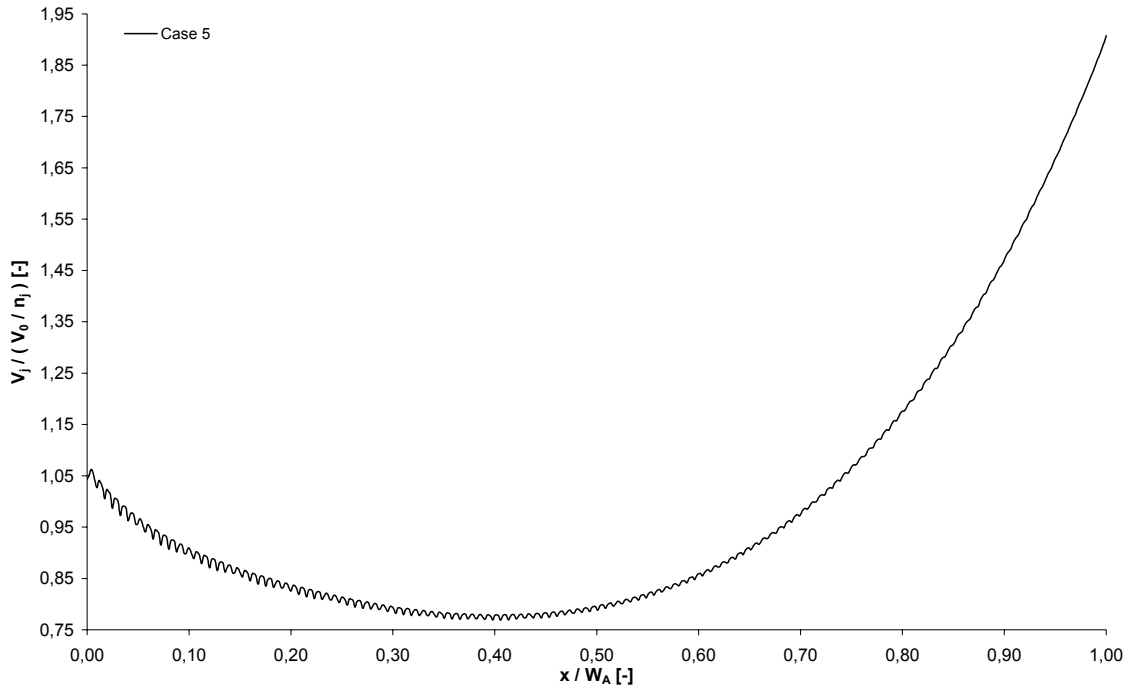

Figure 5.8: Flow Distribution of the Corrugated Sheet Absorber Case 5

Figure 5.9 shows the temperature distribution on the prototype due to the flow-rate and in a transient heating condition. The inlet is on the lower left corner and enters directly into the diverging header. Two peaks are visible on the left and right side of the absorber, similar to the graph in Figure 5.8. The right peak, however, shows a lower temperature and height level than the left one. This effect can be attributed to the long header pipe and an increasing heat loss along this flow path. In the central risers no heat flow occurred, however mainly due to air in some riser channels.

The testing of the corrugated sheet absorber prototype was challenging as the circuit was difficult to bleed. Furthermore, several leakages occurred where the adhesive should connect and seal the sandwich plate to headers and side frames.

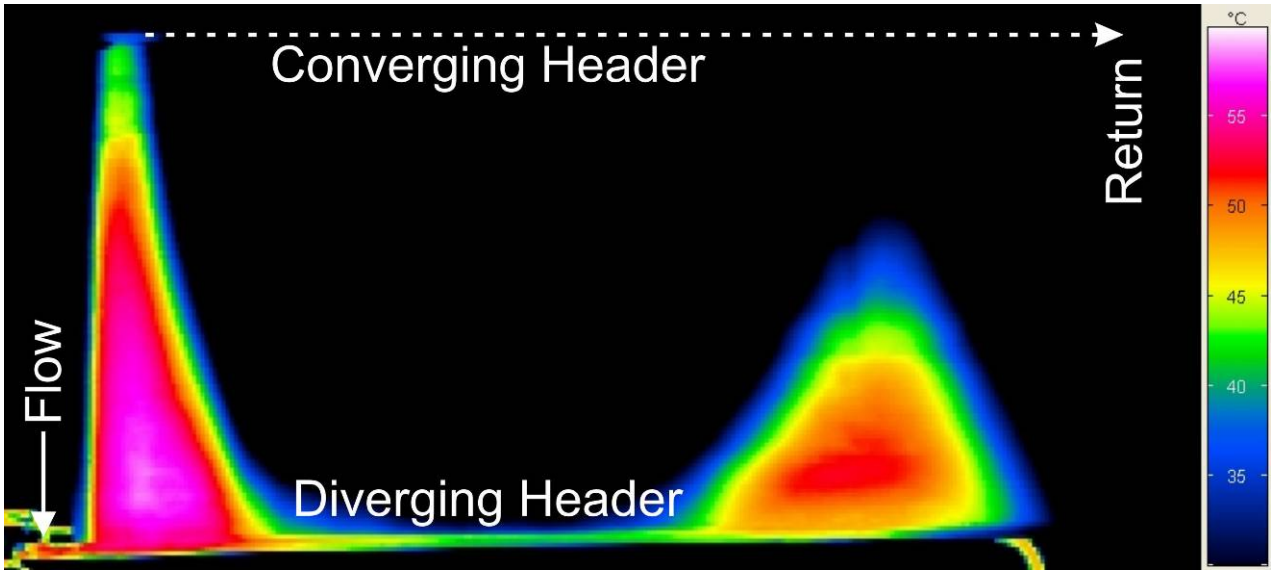

Figure 5.9: Infrared Image of the Corrugated Sheet Absorber (Time from starting the test = 889 s)

Concept 2: Absorber with Corrugated Pattern

The analysis of the flow distribution in the absorber with corrugated pattern follows the classification into different sections as shown in Figure 4.11. For each section an infrared image is provided which shows the temperature distribution in this area.

The flow enters at the inlet on the upper left corner of the left image in Figure 5.10 and is divided in to four channels of the inlet section for the first time. The temperature in the inlet section channels is higher from the left to the right side. Hence, the flow, which corresponds to the graph case 7 – Layer 00 in Figure 4.30, is higher in the right side channels. In the second image an equal temperature and therewith flow distribution is shown in the diverging section. Almost the whole diverging section is streamed until the flow enters the straight channel section. Therefore, a uniform temperature distribution is reached in the straight channel section as visualised in the third image in Figure 5.10. The channels on the right side show a less propagated temperature line due to a longer flow path in the diverging section in combination with higher heat losses. The heat losses of the left side channels of the straight channel section are compensated by the heat flow from the adjacent and warmer inlet section channels. Finally, the flow is combined in the converg-

ing section as illustrated in the right image of Figure 5.10. An equal temperature line entering the first channels of the converging section can be seen. Again, the influence of the inlet section is visible on the left side area. The temperature peak starting from the left side cannot be attributed to a higher velocity in these channels as it already begins to form in the second image. One contributor to this effect are the long islands with high heat conductivity which are directed towards the outlet in these layers (Figure 4.11) and which conduct heat from the inlet channels to the converging section.

By means of the infrared investigations an equal temperature and approximated flow distribution was shown, supporting the results gained from flow simulations. Further infrared images can be found in Appendix F / Table F.1.

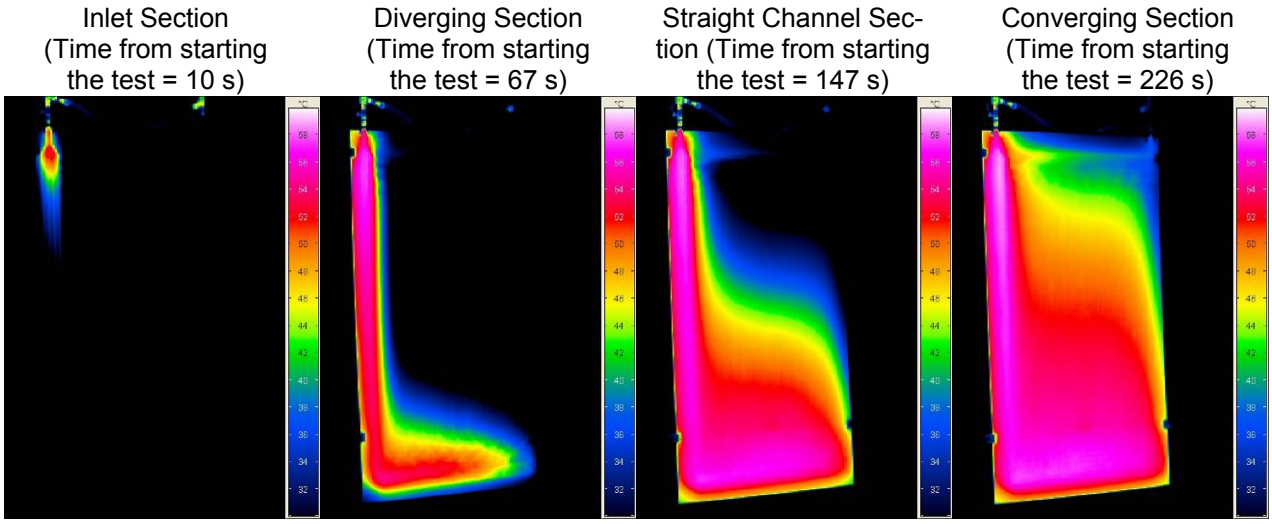

Figure 5.10: Infrared Images of the Absorber with Corrugated Pattern for 60 l h^{-1}

5.3 Pressure Loss

5.3.1 Testing Procedure

The pressure loss tests are carried out in accordance with the regulations given by Deutsches Institut für Normung (2006). A test rig filled with water at room temperature is used for testing as shown in Figure 5.11. The pressure loss is measured in horizontal position of the absorber like the models in the simulation. The flow rates for the pressure loss measurements are given in Table 4.3 and are increased from zero by 30 l h^{-1}. The usual operating flow rate range is given in the following pressure loss figures according to Table 4.3. Previous to the test each absorber is bled and applied with its common operat-

ing pressure. Due to the reasons given in section 5.1 a corrugated sheet absorber could not be tested.

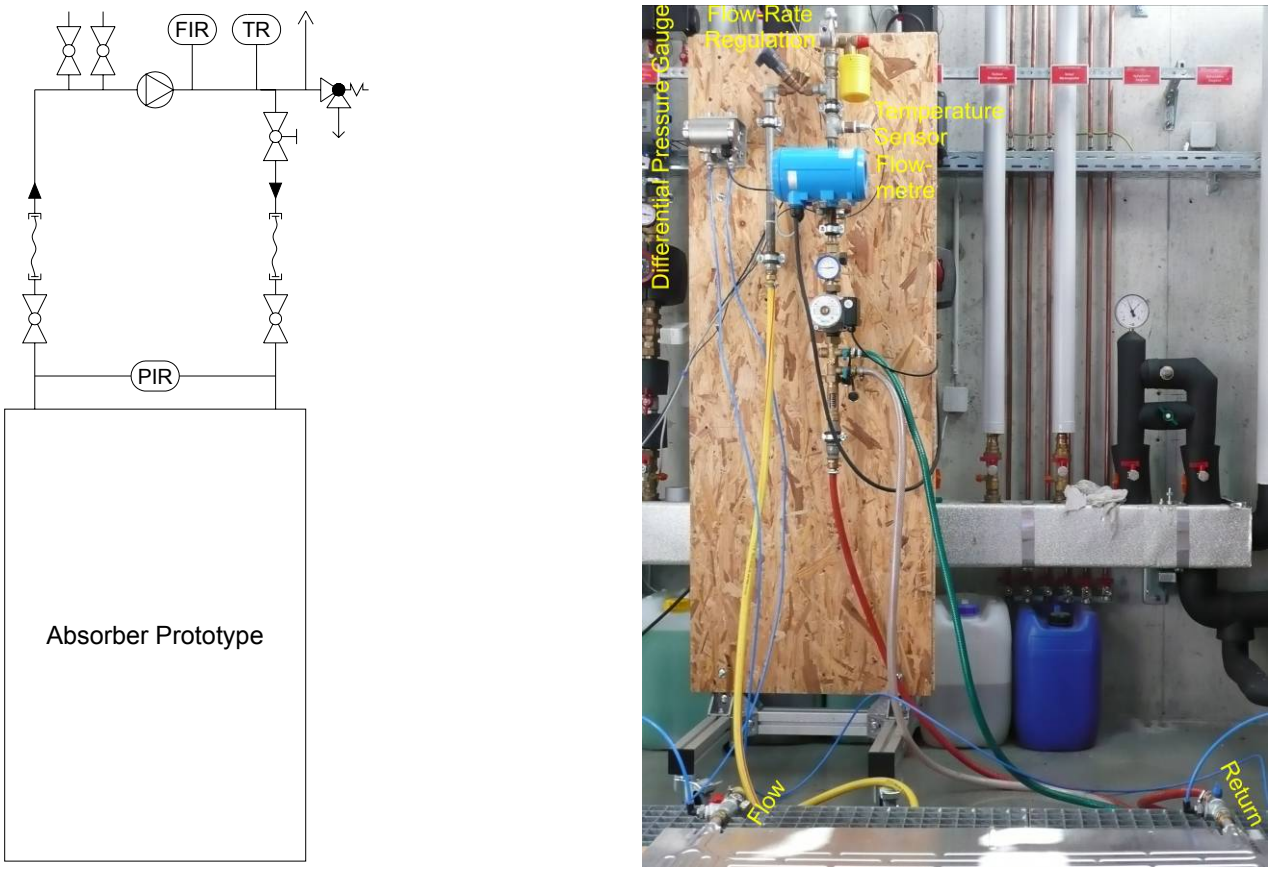

Figure 5.11: Scheme and Experimental Setup for Pressure Loss Tests

5.3.2 Results

State-of-the-Art: Header-Riser Absorber

The simulated header-riser absorber case 5 with extended riser pipes is used as basis for comparison with the state-of-the-art absorber prototype. As shown in Figure 5.12 the pressure loss from simulation corresponds well with the measurements in the whole flow rate range. Especially in the operating region both graphs are nearly congruent.

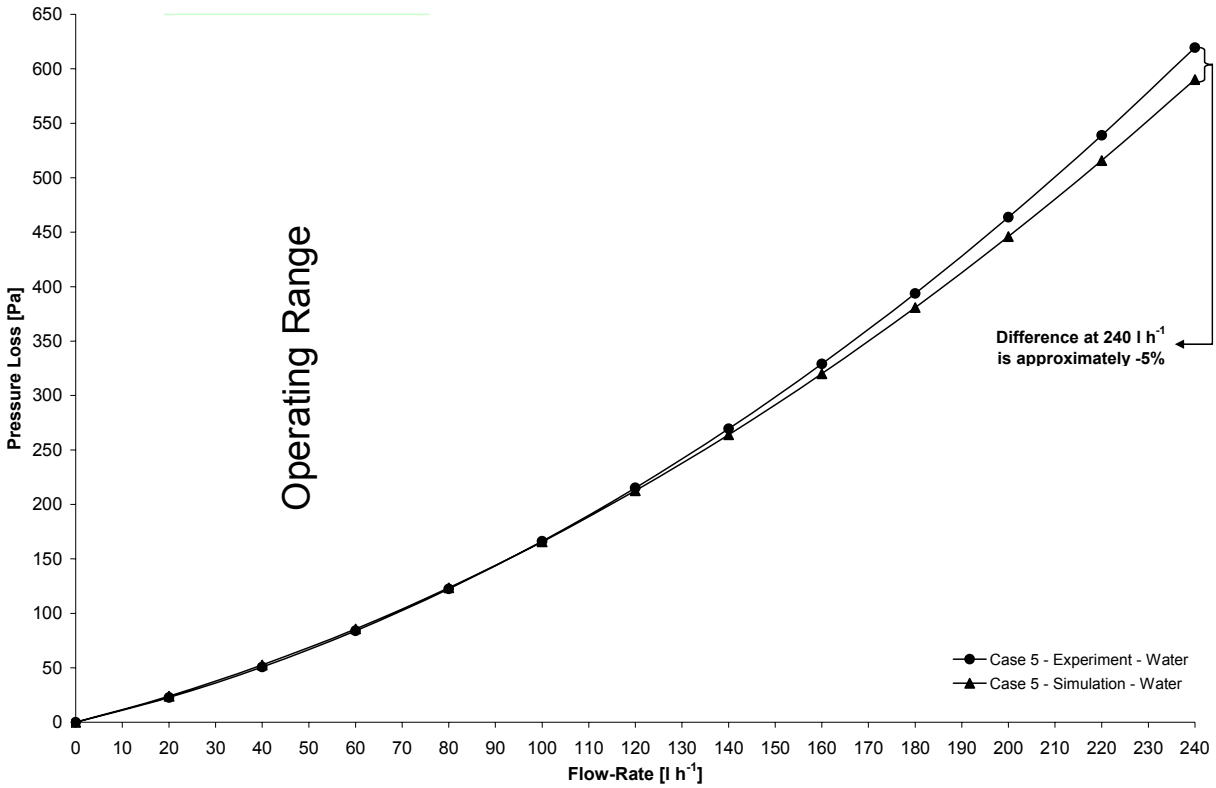

Figure 5.12: Pressure Loss of Header-Riser Absorbers – Simulated and Measured

Concept 2: Absorber with Corrugated Pattern

In contrast to the previous results the comparison of simulation and measurement outcomes shows a significant discrepancy. Figure 5.13 illustrates both pressure loss graphs with a difference of 25% at the top end of the operating flow rate range and up to 38% at the maximum flow rate. However, there are several reasons why the results disagree:

- The channel height differs in the simulation model and the prototype as outlined in section 5.1 due to channels not properly inflated.
- The channel shape is assumed to be rectangular, however, in the real prototype a more complex channel section exists. The rectangular shape was chosen in the early design and simulation phase as the manufacturer could not provide an explicit shape of the channel section.
- The difference between the simulated and measured results increases towards higher flow rates due to transition from laminar to turbulent flow in some areas of the absorber under real test conditions.

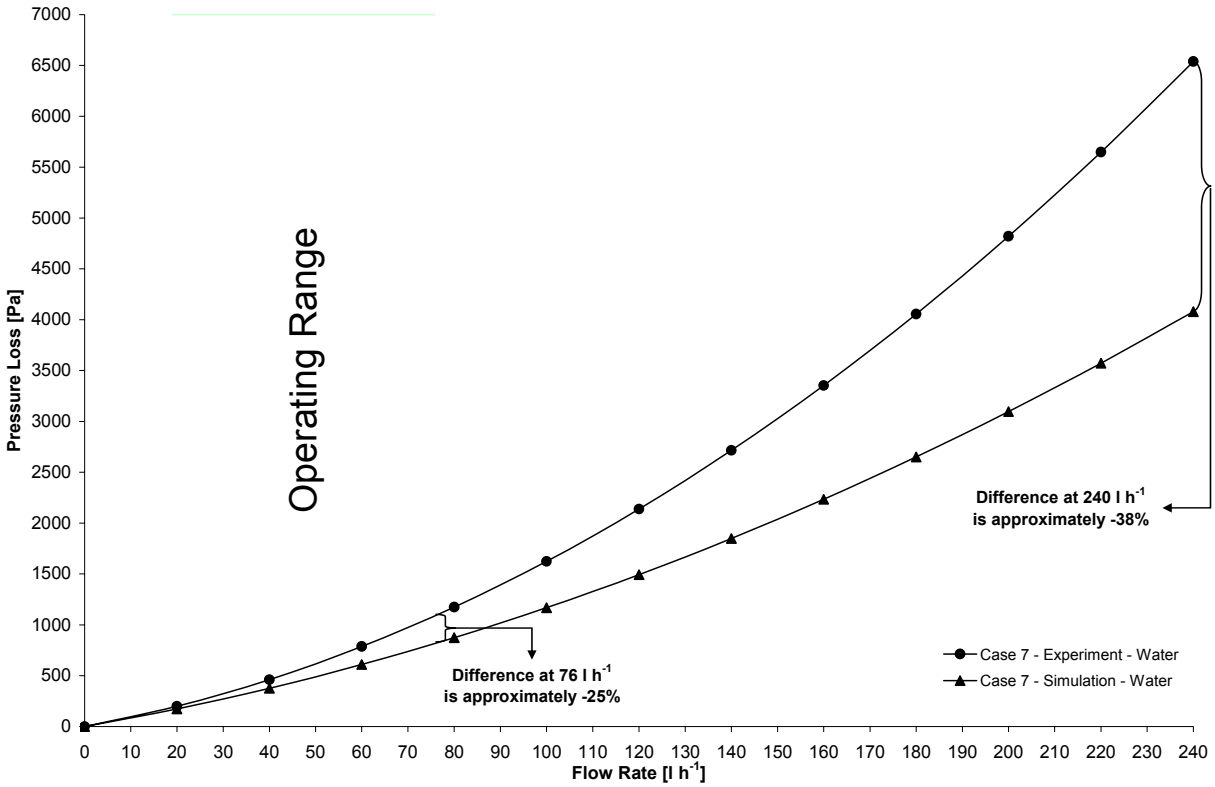

Figure 5.13: Pressure Loss of Absorbers with Corrugated Pattern – Simulated and Measured

5.4 Simulation with Adopted Prototype Properties

This section deals with the implementation of the actual prototype geometry – as outlined in section 5.3.2 – into the simulation model. Furthermore, an analysis of the flow conditions in the channel structure is carried out to figure out those channels with a turbulent flow as well as the flow rate at which transition is likely to start.

The rectangular channel shape is based on measurements and simulations of a test panel provided by the rollbond manufacturing company in the early design phase. That panel has a less complex channel structure, with a channel height of 4 mm. Figure 5.14 shows the pressure loss graphs for the measured test panel as well as the simulated test panel model based on a rectangular channel shape and a channel height of 4 mm. It can be seen, that both graphs agree well with a difference of less than 6%. Furthermore, Figure 5.14 presents simulation results for the test panel with a channel height of 3 mm. Compared to the measured pressure loss of the test panel the strong influence of the absorber height becomes evident.

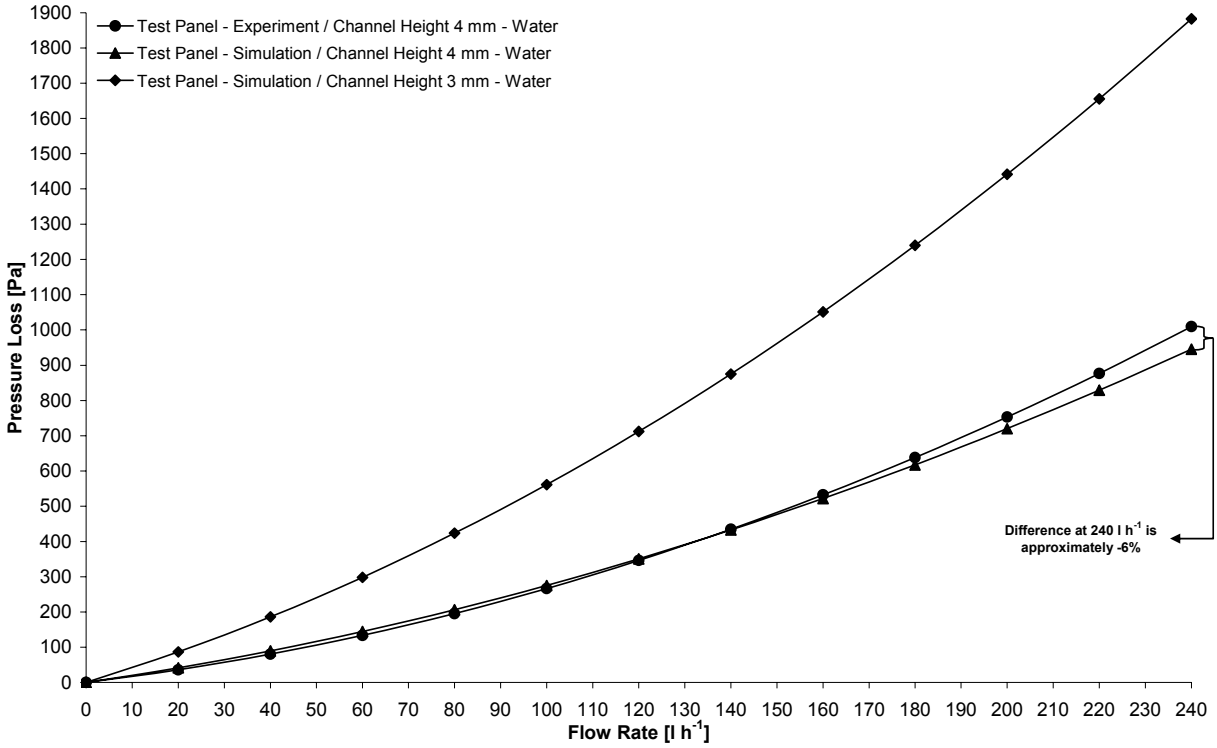

Figure 5.14: Pressure Loss of Test Panel – Simulated and Measured

Consequently the model of the absorber with corrugated pattern is modified as described in Table 5.1.

Table 5.1: Modifications at the Absorber Model with Corrugated Pattern

Modification	Original Simulation Model (Case 1 – Case 7)	Customised Simulation Model
Overall Absorber Height	3.0 mm	3.2 mm Appendix E / Table E.1
Not Properly Inflated Channel Heights	3.0 mm	according to prototype data Appendix E / Table E.1
Channel Shape	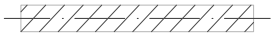	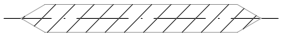

Figure 5.15 illustrates the results for the adapted simulation model. The difference compared to the measured pressure loss of the absorber with corrugated pattern prototype at the maximum flow rate of 240 l h^{-1} is reduced to 16% and at a flow rate of 76 l h^{-1} reduced to 8%. Although the overall absorber height is increased slightly, which would result in a reduced pressure loss as shown in Figure 5.14, there is a reasonable influence on the pressure loss by the constricted channels and the channel shape.

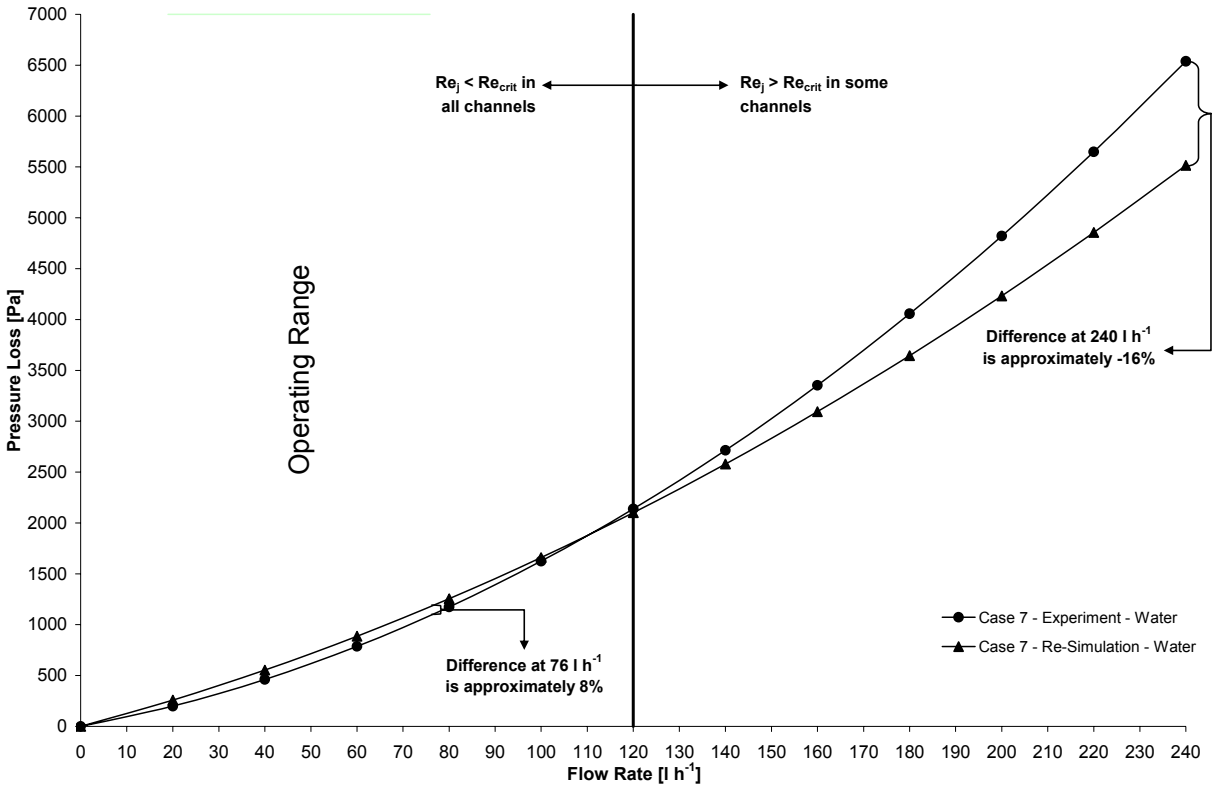

Figure 5.15: Pressure Loss of Absorbers with Corrugated Pattern – Re-Simulated and Measured

Furthermore, Figure 5.15 shows an increasing pressure loss difference between measurement and simulation above 120 l h^{-1}. An analysis of the flow condition in the channels showed, that below 120 l h^{-1} the flow in all channels is laminar, while above 120 l h^{-1} the flow starts to become turbulent. These channels are located in the diverging and especially the converging section as the flow has to be converged into a single channel, while the inlet section distributes the flow into four channels of the diverging section. Therefore, an increased pressure loss at higher inlet flow rates is attributed to higher losses in areas with turbulent flow of the prototype. Figure 5.16 shows the number of channels that are in turbulent condition in the simulated case. A critical Reynolds

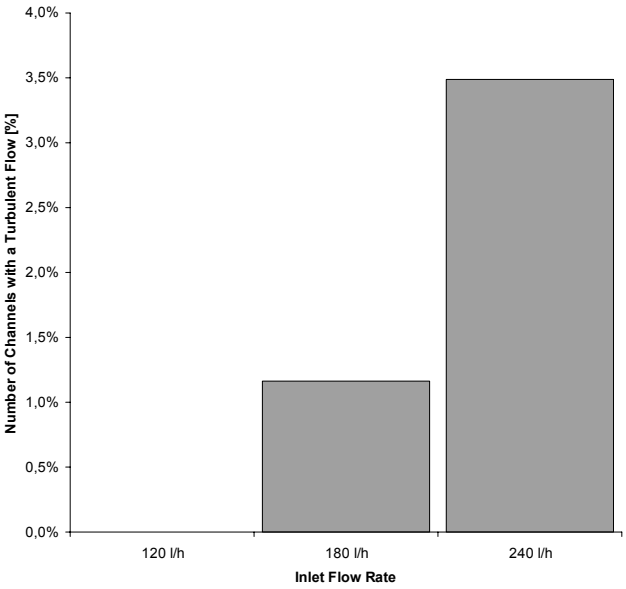

Figure 5.16: Number of Channels with a Turbulent Flow at Various Flow Rates

number Re_{crit} = 2300 is applied according to Martin et al (2002), however, has to be considered carefully as the transition between laminar and turbulent flow is better defined by a Reynolds number range rather than a single point (Martin et al 2002).

5.5 Collector Efficiency Factor

In addition to sections 4.4.1 and 0 this section describes the experimental analysis of the collector efficiency factor. Since the collector efficiency factor cannot be measured directly it is determined by measuring the collector efficiency. The corrugated sheet absorber was not evaluated due to the problems outlined in section 5.1.

5.5.1 Collector Efficiency

The collector efficiency measurements are carried out according to the standard DIN EN 12975-2. In contrast to equation (4-32) with a constant heat loss coefficient U_L the measurement standard is based on a linear heat loss coefficient, resulting in a second order collector efficiency equation:

$$\eta = \eta_0 - a_1 \frac{T_m - T_a}{G} - a_2 G \left(\frac{T_m - T_a}{G} \right)^2 \qquad (5\text{-}1)$$

with

a_1	Linear heat loss coefficient	[W ($m^{-2}K^{-1}$)]
a_2	Parabolic heat loss coefficient	[W ($m^{-2}K^{-2}$)]
T_a	Ambient temperature	[K]
T_m	Mean fluid temperature	[K]
η	Collector efficiency	[-]
η_0	Zero loss efficiency	[-]

T_m is defined by:

$$T_m = \frac{T_{in} + T_{out}}{2} \qquad (5\text{-}2)$$

with

T_{in}	Temperature at collector inlet	[K]
T_{out}	Temperature at collector outlet	[K]

Thus, equation (5-1) takes into account increasing heat losses with a rising temperature difference between absorber and ambient temperature. This is in particular due to the temperature dependency of radiation processes as well as the temperature difference dependency of convective processes between absorber and transparent cover.

5.5.2 Collector Efficiency Factor Theory – Experimental Determination

The calculation of the collector efficiency factor is, especially for sheet-pipe absorbers, well investigated. By contrast, methods for its measurement have been developed and carried out mainly in the last two decades and are related with a more intense use of in-door solar simulators, as greater demands on the measurement equipment are made by the collector efficiency factor tests. However, standards for measuring the collector efficiency factor or similar characteristics still do not exist.

Rockendorf et al (1996) defined an ‘effective internal heat transfer’ and presented three different test methods for its determination. With the effective internal heat transfer and a given equation it is possible to calculate the collector efficiency factor. The first method described by Rockendorf et al (1996) is called ‘integral method’ and is based on the measurement of two collector efficiency curves of a complete collector with and without irradiation. Then, using both parameter sets gained from the measurements, the collector efficiency factor can be calculated and is described in detail by Rockendorf et al (1993). The collector does not need to be equipped with extra measurement which is beneficial. However, the measurement is laborious and requires very constant conditions during both test sequences (Rockendorf et al 1996). With the second test method, absorber strips are irradiated by a solar simulator (Frey et al 1995) or heated electrically from the fin edges (Rockendorf et al 1996). Only one absorber strip needs to be measured, therefore the procedure is fast and simple. However, both absorber concepts, the corrugated sheet absorber and the absorber with corrugated pattern, cannot be tested by this method as they cannot be divided into single stripes. The last method is implemented in a common collector efficiency test with an additional temperature gauge positioned at a

particular position presented by Rockendorf et al (1996). This temperature measured locally is equal to the mean temperature based on the temperature distribution of a whole absorber strip. Again, this method can only be used with sheet pipe absorbers.

Hermann (2005) applied a customised approach according to the second method described above. By this test process a complete absorber is embedded in a collector which is irradiated by a solar simulator. As it can be carried out with the collector efficiency measurements, this testing procedure is also applied in this work. In compliance with equations (4-32) and (4-33) equation (5-1) can be written as:

$$\eta = F'\left(\tau\alpha\right)_{eff} - a_1 \frac{T_m - T_a}{G} - a_2 G \left(\frac{T_m - T_a}{G}\right)^2 \qquad (5\text{-}3)$$

The second and third terms of equation (5-3) can be eliminated when:

$$T_m - T_a \overset{!}{=} 0 \qquad (5\text{-}4)$$

The mean fluid temperature is equal to the ambient temperature. Hence, the heat flux from the absorber to the environment is almost zero and the collector efficiency factor can be calculated according to:

$$F' = \frac{\eta_0}{\left(\tau\alpha\right)_{eff}} \qquad (5\text{-}5)$$

The measurement of the collector efficiency without heat losses η_0 means high demands on the measurement equipment and the test procedure. Therefore, the fluid inlet temperature T_{in} as independent, variable factor in equation (5-2) has to be set in test conditions in accordance with equation (5-4). Furthermore, the effective transmittance and absorptance product has to be known. The values used for calculation are presented in Appendix D / Table D.1.

5.5.3 Testing Procedure

As mentioned in section 5.5.1 the tests are carried out according to the standard DIN EN 12975-2 (Deutsches Institut für Normung 2006). Three different test methods are described therein for glazed collectors, of which two describe tests under steady-state

condition while one is under quasi-dynamic conditions. The method for determination of the collector efficiency factor in this work is based on steady-state conditions using a solar simulator. The advantages compared to steady-state outdoor tests are defined and constant, reproducible conditions, especially for the ambient temperature and the irradiance. These properties are very important for comparison of different absorber designs as carried out between the state-of-the-art sheet-pipe absorber and the absorber with corrugated pattern of concept 2.

The experimental setup of the solar simulator is shown in Figure 5.17, while a scheme is illustrated in Deutsches Institut für Normung (2006).

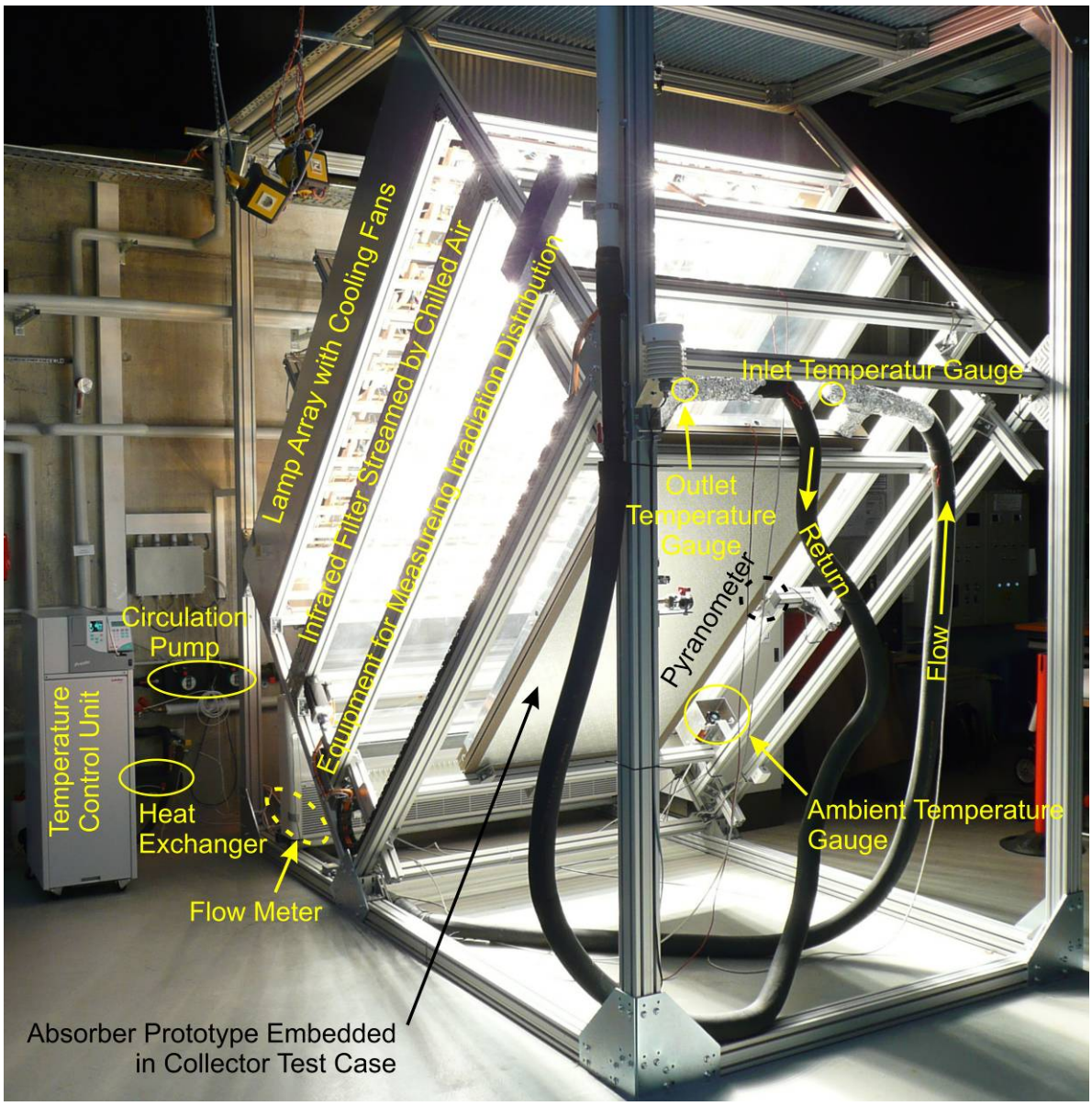

Figure 5.17: Experimental Setup at the Solar Simulator

Due to the influence of the collector heat loss U_L on the collector efficiency factor F' as described by equation (4-36) both absorbers were tested in the same collector casing.

According to the standard at least 8 different temperature levels are set at the collector inlet and kept under steady-state conditions for a defined time. Four of these temperature levels have to be in the range during heat-up starting close to the ambient temperature and the remaining temperature levels have to be measured in steps during cool down from the maximum temperature reached in the test. The evaluation is carried out in compliance with Deutsches Institut für Normung (2006) and is based on the evaluation of equation (4-30) for every temperature step under steady-state conditions. The parameters of the collector efficiency equation (5-1) are calculated by applying a parabolic function with the least-square method.

5.5.4 Results

Usually, collector efficiency curves are the typical result of tests as described above. However, the information given by the curve is essentially referring to the whole collector.

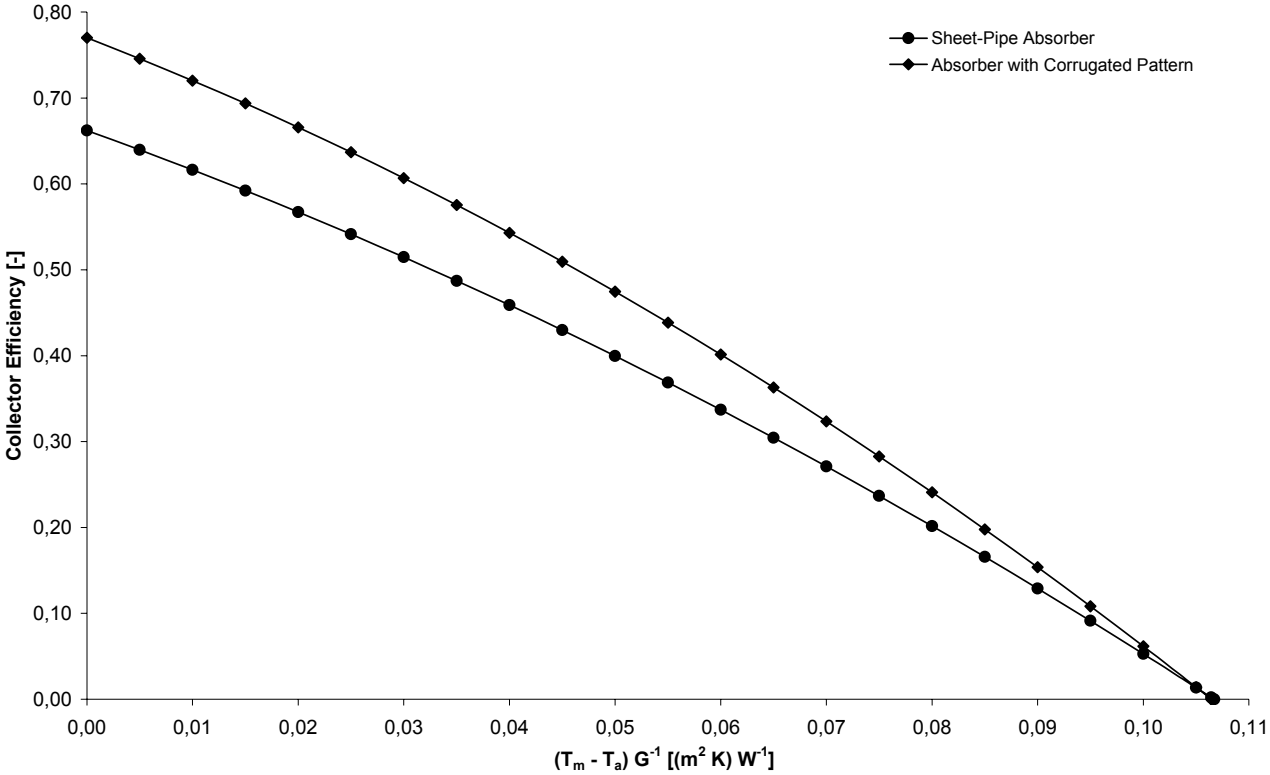

Figure 5.18: Collector Efficiency Curves of the Sheet Pipe Absorber and the Absorber with Corrugated Pattern for an Inlet Flow Rate of 60 l h^{-1}

Figure 5.18 shows the collector efficiency curve for both tested absorbers, while further evaluations were carried out to elaborate the performance of the different absorbers.

Both curves start at different zero loss efficiencies η_0, as can be seen from Figure 5.18. This cannot be attributed solely to the different absorber designs caused by different collector efficiency factors *F'*, but also to the different selective coatings applied to the absorbers. Unfortunately, the absorbers were coated by the manufacturer with unequal selective paints. Hence, both tested absorbers have a different solar absorptance and thermal emittance. However, both curves still intersect close to the abscissa as shown in Figure 5.18 which generally indicates similar heat losses. On the one hand it seems to be obvious as the absorbers were tested in the same collector casing. On the other hand the emittance of the absorber paints is also different, resulting in unequal heat losses. Therefore, the linear and parabolic heat loss coefficient of equation (5-1) is different for both absorbers and higher in case of the absorber with corrugated pattern due to its higher emittance. The better thermal emittance (Appendix D / Table D.2) of the paint applied to the sheet-pipe absorber compensates the better solar absorptance (Appendix D / Table D.2) and the superior collector efficiency factor *F'* (Figure 5.19) of the absorber with corrugated pattern.

Figure 5.19 shows the evaluation of the collector efficiency factor for the state-of-the-art absorber designs, the corrugated sheet absorber and the absorber with corrugated pattern. Unlike the calculations presented in Figure 4.34 with typical selective coating and collector parameters, the calculation results of Figure 5.19 include the parameters represented by the prototypes as described in Table D.2 / Appendix D.

The higher overall collector heat loss coefficient U_L of the prototypes is caused by a higher emittance of both selective paints as well as a non-optimised collector casing compared to state-of-the-art coatings and casings (Appendix D / Table D.2). The higher heat losses have a bigger impact on the sheet-pipe absorbers than on the volumetric absorbers as can be seen by comparing Figure 4.34 and Figure 5.19. Due to its lower thermal resistances the volumetric absorber designs are more favourable in this context and maintain high collector efficiency factors. The calculated collector efficiency factors gained from experiment and theory are in very good agreement. Figure 5.19 shows a difference of about 1.6% between both header-riser absorber calculations and only 0.8%

between the results of the absorber with corrugated pattern. In the theoretical calculations the header-riser absorber case 1 is about 8% lower in collector efficiency factor, the experiments show a similar result at almost 9% lower.

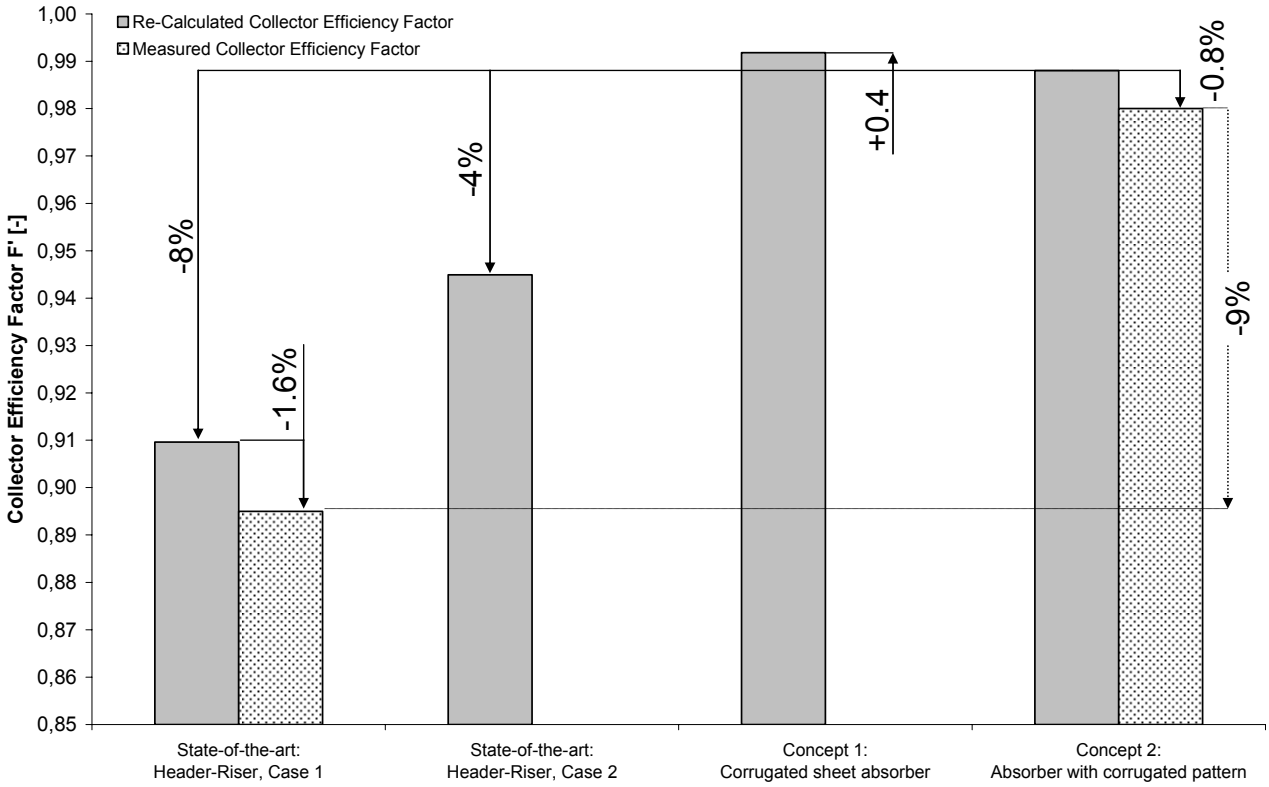

Figure 5.19: Collector Efficiency Factor of Re-Calculated Absorber Concepts Based on the Properties of the Tested Prototypes and Collector Efficiency Factor Calculated from Measurements of the Sheet-Pipe Absorber and the Absorber with Corrugated Pattern

5.6 Conclusions

In the course of the experimental analysis, the properties of different absorber designs were measured. They clearly show a good compliance with the simulated and calculated results presented in the theoretical analysis of chapter 1 and the goals specified in the requirements list of Appendix B.

Flow Distribution

Infrared images of the different absorber designs allow conclusions to be drawn on the flow distribution within the channel structure. Three absorber concepts were tested with two of them having a single diverging unit. Hence, a single infrared image is sufficient to illustrate the temperature distribution along the riser pipes/ducts during heating. In contrast to the header-riser absorber and the corrugated sheet absorber, the absorber with

corrugated pattern is based on several diverging and converging sections. Therefore, an infrared image is presented for the transient condition in every section. The infrared images are in good agreement with the corresponding simulation results when the heat losses in long channel parts as well as areas close to the absorber margins are considered. Furthermore, it can be seen from the infrared images of the header-riser absorber and the absorber with corrugated pattern that the flow distribution was improved in the latter case.

Pressure Loss

The pressure loss is an important parameter for a solar thermal absorber, particularly in influencing operating costs. The absorbers tested are the state-of-the-art header-riser absorber as well as the absorber with corrugated pattern. The header-riser absorber results of simulation and experiment are in good agreement with a deviation of less than 5%. In case of the absorber with corrugated pattern, however, the difference between measured and simulated results is less than 38%. This deviation can be attributed to extremely non-homogeneous inflated channel heights in about 20% of all channels and a different channel section shape. The modified absorber model considering the actual absorber geometry shows a deviation of less than 8% in the operating range of the absorber, hence, a good agreement with the simulation results. Furthermore, experimental and simulated results are shown for a test panel presenting the influence of different absorber channel heights as well as the influence of channel height and channel shape on the pressure loss.

Collector Efficiency Factor

By using the parameters identified from the prototypes and the test collector casing the collector efficiency factor is recalculated for a comparison with the measurement results. Furthermore, the influence of different absorber coating properties on the overall collector heat loss coefficient U_L and the collector efficiency factor F' is shown. The collector efficiency curves also represent these differences due to unequal selective paints, however, still intersect on the abscissa. This phenomenon may be explained by balancing properties of the paints and the different absorber designs used.

Both collector efficiency factors identified from calculation and measurement agree very well with a deviation of 1.6% for the sheet-pipe absorber and 0.8% for the absorber with

corrugated pattern. The absolute collector efficiency factor F' is 0.895 for the sheet-pipe absorber and 0.98 for the absorber with corrugated pattern. Due to the higher overall collector loss coefficients of the prototype collectors, these values cannot be compared with factors presented in section 2.4.3. Therefore, care must always be taken with the parameters relating to the collector efficiency factor, e.g. overall collector heat loss coefficient, flow rate etc.

6 Conclusions and Further Work

The research covers the development of a volumetric thermal absorber for low temperature solar systems. The novel absorber was designed and optimised by numerical simulation and tested by experimental investigation, showing very good agreement. The results show the feasibility of an absorber with corrugated pattern produced by the rollbond manufacturing process. The application of CFD to simulate the absorbers' flow distribution and to optimise them by a unique iterative process delivers excellent results and resulted in a well designed channel structure of the prototype. This new approach including an analysis of the absorber, a detailed engineering process with optimisation and a testing phase resulted in a feasible absorber design. The manufacturing promises mass production at low costs, accompanied by a stable processing (only few parts, no flux, etc.) and a design with a high performance.

In the course of analysing solar thermal collectors, former absorber designs and state-of-the-art technology were reviewed. This clearly showed that volumetric absorbers had been investigated and produced in the past, especially during energy crises. However, these designs suffered from non-homogenous flow distribution, corrosion problems or heavy weight. Due to these problems absorber designs changed to primarily header-riser or meander absorbers which are the state-of-the-art nowadays. The review showed several different connections for those sheet-pipe absorbers, while soldering, ultrasonic and laser welding are the commonly used manufacturing processes today. It was shown that these designs, even if they are the most used ones, suffer from drawbacks which inhibit reducing costs and increasing performance at the same time, while automated processes at a large scale are hard to apply.

The concept development was aimed at a new design approach for the absorber by the application of alternative materials for the whole absorber together with simplified manufacturing processes. The first step was to analyse the absorber within the collector and the solar system and to establish a requirement list defining the necessary properties of future absorbers. Solutions based on the functional analysis and the requirement list resulted in novel concepts with an extended area for heat transfer and were aimed at different manufacturing processes ready for mass production. These concepts were evalu-

ated within the engineering design process by a systematic approach in order to select the most promising concepts for further investigation.

The theoretical analysis was aimed at illustrating and optimising the flow distribution and calculating the absorbers' performance by the collector efficiency factor *F'*. The state-of-the-art header-riser absorber design provided a basis for the flow simulations by CFD. The results are in excellent agreement with the published data of header-riser absorbers. It could be shown that the header-riser design is not equally distributed, although the flow paths along the riser pipes show the same length. Suggestions for improving the flow distribution in the header-riser absorber have been made and the modified models showed results that have a maximum deviation from homogenous flow distribution of less than 5% (case 4), while the original model (case 1) differs more than 20% from ideal flow. Apart from a more homogenous flow, the modified model of case 3 provides a pressure drop that is reduced by 12 percentage points compared to the initial header-riser absorber model. Simple improvements can already be achieved by optimising the branch points between header and risers (comparison between case 1 and case 5) as the flow distribution quality is increased while the pressure drop can be decreased at the same time. These modifications can be carried out with minor changes in the design and minimal increases in costs.

The improvement of the corrugated sheet absorber used the same approach as applied to the header-riser absorber. Due to many more channels, the converging and diverging header has to be modified in order to achieve an acceptable flow distribution. As with the header-riser absorber different approaches for dimensioning the headers were carried out and presented. However, due to limitations in the collector casing dimensions only one approach is applicable practically: that is realised in case 2 and optimised in case 4. The latter shows a maximum deviation to homogenous flow distribution of less than 5% and a very low pressure drop. However, due to idealised conditions of the model a higher pressure loss is expected in real operation, e.g. due to the adhesive residues.

The most challenging research was the simulation and improvement of the absorber with corrugated pattern. Apart from many parameters to be optimised within the channel structure the limits given by the manufacturing process have to be respected. After every simulation the flow rates in the channels were calculated and depending on the deviation

to homogenous flow distribution a new channel width was calculated. This new approach resulted in an optimised channel structure (case 7) with a deviation to homogenous flow distribution in the straight channel section of less than 5%, while the pressure loss only increased slightly compared to the initial model case 1. Although, the pressure drop is higher than that of state-of-the-art header-riser absorber it is still significantly lower than the pressure drop of state-of-the-art meander absorber. Furthermore, the difference in the typical operating flow rate range is much lower than in case of higher flow rates.

Table 6.1 summarises the cases investigated for different absorber designs:

Table 6.1: Summary of Design Characteristics for Theoretically Investigated Absorber Designs

Concept	Case 1	Case 2	Case 3	Case 4	Case 5 / 7
Header-Riser	10 risers + smooth branches + standard headers	15 risers + smooth branches + standard headers	10 risers + smooth branches + modified headers (Martin 1988)	10 risers + smooth branches + modified headers (Wagner 2001)	10 risers + extended branches (CitrinSolar) + standard headers
Corrugated Sheet Absorber	258 risers + standard headers	258 risers + modified headers (Martin 1988)	258 risers + modified headers (Wagner 2001)	258 risers + modified headers (derived from case 3)	526 risers + prototype design
Absorber with Corrugated Pattern	40 risers + initial design (constant channel width)	…	…	…	40 risers + optimised design (varying channel width)

The thermodynamic performance of the different absorber concepts was calculated using an analytical approach based on the model geometries simulated by CFD. The state-of-the-art header-riser absorber was calculated by the well-known collector efficiency formulae, while for the other designs different approaches were used and new formulae were derived. The results show excellent collector efficiency factors for the volumetric absorbers of more than 99%, while the header-riser absorber only reaches typical values in the range of up to 94%. Table 6.2 summarises the characteristics of the evaluated designs regarding flow and thermal behaviour.

Several experimental tests were carried out during the experimental analysis. Infrared photography was used to visualise the flow distribution within the prototypes. The pressure losses were measured for all absorbers in typical flow rate ranges. Finally, collector efficiency curves determined in the solar simulator provided the basis for calculating the collector efficiency factors. All the measurements carried out showed excellent agreement with the calculated data of the theoretical analysis and met the requirements stated in the specification established in the engineering design process. Restrictions have only to be accepted regarding the pressure loss, as the manufacturing process did not work as expected and several channels were not inflated properly. However, the pressure loss is still far below that of state-of-the-art meander absorbers.

Table 6.2: Summary of Energetic Characteristics for Theoretically Investigated Absorber Designs

		State of the Art		**Corrugated Sheet Absorber**		**Absorber with Corrugated Pattern**	
		Case 5	Case 3 (optimised)	Case 1	Case 4 (optimised)	Case 1	Case 7 (optimised)
Flow Distribution min / max deviation to homogenous flow distribution	[-]	- 7 % + 15 %	- 3 % + 5 %	- 25 % + 70 %	- 2 % + 4 %	- 6 % + 4 % (only Layer 10, → details Figure 4.25)	- 1 % + 1 % (only Layer 10, → details Figure 4.30)
Pressure Loss for 60 l h^{-1}	[Pa]	67 *)	59 *)	31	17	527	599
Collector Efficiency Factor (Appendix D / Table D.1)	[-]	0.939	0.939	0.995	0.995	0.993	0.993

*) State of the art meander absorbers: pressure loss for 60 l h^{-1} = 6350 Pa (Treikauskas et al 2008)

For the absorber with corrugated pattern some further tasks can be highlighted:

- Optimisation of the manufacturing process and / or the channel structure in order to avoid unequal channel heights. This process requires strong collaboration with the rollbond manufacturing company and should lead to improvements in the flow distribution and the pressure loss.
- Extended investigations on the overall channel height as results from section 5.4 indicate possibilities for reducing the pressure loss.
- Corrosion of aluminium in solar thermal systems has to be investigated.
- Possibilities for selective coatings have to be determined as state-of-the-art absorber coatings are applied in a continuous process on aluminium or copper coils. Alterna-

tives are galvanic processes, which are also applied in discontinuous processes, however, they suffer from ecological concerns. State-of-the-art selective coatings can be applied discontinuously, but manufacturers ready for a research project have yet to be identified.

Furthermore, the approach of volumetric absorbers is an essential step towards polymer based collectors as their low heat conductivity requires designs totally different from the current sheet-pipe designs. A research programme continuing in this area of research was started in autumn 2007 financed by the *German Federal Ministry for the Environment, Nature Conservation and Nuclear Safety*. This research is also contributing to Task 39 – Polymeric Materials for Solar Thermal Applications – in the International Energy Agency / Solar Heating and Cooling Programme.

References

Acrivos, A.; Babcock, B.D. & Pigford, R.L., 1959. Flow distribution in manifolds. *Chemical Engineering Science*, 10 (1-2), p. 112-124.

Anon, 1999. *Technical Manual: Section 1*: Standard of Products. Cividale del Friuli (Italy): CGA Compagnia Generale Alluminio S.p.A.

Anon, 2008. Rohstoffpreise. Sonnenenergie, 2008 (06), p. 69.

Arnold, R., Hufnagl, E. & Bartl, A.M., 1993. Einsatz technischer Textilien zur Solarenergienutzung. In Ostbayerisches Technologie-Transfer-Institut, *3. Symposium Thermische Solarenergie*. Bad Staffelstein, Germany 14-15 June 1993. Regensburg.

Bäckmann, R., 2001. Sonnschutz- und Solartextilien. *Textilveredelung*, 1/2, p. 13-18

Bassiouny, M.K., 1985. *Experimentelle und theoretische Untersuchungen über Mengenstromverteilung, Druckverlust und Wärmeübergang in Plattenwärmetauschern*. Düsseldorf (Germany): VDI-Verlag.

Berner, J., 2004. Große Hersteller von dünnen Schichten. *Sonne, Wind & Wärme*, 28 (12), p. 53-58.

Bliss, R.W., 1959. The derivations of several „plate-efficiency factors“ useful in the design of flat-plate solar heat collectors. *Solar Energy*, 3 (4), p. 55-64.

Bogaerts, W.F. & Lampert, C.M., 1983. Materials for photothermal solar energy conversion. *Journal of materials science*, 18 (10), p. 2847-2875.

Bohren, A., 2007. *Certification Solarglass – Certification Nr.: IF000612000SGZ*. 23 January 2007, Rapperswil: Institut für Solartechnik.

Cdadapco, 2005a. *StarCD V3.26 – pro-SURF UserGuide*. New York (United States): CD-adapco.

Cdadapco, 2005b. *StarCD V3.26 – pro-STAR UserGuide*. New York (United States): CD-adapco.

Cdadapco, 2005c. *Methodology*. New York (United States): CD-adapco.

Collenz, A. (andrea.collenz@cgaspa.it), 2007a. *Absorber stability vs. channel width.* [E-Mail] Treikauskas, F.D. (treikauskas@fh-ingolstadt.de). Sent Thursday 21 November 2007, 17:22.

Collenz, A., 2007b. *Meeting on General Design Aspects of Rollbond Panels*. [Meeting in Cividale del Friuli (Italy)] (Personal communication, 26 to 27 November 2007).

Cristofari, C., Notton, G., Poggi, P. & Louche, A., 2002. *Modelling and performance of a copolymer solar water heating collector*. *Solar Energy*, 72 (2), p. 99-112.

Davidson, J.H., Mantell, S.C. & Jorgensen, G.J., 2003. Status of the development of polymeric solar water heating systems. In D.Y. Goswami, ed. *Advances in solar energy: an annual review of research and development*. Vol. 15. Boulder, Colo (USA): American Solar Energy Society. Ch. 4.

Dasbach, R., 2008. *Test results of the selective absorber paints coated on the sheet-pipe absorber and the absorber with corrugated pattern*. (Personal communication, 21 November 2008).

Degischer, H.P. & Kriszt, B., 2002. *Handbook of cellular metals: production, processing, applications*. Weinheim (Germany): Wiley-VCH.

Deutsches Institut für Normung, 2006. DIN EN 12975-2:2006-06 *Thermal solar systems and components – Solar Collectors – Part 2: Test methods* – German version EN 12975-2:2006. Berlin (Germany): Beuth Verlag GmbH.

Duffie, J.A. & Beckman, W.A., 2006. Solar engineering of thermal processes. 3rd edition. Hoboken (United States): John Wiley & Sons.

Eicker, U., 2003. *Solar Technologies for Buildings*. 1st edition. Chichester (United Kingdom): John Wiley & Sons.

Eisenmann, W., 2003. Untersuchungen zu Leistungsfähigkeit und Materialaufwand von Sonnenkollektoren mit serpentinen- und harfenartiger Rohrverlegung. Düsseldorf (Germany): VDI Verlag.

Eisenmann, W., Vajen, K. & Ackermann, H., 2004. On the correlations between collector efficiency factor and material content of parallel flow flat-plate solar collectors. *Solar Energy*, 76 (4), p. 387-387.

Epp, B., 2002. Löter-Treffen unter Ausschluss der Öffentlichkeit. *Sonne, Wind & Wärme*, 6, p. 60-61.

Fan, J., Shah, L.J. & Furbo, S., 2007. Flow distribution in a solar collector panel with horizontally inclined absorber strips. *Solar Energy*, 81 (12), p. 1501-1511.

Frey, R.; Frei, U. & Brunold, S., 1995. Bestimmung des Kollektorwirkungsgradfaktors F' an flüssigkeitsführenden Solarabsorbern. In Ostbayerisches Technologie-Transfer-Institut, *5. Symposium Thermische Solarenergie*. Bad Staffelstein, Germany 21-23 June 1995. Regensburg.

Hausner, R. & Fechner, H., 1998. Influence of the flow condition (laminar/turbulent) in the fluid tube on the collector efficiency factor of a fin absorber. In International Solar Energy Society, *2nd ISES-europe solar congress*. Portorož, Slovenia 14-17 September 1998. Birmingham.

Hausner, R. & Fink, Ch., 2002. *Stagnation behaviour of solar thermal systems*. Gleisdorf (Austria): AEEINTEC in assoc. with International Energy Agency – Solar Heating and Cooling Programme – Task 26.

Heck, M., 2005. *Temperaturwechseltests von Absorbern mit verschiedenen Materialkombinationen*. Materialien in solar-thermischen Systemen. Freiburg, Germany 09-10 November 2005.

Henden, L., 2000. *Design and performance studies of a polymer solar collector*. Ph. D. University of Oslo (Norway).

Hermann, M., Koschikowski, J. & Rommel, M., 2002. Corrosion-free solar collectors for thermally driven seawater desalination. *Solar Energy*, 72 (5), p. 415-426.

Hermann, M., 2005. *Bionische Ansätze zur Entwicklung energieeffizienter Fluidsysteme für den Wärmetransport*. Ph. D. University of Karlsruhe (Germany).

Hottel, H.C. & Woertz B.B., 1942. The performance of flat-plate solar-heat collectors. *Transactions of the American society of mechanical engineers*, 64, p. 91-104.

Idelchik, I.E., Steinberg, M.O., Malyavskaya, G.R. & Martynenko, O.G., 1996. Handbook of hydraulic resistance. 3rd ed. New York: Begell House.

Jones, G.F. & Lior, N., 1994. Flow distribution in manifolded solar collectors with negligible buoyancy effects. *Solar Energy*, 52 (3), p. 289-300.

Karni, J., Kribus, A., Rubin, R. & Doron, P., 1998. The „Porcupine“: A novel high-flux absorber for volumetric solar receivers. *Journal of Solar Energy Engineering*, 120 (2), p. 85-95.

Keller J.D., 1949. The manifold problem. *Journal of Applied Mechanics*, 71, p. 77-85.

Konttinen, P.; Lund, P.D. & Kilpi, R.J., 2003. Mechanically manufactured selective solar absorber surfaces. *Solar Energy Materials & Solar Cells*, 79 (3), p. 273-283.

Ladener, H. & Späte, F., 2001. Solaranlagen. 7th ed. Staufen bei Freiburg (Germany): Ökobuch Verlag.

Lampert, C.M., 1997. International development and advances in solar selective absorbers. *Optical materials technology for energy efficiency and solar energy conversion*, 3138 (1), p. 134-145.

Macia, R., 2007. *Meeting on General Design Aspects of Rollbond Panels*. [Meeting in Cividale del Friuli (Italy)] (Personal communication, 12 February 2007).

MacNown J.S., 1982. *Classic papers in hydraulics*. American society of civil engineers: New York (United States).

Mangold, D., 1996. Kostenanalyse der Herstellung von Solarkollektoren und mögliche Kostenreduktionen durch Massenfertigung. In Ostbayerisches Technologie-Transfer-Institut, *6. Symposium Thermische Solarenergie*. Bad Staffelstein, Germany 08-10 May 1996. Regensburg.

Mangold, D., 2004. [Discussion on his Paper (Mangold 1996)] (Personal communication, 19 February 2004).

Martin, H., 1988. *Wärmeübertrager*. Stuttgart (Germany): Thieme.

Martin, H. et al., 2002. *VDI-Wärmeatlas – Berechnungsblätter für den Wärmeübergang*. 9th ed. Düsseldorf (Germany): VDI-Verlag.

Meir, M. & Rekstad, J., 2003. The development of a polymer collector with glazing. In Polymer Competence Center, *Erstes Leobener Symposium "Solartechnik – Neue Möglichkeiten für die Kunststoffbranche"*. Leoben, Austria 7-8 October 2003. Leoben

Metawell, 2008. Datasheet of the sandwich plate: alu hl 05-02-05 / H5.2. [Online]. (Updated 10 Oct 2008) Available at: http://www.metawell.de/pdf/e_alu_hl_05-02-05_hl_h6.pdf [accessed 8 December 2008].

Niklasson, G.A. & Granqvist, C.G., 1991. Selectively solar-absorbing surface coatings: Optical properties and degradation. In C.G. Granqvist, ed. *Materials science for solar energy conversion systems*. Oxford: Pergamon Press. Ch. 4.

Niklasson, G.A. & Granqvist, C.G., 1983. Surfaces for selective absorption of solar energy: an annotated bibliography 1955-1982. *Journal of materials science*, 18 (12), p. 3475-3534.

Orel, B. et al., 2007a. Silicone-based thickness in sensitive spectrally selective (TISS) paints as selective paint coatings for coloured solar absorbers (Part I). *Solar Energy Materials & Solar Cells*, 91 (2-3), p. 93-107.

Orel, B. et al., 2007b. Selective paint coatings for coloured solar absorbers: Polyurethane thickness insensitive spectrally selective (TISS) paints (Part II). *Solar Energy Materials & Solar Cells*, 91 (2-3), p. 108-119.

Pahl, G., Beitz, W., Feldhusen, J. & Grote, K.H., 1996. *Engineering Design – A systematic Approach*. 2nd ed. London (United Kingdom): Springer-Verlag.

Peuser, F.A. & Riemer, H., 1985. Projektbegleitendes Messprogramm zum Zukunftsinvestitionenprogramm / Abschlussbericht zum Teilprojekt ET 4435,1. Bonn (Germany): ZfS – Rationelle Energietechnik GmbH.

Peuser, F.A.; Croy, R.; Schumacher, J. & Weiß, R., 1997. *Langzeiterfahrungen mit thermischen Solaranlagen*. Hilden (Germany): ZfS – Rationelle Energietechnik GmbH.

Peuser, F.A.; Remmers K.H. & Schnauss M., 2002. *Solar thermal systems, successful planning and construction*. Berlin (Germany): Solarpraxis.

Remmers, K.H., 1999a. *Große Solaranlagen*. Berlin (Germany): Solarpraxis.

Remmers, K.H., 1999b. Ermittlung von Richtpreisdiagrammen zur rationellen Kostenschätzung und wirtschaftlichen Planung von Solaranlagen. In Ostbayerisches Technologie-Transfer-Institut, *9. Symposium Thermische Solarenergie*. Bad Staffelstein, Germany 05-07 May 1999. Regensburg.

Rockendorf, G.; Falk, S. & Wetzel W., 1996. Bedeutung und Bestimmung des Kollektorwirkungsgradfaktors bei Sonnenkollektoren. In Ostbayerisches Technologie-Transfer-Institut, *6. Symposium Thermische Solarenergie*. Bad Staffelstein, Germany 08-10 May 1996. Regensburg.

Rockendorf, G.; Schreitmüller, K.R. & Wetzel, W., 1993. Thermal collector test methods – A comparison of the heat loss measurement and a measurement under radiation. In Eszter Kaboldy, ISES Solar World Congress 1993, *Harmony with nature – Volume 5 Active systems*. Budapest, 23-27 August 1993, Hungarian Energy Society: Budapest.

Rotz von, St., 2002. Anwendungsspezifische Optimierung von Harfen- und Mäanderabsorbern mit dem Programm «Absorber-Master». In Ostbayerisches Technologie-Transfer-Institut, *12. Symposium Thermische Solarenergie*. Bad Staffelstein, Germany 24-26 April 2002. Regensburg.

Sandler, M., 2004. Vollflächig durchströmter Solarabsorber mit Schlitzeinströmung und integrierten Sammelleitungen. In Ostbayerisches Technologie-Transfer-Institut, *14. Symposium Thermische Solarenergie*. Bad Staffelstein, Germany 12-14 May 2004. Regensburg.

Siemens, 2008. [Online]
http://www.plm.automation.siemens.com/en_gb/products/velocity/solidedge/index.shtml
[accessed 17 December 2008]

SPF, 2005. *Solar collector factsheet: SPF-Nr. C712*. [internet]. Rapperswil (Switzerland) Available at: http://www.solarenergy.ch/factsheets/scf712en.pdf [accessed 22 August 05]

Tiwari, G.N., 2002. *Solar energy – fundamentals, design, modelling and applications*. Pangbourne (United Kingdom): Alpha Science International.

Touloukian, Y.S. & DeWitt, D.P., 1972. *Thermal radiative properties: Nonmetallic solids (Volume 8)*. London: Heyden & Son.

Treikauskas, F.D.; Zörner, W. & Hanby, V., 2005. Optimised absorbers for solar-thermal collectors – Weaknesses of state-of-the-art sheet-pipe absorbers. In ESTIF (European Solar Thermal Industry Federation), *2nd European Solar Thermal Energy Conference*. Freiburg, Germany 21-22 June 2005. Freiburg.

Treikauskas, F.D.; Zörner, W. & Hanby, V., 2008. Volumetrische Absorber: Die neue Generation von Solarabsorbern in Theorie und Praxis. In Ostbayerisches Technologie-Transfer-Institut, *18. Symposium Thermische Solarenergie*. Bad Staffelstein, Germany 23-24 April 2008. Regensburg.

Wagner, W., 2001. *Strömung und Druckverlust*. 5th ed., Würzburg (Germany): Vogel-Verlag.

Wagner, I., Hintz, C. & Sahm, P.R., 2000. Precision cast near net shape components based on cellular metal materials. In Clyne, T.W. & Simancik, F., eds. *Metal matrix composites and metallic foams: EUROMAT99–Volume 5*. Weinheim (Germany): Wiley-VCH, p. 40-45.

Wang, X.A. & Wu L.G., 1990. Analysis and performance of solar collector arrays. *Solar Energy*, 45 (2), p. 71-78.

Weitbrecht, V.; Lehmann, D. & Richter, A., 2002. Flow distribution in solar collectors with laminar flow conditions. *Solar Energy*, 73 (6), p. 433-441.

Whillier, A., 1953. *Solar energy collection and its utilization for house heating*. Ph.D. Massachusetts Institute of Technology.

Appendix A:

Former Absorber Designs

Table A.1: Former Absorber Designs

	Sheet-Pipe Absorber by Substance-to-Substance Connection	**Sheet-Pipe Absorber with Pipes Connected by Pressing**
Absorber	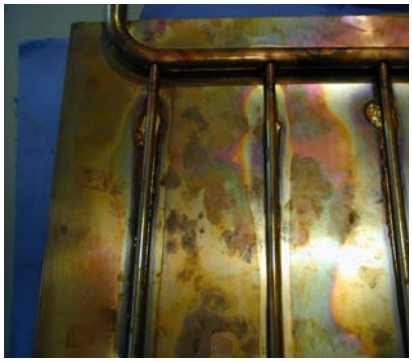	 (Peuser et al 1997)
Configuration	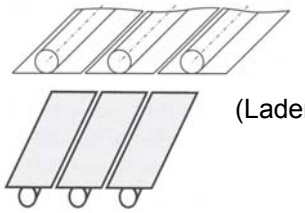 (Ladener & Späte 2001)	
Material	• Aluminium sheet / copper pipe • Copper sheet / copper pipe	• Aluminium sheet / copper pipe • Copper sheet / copper pipe
Processing	• Table 2.4	• Bending of absorber sheet • Clamping of pipe and sheet
Advantage	• Operating pressure ↑ • Volume of heat carrier fluid ↓ • Thermal response time ↓ • Acceptable weight	• Operating pressure ↑ • Volume of heat carrier fluid ↓ • Thermal response time ↓ • Acceptable weight
Disadvantage	• Moderate thermal transfer because of distances between heat carrier pipes • Partially problems with manufacturing and / or strength at higher temperatures during operation	• Moderate thermal transfer because of distances between heat carrier pipes • Various material combinations

Table A.1: Former Absorber Designs (continued)

	Sheet-Pipe Absorber with Embedded Pipes	**Steel Panel Absorber**
Absorber	 (Peuser et al 1997)	
Configuration	 (Ladener & Späte 2001)	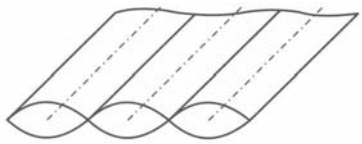 (Ladener & Späte 2001)
Material	• Aluminium sheet / copper pipe • Aluminium sheet / stainless steel pipe	• Steel • Stainless Steel
Processing	Alternative 1 • Moulding of sheets • Application of an adhesive layer into the recess and the pipe • Insertion of the pipes • Bonding of sheets Alternative 2 • Moulding of sheets • Insertion of the pipes • Hot rolling of both sheets	• Moulding of sheets • Seam welding along lines of contact beside the fluid channels
Advantage	• Operating pressure ↑ • Volume of heat carrier fluid ↓ • Thermal response time ↓	• Heat transfer area ↑ • Thermal transfer ↑ • One material
Disadvantage	• Moderate thermal transfer because of distances between heat carrier pipes • Various material combinations • Weight ↑ (depending on material combinations between pipe and sheet)	• Weight ↑ • Corrosion • Volume of heat carrier fluid ↑ • Heat capacity ↑ • Thermal response time ↑

Table A.1: Former Absorber Designs (continued)

	Steel-Cushion Absorber	**Rollbond Absorber**
Absorber	 (Peuser et al 1997)	
Configuration	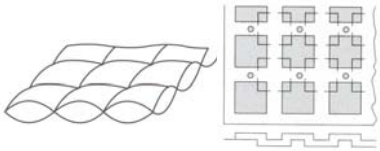 (Ladener & Späte 2001)	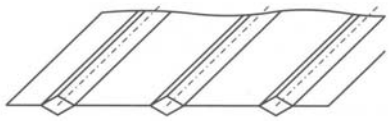 (Ladener & Späte 2001)
Material	• Steel • Stainless Steel	• Aluminium
Processing	Alternative 1 • Moulding of sheets • Spot welding of two sheets at their contact points Alternative 2 • Spot welding of two sheets in a predefined pattern • Inflation of welded sheets by compressed air or fluid	• Coating with special coating compounds (e. g. graphite-based) along intended fluid channels by printing methods • Pressed with high pressure → Roll forming (no connection along coating) • Inflation by compressed air along coated areas → fluid channels
Advantage	• Heat transfer area ↑ • Thermal transfer ↑ • One material	• Number of channels ↑ • Thermal transfer ↑ • Weight ↓ • One material
Disadvantage	• Operating pressure ↓ • Weight ↑ • Corrosion • Volume of heat carrier fluid ↑ • Heat capacity ↑ • Thermal response time ↑	• Operating pressure ↓ • Corrosion because of coating compound for fluid channels

Appendix B:

Requirements List

Requirements List

Research Project: Development of a volumetric solar thermal absorber

Issued on: 4th December 2007

No.	Description	Values	Demand	Wish
1	**Function**			
	Conversion of radiation into heat and transmission to a liquid fluid			
1.1	Subfunction			
	Conversion of solar radiation into thermal energy			
	Heat conduction by the converting device			
	Heat transfer to a liquid fluid			
	Transport of liquid fluid			
1.2	Auxiliary Functions			
	Implementation into a casing			
	Connection to supply-piping			
2	**Geometry**			
2.1	Dimensions			
	Maximum width of absorber	985 mm	**D**	
	Maximum length of absorber	1925 mm	**D**	
	Maximum height of absorber	< 10 mm	**D**	
	Absorber surface	1.90 m²	**D**	
	Fluid volume	<< 8.0 l		**W**
2.2	Connection			
	Number of connections to supply-piping	2	**D**	
	Pipe diameter of flow and return	18 mm		**W**
	Attachment for temperature gauge		**D**	
3	**Load**			
3.1	Internal Pressure			
	Maximum operating pressure (security valve pressure)	3.0 bar	**D**	
	Test pressure (according to: Deutsches Institut für Normung 2006)	4.5 bar	**D**	
3.2	Temperature			
	Minimum absorber temperature	-30°C	**D**	
	Maximum absorber temperature	300°C	**D**	
3.3	Maximum weight of absorber (not filled)	< 8 kg		**W**

Requirements List

Research Project: Development of a volumetric solar thermal absorber

Issued on: 4th December 2007

No.	Description	Values	Demand	Wish
4	**Performance**			
4.1	Coating			
	Selective coating		**D**	
	Quality of selective coating			
	Absorptance	$\alpha > 0.90$		**W**
	Emittance	$\varepsilon < 0.15$		**W**
4.2	Absorber performance			
	Collector efficiency factor *F'*	> 0.95	**D**	
	Collector heat capacity	<< 40 kJ K^{-1}	**D**	
5	**Material**			
5.1	Physical characteristics (absorber material)			
	Diffusion tight		**D**	
	Density	<< 7,800 kg m^{-3}	**D**	
	Heat conductivity	>> 10 W $m^{-1}K^{-1}$		**W**
	Heat capacity	< 1,000 J kg^{-1} K^{-1}		**W**
	Temperature stability	~ 280°C	**D**	
5.2	Chemical characteristics (absorber material)			
	Flame resistant		**D**	
	Weather-proof (UV-resistant)		**D**	
	Corrosion resistant		**D**	
	Saltwater-proof			**W**
	Non-ageing		**D**	
	Resistant against heat carrier fluids		**D**	
6	**Interfaces**			
	Absorbing surface ⇔ Selective coating			
	Absorber ⇔ Collector casing			
	Absorber flow and return connections ⇔ Supply-piping			
7	**Life cycle / Maintenance**			
	Life cycle	> 15 a	**D**	
	No maintenance during life cycle		**D**	

Appendix C:

Tables and Data for Concept Evaluation

Table C.1: Definition of Weighting Factors for the Evaluation Criteria

Number of "+"			Weighting Factor
0	-	0	1
1	-	2	2
3	-	4	3
5	-	6	4

Technical Assesment Criteria	*Fluid Mechanic and Thermodynamic Criteria*	Pressure Drop	Thermal Resistance & F'	Heat Capacity	*Operating Criteria*	Operating Pressure	Temperature Stability of Absorber	Corrosion Resistance	Weight	*Criteria Associated with Production*	Number of Components	Number of Steps in Production	**Economic Assessment Criteria**	Material Costs	Production Costs	Number of "+"	Weighting Factor
Technical Assesment Criteria																	
Fluid Mechanic and Thermodynamic Criteria																	
Pressure Drop			-	○		+	-	-	+		-	-		-	-	2	2
Thermal Resistance & F'		+		+		+	○	○	+		○	○		○	○	4	3
Heat Capacity		○	-			○	-	-	○		-	-		-	-	0	1
Operating Criteria																	
Operating Pressure		-	-	○			-	-	+		○	○		○	○	1	2
Temperature Stability of Absorber		+	○	+		+		○	+		+	+		○	○	6	4
Corrosion Resistance		+	○	+		+	○		+		+	+		○	○	6	4
Weight		-	-	○		-	-	-			-	-		-	-	0	1
Criteria Associated with Production																	
Number of Components		+	○	+		○	-	-	+			○		-	-	3	3
Number of Steps in Production		+	○	+		○	-	-	+		○			-	-	3	3
Economic Assessment Criteria																	
Material Costs		+	○	+		○	○	○	+		+	+			-	5	4
Production Costs		+	○	+		○	○	○	+		+	+		+		6	4

Table C.2: Definition of Points for Each Concept on the Basis of the Evaluation Criteria

	Range	Possible Points	Sheet-Pipe Absorber	Absorber with Corrugated Pattern	Corrugated Sheet Absorber	Metal-Matrix Absorber	Roll-Bond Absorber
Technical Assesment Criteria							
Fluid Mechanic and Thermodynamic Criteria							
Pressure Drop	0 mbar < $\Delta p \leq$ 20 mbar	4	4	3	4	3	3
	20 mbar < $\Delta p \leq$ 60 mbar	3					
	60 mbar < $\Delta p \leq$ 120 mbar	2					
	$\Delta p >$ 120 mbar	1					
Thermal Resistances & F' (Number of Thermal Resistances is used for evaluation)	1	4	1	4	3	4	2
	2	3					
	3	2					
	4	1					
Heat Capacity	0 kJ K^{-1} < c ≤ 10 kJ K^{-1}	4	4	2	2	2	3
	10 kJ K^{-1} < c ≤ 20 kJ K^{-1}	3					
	20 kJ K^{-1} < c ≤ 30 kJ K^{-1}	2					
	c > 30 kJ K^{-1}	1					
Operating Criteria							
Operating Pressure	p > 4 bar	4	4	2	3	2	4
	3 bar < p ≤ 4 bar	3					
	2 bar < p ≤ 3 bar	2					
	0 bar < p ≤ 2 bar	1					
Temperature Stability of Absorber	T > 220 °C	4	3	4	3	4	4
	200°C < T ≤ 220 °C	3					
	180°C < T ≤ 200 °C	2					
	T < 180 °C	1					
Corrosion Resistance	Cu	4	4	3	3	3	3
	Al	3					
	Cu + Al	2					
	Steel or more different materials	1					
Weight	0 kg < m ≤ 5 kg	4	3	4	4	3	4
	5 kg < m ≤ 10 kg	3					
	10 kg < m ≤ 15 kg	2					
	m > 15 kg	1					
Criteria Associated with Production							
Number of Components	1 - 2	4	3	3	4	3	4
	3 - 4	3					
	5 - 6	2					
	> 6	1					
Number of Steps in Production	1 - 3	4	2	3	3	1	4
	4 - 6	3					
	7 - 9	2					
	> 9	1					
Economic Assessment Criteria							
Material Costs (MC)	0 € < MC ≤ 15 €	4	2	3	1	1	3
	15 € < MC ≤ 30 €	3					
	30 € < MC ≤ 45 €	2					
	MC > 45 €	1					
Production Costs (PC)	0 € < PC ≤ 15 €	4	2	3	4	3	3
	15 € < PC ≤ 30 €	3					
	30 € < PC ≤ 45 €	2					
	PC > 45 €	1					

Table C.3: Rating Matrix

	Weighting Factor	Sheet-Pipe Absorber		Absorber with Corrugated Pattern		Corrugated Sheet Absorber		Metal-Matrix Absorber		Roll-Bond Absorber		Perfect Concept	
		State of the Art		Concept 1		Concept 2		Concept 3		Concept 4		Perfect Concept	
		Points	Product	*Points*	Product	*Points*	Product	*Points*	Product	*Points*	Product	*Points*	Product
Technical Assessment Criteria													
Fluid Mechanic and Thermodynamic Criteria													
Pressure Drop	2	*4*	8	*3*	6	*4*	8	*3*	6	*3*	6	*4*	8
Thermal Resistances & F'	3	*1*	3	*4*	12	*3*	9	*4*	12	*2*	6	*4*	12
Heat Capacity	1	*4*	4	*2*	2	*2*	2	*2*	2	*3*	3	*4*	4
Operating Criteria													
Operating Pressure	2	*4*	8	*2*	4	*3*	6	*2*	4	*4*	8	*4*	8
Temperature Stability of Absorber	4	*3*	12	*4*	16	*3*	12	*4*	16	*4*	16	*4*	16
Corrosion Resistance	4	*4*	16	*3*	12	*3*	12	*3*	12	*3*	12	*4*	16
Weight	1	*3*	3	*4*	4	*4*	4	*3*	3	*4*	4	*4*	4
Criteria Associated with Production													
Number of Components	3	*3*	9	*3*	9	*4*	12	*3*	9	*4*	12	*4*	12
Number of Steps in Production	3	*2*	6	*3*	9	*3*	9	*1*	3	*4*	12	*4*	12
Sum		69		74		74		67		79		92	
Technical Rating X		0,75		0,80		0,80		0,73		0,86		1,00	
Economic Assessment Criteria													
Material Costs	4	*2*	8	*3*	12	*1*	4	*1*	4	*3*	12	*4*	16
Manufacturing Costs	4	*2*	8	*3*	12	*4*	16	*3*	12	*3*	12	*4*	16
Sum		16		24		20		16		24		32	
Economic Rating Y		0,50		0,75		0,63		0,50		0,75		1,00	

Appendix D:

Parameters for Collector Efficiency Calculation and Measurement

Table D.1: State-of-the-Art Parameters for Collector Efficiency Factor Calculation

Parameter	Variable	Value	Source
Absorptance	α	0.94	Eicker (2003)
Ambient temperature	T_a	25°C	
Bond conductance	C_b	∞ W m^{-1}K^{-1}	Eicker (2003)
Collector overall heat loss coefficient *)	U_L	4.0 W m^{-2}K^{-1}	Eicker (2003)
Thermal conductivity of heat transfer fluid – water	λ_F	0.607 W m^{-1}K^{-1}	Martin et al (2002)
Thermal conductivity of aluminium	λ_S	220 W m^{-1}K^{-1}	Martin et al (2002)
Reflectance – low-iron solar solar glass	ρ	0.08	Touloukian and DeWitt (1972)
Transmittance – low-iron solar solar glass	τ	0.92	Bohren (2007)

Table D.2: Modified Parameters for Collector Efficiency Factor Re-Calculation Based on the Properties of the Prototype Absorbers and Collector

Parameter	Variable	Value	Source
Absorptance	α		
sheet-pipe absorber		0.79	Dasbach (2008)
absorber with corrugated pattern		0.84	Dasbach (2008) [1)]
Emittance	ε		
sheet-pipe absorber		0.44	Dasbach (2008)
absorber with corrugated pattern		0.57	Dasbach (2008)
Collector overall heat loss coefficient	U_L		
sheet-pipe absorber		6.2 W m^{-2}K^{-1}	[2)]
absorber with corrugated pattern		6.4 W m^{-2}K^{-1}	[2)]

[1)] The absorptance identified by Dasbach (2008) was measured for a selectively painted and flat absorber piece taken from the tested absorber with corrugated pattern. This value had to be corrected for the angular dependence of solar absorptance according to Duffie and Beckman (2006) due to the chamfers of the channel structure.

[2)] The collector overall heat loss coefficient is calculated using the measurement results of the sheet-pipe absorber and the absorber with corrugated pattern, respectively. In contrast to the evaluation suggested by Deutsches Institut für Normung (2006) the linear approach according to equations (4-30) - (4-33) is applied.

Appendix E:

Prototype – Absorber with Corrugated Pattern

Figure E.1: Incompletely Inflated Channels in the Converging Section

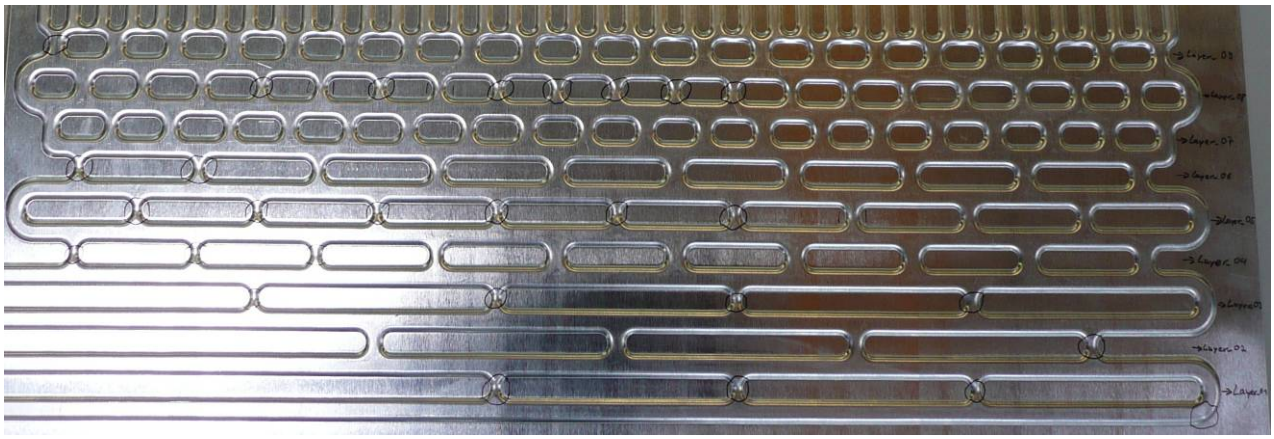

Figure E.2: Incompletely Inflated Channels in the Diverging Section

Appendix C

Table E.1: Channel Heights of the Absorber with Corrugated Pattern

	Channel Number																																	
	01	02	03	04	05	06	07	08	09	10	11	12	13	14	15	16	17	18	19	20	21	22	23	24	25	26	27	28	29	30	31	32	33	34
Layer_00	3.2	3.2	3.2	3.2																														
Layer_01	2.2	2.2	2.1	3.2																														
Layer_02	3.2	3.2	3.2	2.7																														
Layer_03	2.1	2.2	2.3	3.1	3.2																													
Layer_04	2.0	2.1	2.9	3.2	3.2	3.2	3.2	3.2	3.2	3.2																								
Layer_05	3.2	2.0	2.1	2.1	2.2	2.3	3.0	3.2	3.2	3.2	3.2																							
Layer_06	2.1	2.9	3.2	3.2	3.2	3.2	3.2	3.2	3.2	3.2																								
Layer_07	3.2	3.2	3.2	3.2	3.2	3.2	3.2	3.2	3.2	3.2	3.2	3.2	3.2	3.2	3.2	3.2	3.2	3.2	3.2	3.2														
Layer_08	3.2	3.2	3.2	3.2	3.1	3.2	3.0	3.2	3.0	3.1	3.1	3.1	3.2	3.2	3.2	3.2	3.2	3.2	3.2	3.2	3.2													
Layer_09	3.1	3.2	3.2	3.2	3.2	3.2	3.2	3.2	3.2	3.2	3.2	3.2	3.2	3.2	3.2	3.2	3.2	3.2	3.2	3.2														
Layer_10	3.2	3.2	3.2	3.2	3.2	3.2	3.2	3.2	3.2	3.2	3.2	3.2	3.2	3.2	3.2	3.2	3.2	3.2	3.2	3.2	3.2	3.2	3.2	3.2	3.2	3.2	3.2	3.2	3.2	3.2	3.2	3.2	3.2	3.2
Layer_11	3.2	3.2	3.2	3.2	3.2	3.2	3.2	3.2	3.2	3.2	3.2	3.2	3.2	3.2	3.2	3.2	3.2	3.2	3.2	3.2														
Layer_12	3.2	3.2	3.2	3.2	3.2	3.2	3.2	3.2	3.2	3.2	3.2	3.1	3.1	3.1	3.1	3.1	3.1	3.2	3.2	3.2	3.2													
Layer_13	3.2	3.2	3.2	3.2	3.2	3.2	3.2	3.2	3.2	3.2	3.2	3.2	3.2	3.2	3.2	3.2	3.2	3.2	3.2	3.1														
Layer_14	3.2	3.2	3.2	3.2	3.2	3.2	3.2	3.2	3.2	2.9																								
Layer_15	3.2	3.1	2.9	2.8	2.9	2.6	2.3	2.2	2.2	2.6	3.2																							
Layer_16	3.2	3.2	3.2	3.2	3.2	3.2	3.2	3.2	2.1	1.9																								
Layer_17	3.2	3.1	2.6	2.3	2.2	3.0																												
Layer_18	3.2	3.2	3.2	2.3	2.0																													
Layer_19	3.2	3.2	3.2	3.2	2.2	2.1																												

Appendix F:

Infrared Sequences of the Absorber with Corrugated Pattern

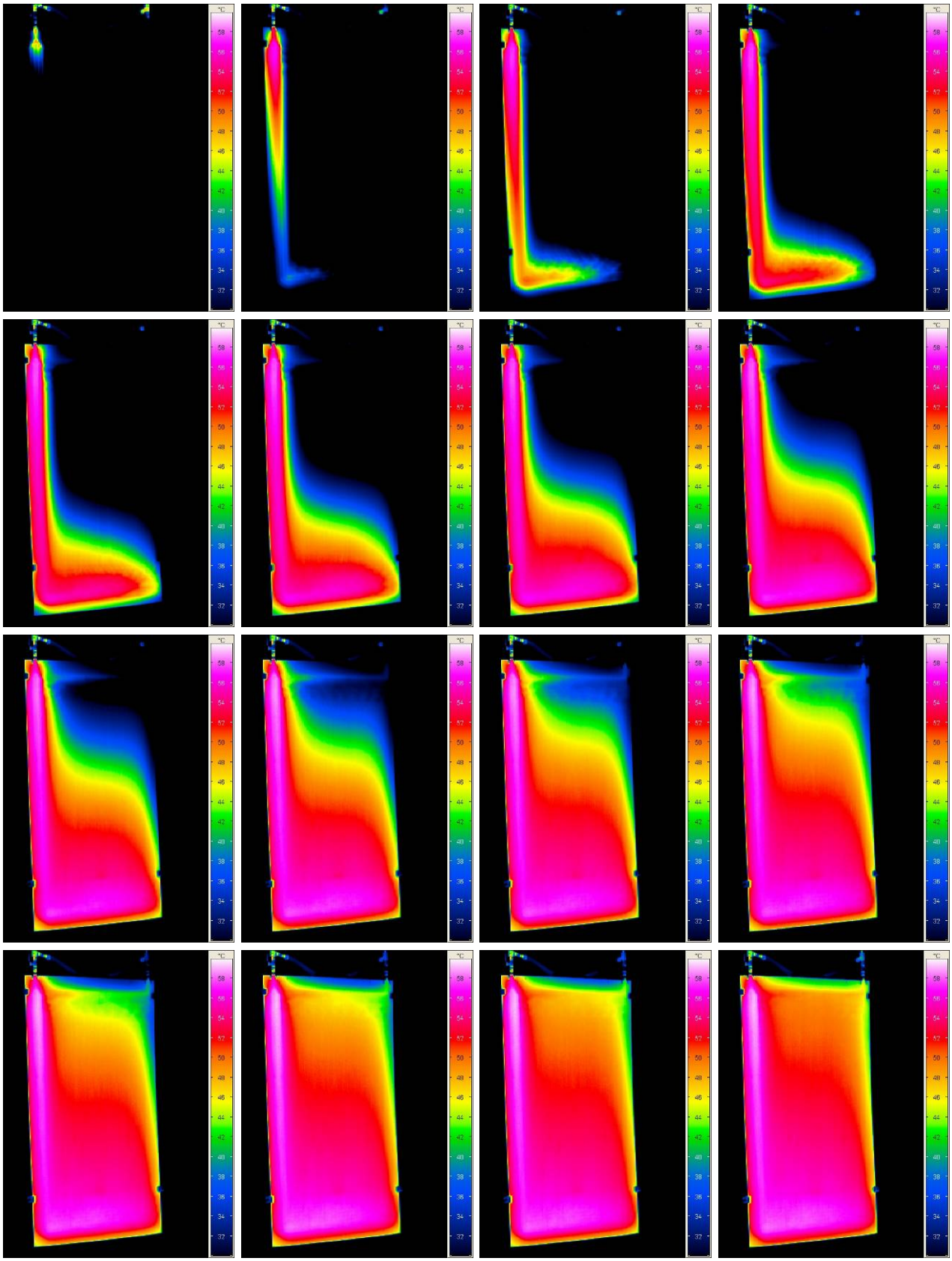

Figure F.1: Infrared Sequence for an Inlet Flow-Rate of 60 l h^{-1}
(time between two images is approximately 20 s)

Appendix G:

Publications

Treikauskas, F.D.; Zörner, W. & Hanby, V.
Absorbers for Solar-Thermal Flat Plat Collectors – Weaknesses of Today's Sheet-Pipe-Design Absorbers. 15. Symposium Thermische Solarenergie. Bad Staffelstein, Germany, 27-29 April 2005. (in German)

Treikauskas, F.D.; Zörner, W. & Hanby, V.
Optimised Absorbers for Solar-Thermal Collectors – Weaknesses of State-of-the-Art Sheet-Pipe Absorbers. 2nd European Solar Thermal Energy Conference (estec2005). Freiburg, Germany, 21-22 June 2005.

Treikauskas, F.D.; Zörner, W. & Hanby, V.
Concept Development of Solar–Thermal Absorbers for Flat-Plate Collectors. 16. Symposium Thermische Solarenergie. Bad Staffelstein, Germany, 17-19 May 2006. (in German)

Treikauskas, F.D.; Zörner, W. & Hanby, V.
Numerical Simulation of Volumetric Absorbers. 17. Symposium Thermische Solarenergie. Bad Staffelstein, Germany, 09-11 May 2007. (in German)

Treikauskas, F.D.; Zörner, W. & Hanby, V.
Optimised Absorbers for Solar-Thermal Collectors – CFD–Simulations of Volumetric Absorbers. 3rd European Solar Thermal Energy Conference (estec2007). Freiburg, Germany, 19-20 June 2007.

Treikauskas, F.D.; Zörner, W. & Hanby, V.
Volumetric Absorbers: The New Generation of Solar Absorbers in Theory and Practice. 18. Symposium Thermische Solarenergie. Bad Staffelstein, Germany, 23-24 April 2008. (in German)

Treikauskas, F.D.; Zörner, W. & Hanby, V.
Aluminium-Rollbond – die neue/alte Lösung für den solar-thermischen Kollektor-Absorber. 19. Symposium Thermische Solarenergie. Bad Staffelstein, Germany, 06-08 May 2009. (in German / to be published)

Treikauskas, F.D.; Zörner, W. & Hanby, V.
Aluminium Rollbond Absorber – Detail Engineering and Testing. 4th European Solar Thermal Energy Conference (estec2009). München, Germany, 25-26 May 2009. (to be published)